ABSTRACT

Title of Document: EVOLUTION OF FLAME TO SURFACE HEAT FLUX DURING UPWARD FLAME SPREAD ON POLYMETHYL METHACRYLATE (PMMA)

Isaac T. Leventon, Master of Science, 2011

Directed by: Dr. Stanislav Stoliarov, Professor,
Department of Fire Protection Engineering

The heat feedback profile across 5 cm wide, 15 cm tall samples of PMMA is measured as a flame spreads vertically across its surface. Incident heat flux to a water cooled gauge is determined with peak values averaging to 36kW/m^2 across the height of the sample. This heat flux has been separated into its convective and radiative components and, at this scale, radiative heat transfer is shown to account for between five and fifteen percent of total flame to surface heat flux. Based on these measurements, net heat flux into the pyrolyzing material can be determined. Correlations, expressed solely as a function of sample burning rate, predicting net heat feedback to the material's surface are developed.

Keywords: Flame heat flux, upward flame spread, energy feedback, PMMA

Evolution of Flame to Surface Heat Flux During Upward Flame Spread On Polymethyl Methacrylate (PMMA)

By

Isaac T. Leventon

Thesis submitted to the Faculty of the Graduate School of the
University of Maryland, College Park, in partial fulfillment
of the requirements for the degree of
Master of Science
2011

Advisory Committee:
Professor Stanislav I. Stoliarov, PhD, chair
Professor James G. Quintiere, PhD
Richard E. Lyon, PhD

Acknowledgements

Every time I read through an old thesis, the first acknowledgement that I come across is inevitably a requisite thank you from the author to his or her advisor. Sometimes the student offers a long, meandering expression of love for the opportunity they've been afforded and how enjoyable it's somehow been to work on (despite the ridiculous hours they must have put in to finish). Often they'll pay tribute to the many long conversations spent pouring their mind and soul out to their advisor when they needed guidance, help with a particularly interesting (re- unexpected, bewildering, and frustrating) problem, or simply encouragement that this will all be worth it in the end, somehow.

I would read these and think, "Well that's nice. Looks like they really, really don't want to lose their funding.." but now I realize that these remarks are not a stretch by any means, rather they're genuine expressions of gratitude. That being said, for all of these reasons I've just stolen, and for somehow trusting me as an undergrad nearly two years ago to begin making this project my own- thank you, Dr. Stas. This work wouldn't be close to what it is today without your help.

Along the way, I've also had some help from a few others that I would like to mention here.

Olga, you somehow managed to make me (and my work) look reasonably competent during my first months in lab. I'm not quite sure how you made that possible, so thank you.

Nicolas, tu travaillais si dur pendant l'été passé et j'avais confiance totale de tes efforts et de tes résultats. A mesure que j'écrivais et que je lisais tous les autres renseignements que nous utilisons pour écrire cette thèse, tu continuais à faire les expériences dont j'avais besoin. En fait, pendant ce temps, tu m'as permettais à rester sain d'esprit; merci beaucoup.

Dr. Lyon and the FAA, you've kept us funded for more than a year now, through the magic that is Grant Number 09-G-018; that's been pretty great. Quite literally this could not have been done without your support. More importantly, on a personal level at least, Dr. Lyon, when we did get the chance to meet this summer, you showed a genuine interest in my work- that really helped me to believe that my efforts here actually matter.

To the friends who have put up with the last 16 months of frustration, rants, exclamations, irritability, and random bouts of insanity and cake only to still be there on the occasional night I would take off, thank you.

Finally, Jackie, I've been trying to keep up with you for years now and even though I don't think I'll ever catch up and while you still may not believe that there's an actual bar, thanks for setting it so high. Learning about all of the wonderful things that are coming for me (the silly hours and painful work, the absolute party that's known as Quals, and uncaring, soul crushing data) before they actually arrive for the first time has been a great help. Even more importantly, knowing that you're there if and when everything falls apart (even if I don't reach out) has been an immeasurable help.

Thank you.

Table of Contents

List of Tables

List of Figures

List of Symbols

a	scaling constant (dependence of flame height on mass loss rate)
b	constant (dependence of flame height on mass loss rate)
c	scaling parameter (dependence of q_{rad}(%) on sample height, x)
C_p	specific heat [J/mol-K]
d	constant (dependence of q_{rad}(%) on height)
e	constant (dependence of q_{rad}(%) on height)
f	constant (quasi-steady state heat flux at $2\text{ cm} < x < 5\text{ cm}$)
g	constant (quasi-steady state heat flux at $x > 15\text{ cm}$)
h	convective heat transfer coefficient
k	thermal conductivity [W/m-K]
$\frac{dm'}{dt}$	mass loss rate per unit width [g/s-m]
$\frac{dm''}{dt}$	local burning rate [g/s-m^2]
p	pressure
PMMA	Poly(methyl Methacrylate)
q_{rad}(%)	percentage of flame to surface heat flux transferred by radiation
q"	heat flux [kW/m^2]
Q’	heat release rate per unit width [kW/m]
r	reflectivity
t	time [seconds]
T	temperature [K, °C]
w	sample width
x	coordinate along the slab surface in the vertical direction
x_f	flame height
x_p	pyrolysis height
V_s	flame spread rate

Greek Symbols

α	scaling parameter (dependence of q^* on x^*)
β	exponential parameter (dependence of q^* on x^*)
γ	exponential parameter (dependence of β on $\dot{m}'$)
δ_f	flame standoff distance, thickness
λ	conductivity [W/m-K]

ν	kinematic viscosity [m^2/s]
ρ	density [kg/m^3]
σ	Stefan-Boltzman constant ($5.67 \bullet 10^{-11}$ [kW/m^2K^4])
τ	scaling constant (dependence of β on mass loss rate)
φ	view factor
ω	scaling constant (dependence of β on mass loss rate)

Subscripts

∞	ambient
conv	convection
fl	flame
HFg	heat flux gauge
max	maximum
net	net (heat flux into a material)
pyr	pyrolysis
rad	radiation
rerad	reradiation
steady	quasi steady state
surf	surface
TBL	thermal boundary layer

1. Introduction

1.1 The Fire Problem

Material flammability is a complex phenomenon that is defined by multiple factors including ignitability, flame spread, heat release rate and the generation of different hazardous products of combustion. In an effort to better protect people and property from the dangers that unwanted fires pose, it is therefore important to not only better understand each of these processes but to evaluate different materials by the appropriate metrics given their intended use.

It has been strongly suggested [1] that heat release rate is the most important variable in fire hazard; however, Ito and Kashiwagi have effectively argued that, "in the initial stages of building fires, flame spread over the surface of combustible solid materials such as a floor covering, a wall, or interior finishings is the key determinant of the rate of fire growth." [2] Furthermore, upward flame spread has been recognized as especially important because it is so often present during the development of fires. [3] While materials burn in this configuration, flame spread rate is particularly significant because it is most rapid and thus the flame spread process is most hazardous[4].

Further complicating this problem is a practice highlighted by Quintiere that unfortunately still continues today with, for example, the widespread use of the standard safety test for plastic material flammability, UL94 [5]. In 1988 Quintiere stated, "Many different tests for assessing flammability of materials… in general ... express their results in terms of some observations or measurements used to derive a relative ranking scale. None attempts to relate their measured test results to theories of ignition, spread or combustion. Consequently, the test results are limited in their use, but often widely applied." [6]

While material thermal properties have an important influence on the rate of surface flame spread, numerous studies have identified heat transfer from the flame to the unburnt material as the controlling mechanism of upward flame spread. This makes knowledge of the flame to surface heat flux profile crucially important and the flame extension length, or preheat distance, the length scale of interest for the problem [2][7][8][9]. The importance of these two factors is stressed quite explicitly by Quintiere et al.- "Consequently, the knowledge of $q_f^{"}$ [flame to surface heat flux] and δ_f [characteristic flame length] would complete the required information for wall flame spread."[10]

As the prevalence of synthetic polymers in buildings and other structures grows, the need to evaluate and understand these materials and the hazards they pose, specifically in fire scenarios, increases as well. Because of its ideal burning behavior—it does not drip heavily or char and it has well known thermophysical properties—Poly(methyl Methacrylate), or PMMA, is the de facto choice for flame spread research.

1.2 Early Models of Upward Flame Spread

Given its significance in the fire safety field, it is unsurprising that flame spread has been studied for more than fifty years [11] via.[9]. By 1969, DeRis [12] presented his theoretical description for the opposed flow spread of a laminar diffusion flame. This early work presented a thermal energy balance to predict flame spread rate that was driven by heat transfer by conduction. It did not have to account for convective heat transfer to the unburned fuel bed as it studied a system where the air stream was counter to the flame spread direction (opposed flow) and, for simplicity, it also neglected the

effects of radiation in its solution of the thin fuel bed problem. Despite these simplifications and some other assumptions[A], the results of this work reveal much of the physics involved in this system and were "not inconsistent" with the experimental data available at the time.

Several years later, the first theoretical descriptions of upward flame spread approached the problem similarly by neglecting radiative heat transfer and assuming a two-dimensional, laminar flame[4] [13] [14] . Theoretical predictions of these models qualitatively agree with experimental measurements but further work continues to improve their accuracy by offering better data as inputs and accounting for second order factors that are not present in the ideal two-dimensional models of flame spread.

A first order approximation for upward flame spread rate, V_s, on thermally thick materials can be expressed as [15]:

$$V_s \approx \frac{4\left(q_f^{"}\right)^2 \delta_f}{\pi(k\rho c_p)\left(T_{ig}-T_s\right)^2} \tag{1}$$

Here, $q_f^{"}$ is the heat transfer to the unburned fuel surface and δ_f is the length over which it occurs, $k, \rho,$ and c_p are, respectively, the material's thermal conductivity, density, and specific heat (collectively known as the material's thermal inertia) and T_{ig} and T_s are the ignition (or pyrolysis) and initial surface temperatures of the unburned material, respectively. In such a simplified model, only the fundamental factors that control the flame spread rate are considered, thus highlighting the importance of understanding the gas phase quantities of $q_f^{"}$ and δ_f and improving knowledge of material thermal behavior in the solid phase.

[A] Combustion is allowed only to occur in the gas phase and is treated as an infinitely fast, one step global reaction at the flame sheets so as to allow for a solution that does not involve reaction kinetics. Gas velocity and state properties (ρ, p, λ, C_P, D) as well as the Lewis number are all assumed constant as well.

1.3 Second Order Influences on Flame Spread Rate

Material orientation and hence whether the flame spreads laterally or downward (opposed flow) or upward (concurrent flow) has a significant impact on flame spread over a material. As the most rapid and thus most dangerous mode, upward flame spread has been extensively studied and will be the focus of this report. Additional influences on flame spread rate — which have been thoroughly examined and must be accounted for when designing experiments, comparing results from different tests, and modeling flame spread — include sample geometry, entrainment of air into the flame, and non-ideal burning behaviors such as charring, soot deposition, melting and dripping.

1.3.1 Sample geometry

The thickness of a sample can affect how burning rate develops while a flame spreads across its surface. Depending on whether the sample can be treated as thermally thick or thin, in depth heat transfer from the flame into the material will vary, resulting in a corresponding change in burning rate. Consider a polymer slab that is burning on its front face, but insulated at its back. In the thermally thick case, the heat wave from the surface can extend indefinitely through the material; however, in thinner materials, this heat wave eventually encounters the insulating layer and is stopped, thus augmenting the heat transfer into the material and correspondingly enhancing the burning rate.

Furthermore, as the local burning rate, $\frac{dm''}{dt}$, can vary between initial, peak, and burnout values, if the sample is not sufficiently thick, $\frac{dm''}{dt}$ cannot ultimately reach a single constant value across the entire sample face. Thus, although surface regression is on the

order of 1/100th of the rate of flame spread[16], if a sample cannot be treated as infinitely thick, its effects must be accounted for. Care must therefore be taken to include these effects in flame spread models, restrict the length of experiments to time scales so that they won't occur, or to choose a sample thickness a priori that precludes this difficulty.

Studies measuring the effects of finite sample width on vertical flame spread have shown that, without modification, the two dimensional burning rate theory may also have difficulties predicting vertical flame spread rate over narrow samples. For example, Tsai and Wan [17] showed that flame standoff distance and spread rate decrease for samples less than 0.3 m wide.

Rangwala et al. [18] also reported this reduced standoff distance and further modified their theory to include a Fick's Law diffusion term to account for lateral diffusion of gaseous pyrolysis products as well. They suggested that this diffusion would account for the decreased burning rate seen in < 0.2 m samples and for reduced flame height. Although both of these papers report these variations as occurring for samples narrower than 0.2 or 0.3m, it should be noted that these differences are slight at the threshold values and only become notable at very narrow widths ($w < 5cm$).

Pizzo et. al [3] also reported that as sample width decreases, flame heights are shortened thus resulting in a corresponding decrease in flame spread rate. They refer to the work of Rangwala et al. to say that this behavior could result from lateral fuel diffusion, but also propose that it could be due to lateral entrainment of fresh air into the plume. Introduction of fresh air intensifies with flame turbulence and can also occur simply due to drafts; correspondingly, care is taken in most experiments to ensure that bulk air velocity remains one-dimensional in the vertical direction. This is done

passively by maintaining quiescent conditions during testing and sometimes directly by the use of screens, curtains or side walls.[15][19]

While it was shown that burning rate is affected as sample width decreases below 20 cm, the effect is much greater in very narrow samples. [20] This effect was highlighted experimentally by tests that showed that burning rate, when normalized by sample width, is actually quite consistent between tests performed on 5, 10, 15 and 20 cm samples but markedly lower for 2.5 cm wide samples.

At this narrow sample width, three-dimensional effects become readily apparent in the regression pattern at the face of the solid polymer. Rather than forming a flat, uniform regression front into the surface as predicted by the two-dimensional theory, 2.5 cm samples exhibited a curved front that was markedly deeper at its center than at the sample edges. This front had an effective radius of curvature comparable to the sample width itself and provided clear evidence of a non-uniform burning rate across the width of the sample whereby $\frac{dm''}{dt}$ decreases from the center of the sample towards its edges.

1.3.2 Transition to Turbulence

A narrow sample width has also been reported as reducing the heat release rate per unit width, Q', at which the transition from laminar to turbulent burning occurs. [20] Although correct, this relationship may not imply causality as Pizzo et al. [3] later reported that the same Q' corresponds to a higher pyrolysis height, x_p, in thinner samples. This report also expresses x_f as a function of x_p, which in turn suggests that the transition to turbulence might be better predicted by a geometric parameter rather than by a measure of heat release rate.

This transition is important because it coincides with a fundamental change in the heat transfer mechanism above the burning material's surface- in the laminar region where the flame is thinnest and closest to the material's surface, heat transfer from the flame to the surface occurs primarily by convection; however, with an increase in the flame height and hence turbulence and flame thickness, radiation becomes dominant.[16]

Numerous sources note this transition as occurring somewhere between 10 and 20 cm (reported as either as the flame height or the height above the base of the ignition source or burner) [3] [18] [20] [21] [22] with a corresponding Grashof number listed in one paper as ~$5x10^7$. This value is slightly below the standard transitional value of 10^8-10^9 that is suggested for simple buoyancy induced flow along a heated vertical wall[23]; however, it is remarkably close for such a comparatively more complex system.

This analogy is made because it helps to visualize the flow field induced by a vertically spreading flame in a simplified manner that has been well studied- a hot wall immersed in a cold environment will create a similarly behaving buoyancy induced flow. Although the presence of a flame in this reacting system makes the physics of the flame spread problem much more complex, it is a valid and useful first order approximation.

The importance of this laminar to turbulent transition is highlighted here because $\dot{Q}'$ has also often been used along with x_p, to estimate flame height, x_f, in a relationship of the form:

$$x_f = a\left(\dot{Q}'^{*}\right)^n x_p \qquad (2)$$

Here, $Q^{'*}$ is a Froude Number[B] and a and n are constants that Consalvi et al. suggest should take one of two values depending on whether or not a critical value of sample heat release rate, $Q^{'} = 20$ kW/m, is exceeded.[24]. Simplified versions of this correlation (of the form $x_f = ax_p^n$) have also been produced from both experimental and numerical data [15] [25] [26] and [27] via[24].

The required a and n values in each of these reports come from fits of individual data sets and while they do vary, it is suggested that this occurs largely because of great discrepancies in how x_f is measured. Recent work has been performed that proposes a standard definition of this flame height based up a threshold measure of heat flux [8]; however, as will be discussed later in this report, a single method has yet to become universally adopted. Ultimately, values of $n \approx 1$ and $n = 2/3$ are suggested for the case where $Q^{'}$ is less than or greater than, respectively, 20 kW/m.

This value (20 kW/m) appears to have been chosen to provide a way to account for the changing flame spread behavior resulting from a transition to turbulence but, as has previously been stated here, it may be possible to mark this transition equally well, if not better, by a critical length scale or a dimensionless parameter such as the Rayleigh or Grashof numbers.

While it is a commonly accepted practice to measure fire size by heat release rate, Pizzo et al.[3] have shown that a single value of Q' cannot be universally applied to mark this transition. Specifically, for 5 and 2.5 cm wide slabs this threshold value reduces to 17 and 9 kW/m, respectively. This occurs, they explain, because the same value of Q' occurs at significantly greater pyrolysis heights (and thus flame heights) in narrow

[B] $\dot{Q}'^{*} = \frac{\dot{Q}'}{\rho_\infty C_P T_\infty \sqrt{g x_p} x_p}$,

samples. Consequently, if a geometric parameter can indicate this transition in a greater number of systems without being altered, it may be considered as a better indicator of the transition from laminar to turbulent burning behavior.

1.4 Describing the Heat Feedback Profile

Some of the earliest models predicting upward flame spread rate assumed a priori that it was was steady or exponentially increasing. [24] Since then, dutiful research has been performed to determine the thermophysical characteristics of commonly used wall materials and how to predict pyrolysis and flame lengths as functions of their burning rate. With the advent of more powerful and reliable solid phase thermal models, flame spread models advanced in their complexity and ability to provide accurate predictions of fire growth. [9]

Today, with ever more powerful solid phase conduction models [28], the solid phase reactions crucial to the flame spread problem can be well modeled given accurate knowledge of material thermal properties. The next step in improving how flame spread is predicted is thus to better understand gas phase conditions in the flame - most importantly, the flame to surface heat feedback profile.

The simplest method used to model flame to surface heat flux during vertical flame spread is to approximate it as a constant value for $x < x_f$ and zero beyond (downstream of) that region. Together, the papers written by Tsai et al. [24] and Consalvi et al. [29] provide summaries of twelve different studies that modeled upward flame spread with such a heat flux profile. Between them, flame spread was modeled on a range of different wall materials using constant heat fluxes between 20 and 35 kW/m^2

(most often, 25 or 30kW/m^2). Similar work presented by Delichatsios expanded the use of such a heat flux profile by modeling upward flame spread on various cylinders. [30]

A more complex description of the flame to surface heat transfer that allows for a constant heat flux where $x/x_f < 1$ and an exponentially decaying value as x increases farther downstream is suggested by several other works [9] [29] [31] via [24]. Finally, Consalvi et al. suggest a flame height definition that seems to correlate well across multiple materials, which provides a constant heat flux from $x/x_f < 0.8$ and an exponentially decaying heat flux for larger x. Here, flame height is defined as the point in the flame where "wall heat flux" reaches a certain threshold, $q''_{wall} = 10kW/m^2$. [8]

The value of q'' used as inputs into these models is usually taken from steady state testing or measurements of peak heat flux during spreading tests. Brehob et al. suggest that q'' can be regarded as a "fire property" of the wall lining material and, as part of their research, they showed that q''_{max} (the peak measured flame heat flux) does not increase with sample height, at least up to 1.2m [9]. Although the transition to turbulence may alter the method of heat transfer, it has been noted that variations in q'' with respect to turbulence is slight and that "the effect of the flow turbulence on the flame spread rate takes place primarily through flame length." [32]

1.5 Thermal Model

Before advancing into a discussion on how flame to surface heat feedback is studied in this work, it is important to introduce the thermal model that is used to describe this system. As seen in Figure 1, a non-premixed, primarily laminar flame fixed at the base, $x = 0$, of the sample is supported between the polymer and an idealized thermal boundary layer, TBL, providing a relatively constant heat flux from $x = 0$ to $x = x_f$. In the pyrolysis region, $0 \leq x \leq x_p$, a constant surface temperature equal to the pyrolysis temperature of the sample (for PMMA, ~630K [33]) is maintained as heat transfer from the flame is balanced by reradiation, in depth conduction, and the endothermic process of pyrolysis.

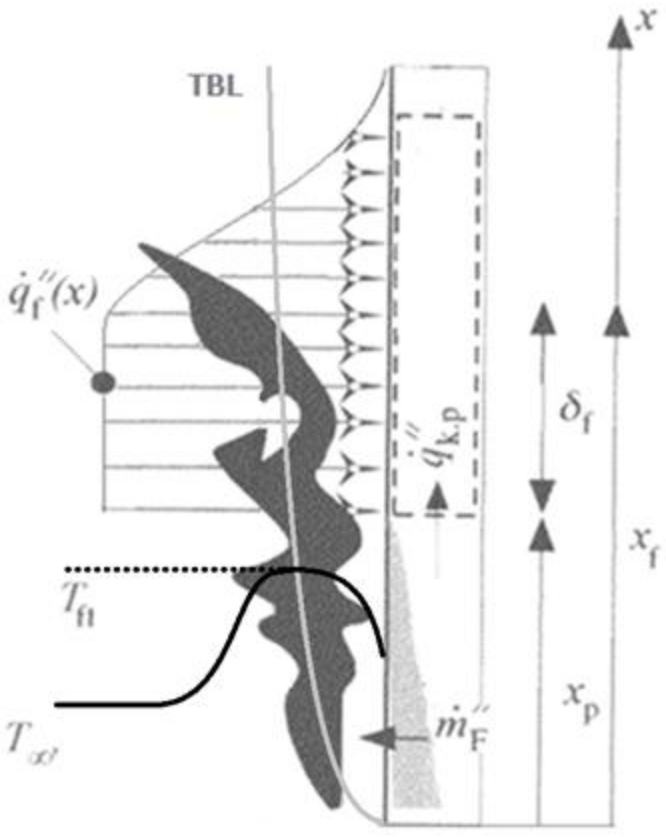

Figure 1. Thermal model for surface flame spread, adapted from *Fundamentals of Fire Phenomena* [34].

The vaporized fuel moves upward by natural convection, reacting with the ambient oxidizer to burn above the pyrolysis region and beyond the pyrolysis front until it is entirely consumed. As these vaporized products burn from $x_p < x < x_f$ they heat the unburnt solid surface until it reaches its pyrolysis temperature and begins to vaporize. Beyond the flame height, a thermal plume exists that preheats the unburned sample, though at a lower rate than in the flaming region.

Exclusively in our model, we propose that the energy needed for pyrolysis of the unburnt sample comes primarily from gas phase, flame to surface heat transfer. It has been reported by Ito and Kashiwagi that in this configuration, conduction through the solid (PMMA) itself is negligible (accounting for 6% of total heat transfer to the unburned fuel) [2]. Thus, our measurements will determine the distribution of just the primary heat source into the unburnt fuel. While this should be sufficient for later correlations predicting flame spread, the solid phase combustion solver that will later be used here will be able to predict and account for conduction through the material, parallel to the direction of flame spread.

As a mostly laminar and fairly transparent flame, the measured flame to surface heat flux should be primarily convective in nature and have but a small radiative component. As such, when determining this heat transfer to the sample, it is treated as arising from the hot gases of the thermal boundary layer that flow naturally across the sample surface rather than simply just from the flame itself. Thus, even though the flame is clearly the energy source for this stream of gases, at higher sample heights where the flow begins to transition from laminar to turbulent, this heat flux will not simply drop to zero if and when the flame flickers.

As will be discussed later in this report, by explicitly measuring radiative heat transfer and treating the remaining component of net heat flux as pure convection, more useful details of this flow field can be estimated; namely, an effective convective heat transfer coefficient and temperature profile of the evolving boundary layer. This temperature profile is shown in Figure 1 as a solid black curve and idealized beyond the flame as a constant value (dotted line). In this way, flame to surface convective heat transfer, q''_{conv}, can be described conventionally as [23] :

$$q''_{conv} = h_{conv}(T_{fl} - T_{surf}) \tag{3}$$

where h_{conv} is the convective heat transfer coefficient, T_{fl} is an effective flame temperature, that of the boundary layer flow, and T_{surf} is surface temperature.

1.6 Purpose of this study

While thorough research has been done to better understand vertical flame spread, a number of important challenges still remain. One commonly faced - is ambiguity concerning the definition of flame height. This definition of x_f becomes critically important when one considers that most models describe a flame to surface heat flux distribution that varies as a function of x/x_f.

Experimentally, x_f is often recorded by eye during testing or by a threshold value of luminous intensity in subsequent reviews of test video. These measurements, already inherently inconsistent as they change based on which researcher is performing the test, are also very difficult to incorporate in computer models of flames spread. Alternatively, parameters which may be easier to calculate in models (such as a local equivalence ratio)

may be good predictors of flame location, but incredibly challenging to measure in real world testing.

In addition to the challenges faced in accurately modeling the profile of a burning sample's flame to surface heat feedback, reservations exist concerning the values of q'' that are reported (usually greater than, but near, $30kW/m^2$ [35]). Most often, input values of q'' come from measurements taken by a water cooled heat flux gauge. Idealizing convective heat transfer as in equation (3), it becomes readily apparent that, uncorrected, this measurement is too high to represent flame to surface heat transfer because the heat flux gauge's temperature (here, T_{surf}) may be significantly lower than that of the pyrolyzing material that surrounds it.

Furthermore, such a measurement also does not account for reradiation from the surface of the pyrolyzing sample, which reduces net heat transfer into the sample at its surface. In the presence of a flame, this reradiation is so significant that it has been reported that net radiative heat transfer may be away from the solid fuel surface. [36]

Several studies have suggested that commonly used peak heat flux values may not be the best representation of actual conditions. Unfortunately, these works do not seem to have had a major impact on common modeling practice, very likely because errors in predicted q'' can always be corrected for in other ways- for example, by using effective thermal properties for the material to force model predictions to match observed behavior.

Tsai et al. [29] expressed caution in using high values of q'' when simplifying the flame heat flux profile as a constant value for $x < x_f$ and zero beyond. However, their suggestion to instead use an average heat flux, $q'' = \frac{q''_{peak}+q''_{flame\ tip}}{2} \approx 18.8kW/m^2$, is not only quite low to still be considered as representative of the system, but it retains the

inherent weaknesses associated with using a step function to describe the flame to surface heat flux profile.

Ito and Kashiwagi [2] very accurately determined this flame to surface heat flux distribution by measuring the temperature distribution within solid samples of PMMA with a holographic iterferometry technique. Their result indicated a lower peak heat flux that may be a better indication of true conditions. Unfortunately, their method is comparatively more difficult than it is to use a heat flux gauge and it can only be applied to a limited number of polymers as opaque materials cannot be studied in this manner.

We propose another, comparatively simpler, method to accurately determine the net flame to surface heat flux, $q^{"}_{net}$, into a material that requires the deconvolution of readings taken by a total heat flux gauge, $q^{"}_{HFg}$, into its convective and radiative components. These two heat transfer measurements can be represented symbolically as:

$$q^{"}_{HFg} = q^{"}_{conv} + q^{"}_{rad} \tag{4}$$

and

$$q^{"}_{\text{net}} = q^{"}_{conv} + (1 - \text{r})q^{"}_{rad} - q^{"}_{rerad} \tag{5}$$

where r is sample reflectivity, $q^{"}_{rad}$ is radiation incident on the sample's surface and $q^{"}_{rerad}$ is reradiation from the sample itself. Reradiation is defined as:

$$q^{"}_{rerad} = \sigma(1 - r)\left(T^4_{surf}\right) \tag{6}$$

As incident radiation is invariant regardless of the target's surface temperature, the radiation measured by a water cooled gauge will be identical to that incident upon the material of interest (with appropriate corrections for varying surface reflectivity, of course). If this measured radiative component, $q^{"}_{rad}$, can be accurately determined and

then subtracted from q''_{HFg} it would then provide a measure of convective heat transfer, q''_{conv}, to the gauge.

With this q''_{conv} , given that T_{HFg} is known and treating T_{fl} as equal to the stoichiometric adiabatic flame temperature when the flame is fully established above the gauge and still primarily laminar, a convective heat transfer coefficient can be determined for this system from equation (3). When modeling flame spread, these values would be used as gas phase inputs, thus allowing for a better prediction of convective heat transfer into the polymer based on its instantaneous surface temperature.

Current estimates of q''_{rad} have been reported by several authors as possibly ranging from $2 - 15 kW/m^2$ [17] [37] [38]. Perhaps the most thorough work (in which q''_{rad} was determined by three independent methods) reports this value with a reasonably large margin of error. [37] Specifically, for vertical slabs of black PMMA, out of a total calculated heat flux of $25 \pm 10 \mathrm{kW/m^2}$, the radiative component was predicted to be $7 \mathrm{kW/m^2} \pm 8 \mathrm{kW/m^2}$.

Unfortunately, work done to understand the radiative component of q''_{net} from small laminar flames is incomplete or, when reported, done so with significant uncertainty. This is likely because radiation is not the dominant method of heat transfer in wall fires until the flame grows such that it is wholly turbulent and so for smaller samples, q''_{rad} is commonly treated as negligible. Thus, flame to surface heat transfer is often idealized at these scales as purely convective or the distinction is simply not made.

Our work improves the understanding of heat feedback in this system by taking highly resolved measurements of flame to surface heat flux specifically under the conditions where upward flame spread is the most important fire hazard to consider. To

do this, the heat flux profile of a flame spreading upward across small (15 cm tall, 5 cm wide) samples of PMMA is accurately measured. This length scale more closely corresponds to conditions encountered under likely ignition scenarios as opposed to tests on much larger samples, which face similar conditions as seen in fully developed fires, where, arguably, heat release rate becomes the more important fire hazard.

The measured heat flux, $\dot{q}''_{HFg}$, is separated into its convective and radiative components and treated and expressed solely as a function of sample mass loss rate and position. In this two component form, discrepancies in the heat flux measured by the gauge and that felt by the sample due to the sample's higher temperature can finally be accounted for. With a powerful solid phase conduction solver that determines burning rate as a response to this heat flux, flame spread can be more accurately predicted in a myriad of different conditions. The effects of finite sample width on the measured heat flux profile are also studied.

2. Experimental Work

2.1 Test Apparatus Design and Construction

As detailed measurements of transient flame to surface heat transfer have not been produced at this scale with such a fine resolution, we needed to design and build a test apparatus that could support samples in the necessary orientation, limit heat losses, allow for repeatable, unrestricted, and well defined one-dimensional vertical flame spread, and provide a way to accurately measure both sample mass loss rate and heat transfer from the flame to the sample surface during experiments. Several design options were considered and the final test apparatus can be seen in Figure 2.

In this apparatus, 5 cm wide, 5 mm thick plastic samples, which have been previously prepared and set in Kaowool PM insulation, can be securely fixed within a steel holder. Prepared samples are pressed forward into the front of the holder leaving 0.5 cm of exposed insulation on either side of the sample face to allow for unimpeded lateral entrainment of air. Each sample is also secured such that its base is 1.5 cm above the bottom of the holder window and at its top rests a single 0.95 cm, water cooled, Schmidt-Boelter heat flux gauge.

A hole is drilled at the top and along the centerline of prepared samples allowing the gauge to be tightly inserted such that its center is directly on the divide between the uppermost part of the sample and the base of the strip of insulation above that. The gauge is held in place at its front by the sample insulation itself and in back by a sliding, lockable support such that the front face of the gauge rests flush with that of the sample.

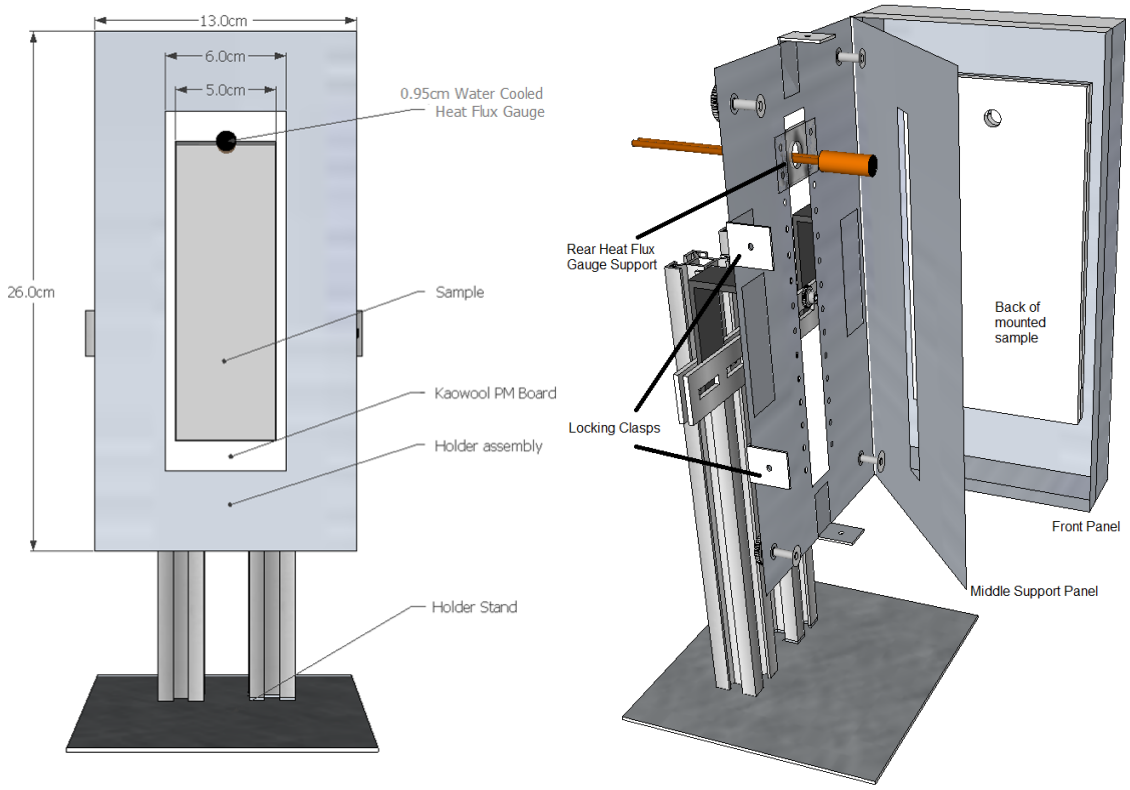

Figure 2. Test Apparatus
(a) Front view showing a 15 cm sample mounted on insulation and set in place within the holder.

(b) Side view showing heat flux gauge and sample supports. When the front panel is rotated closed, it is locked in place by four (top, bottom and sides) clasps. The middle panel is pressed forward by thumbscrews at all four corners when the holder is closed to hold the sample securely in place against the front panel.

As seen in Figure 3, during testing, the holder apparatus is surrounded by fire curtains to limit horizontal perturbations of air and placed underneath a fume hood to capture combustion products. Also shown here is a mass balance that rests beneath the entire apparatus, supporting it during mass loss rate experiments.

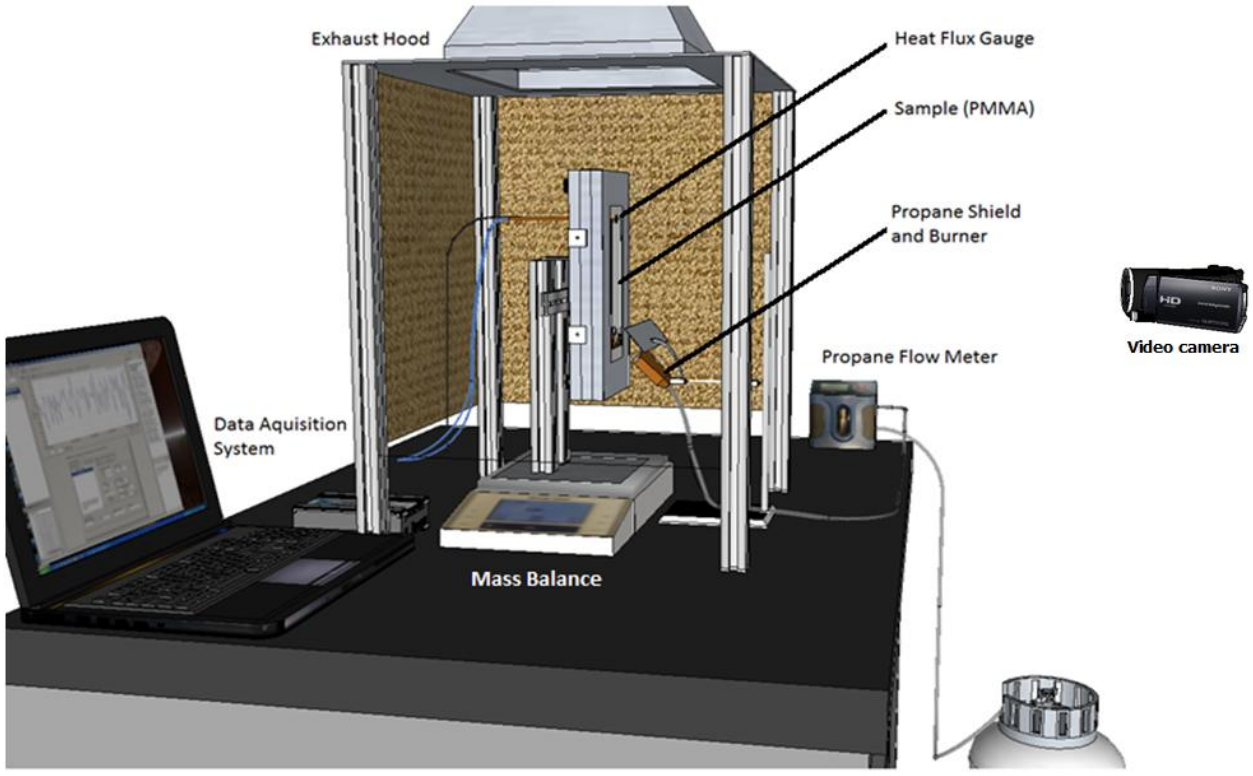

Figure 3. Experimental setup showing required equipment used in each test.
The near side fire curtain, normally present during tests to restrict lateral air flow, has been removed in this schematic for the sake of transparency

A straightforward method of measuring the heat flux profile across these samples would be to canvass the sample with multiple heat flux gauges; however, this would create two significant challenges. First, such a large number of water cooled gauges would fundamentally change the conditions (e.g. lower the temperature) both within the sample and in the flow field above. Second, even without these effects, as the polymer heats up during the test, some of it begins to drip down. These drippings would destroy, or at the very least strongly alter, the face of the gauge by the end of each test thus rendering final measurements unusable.

Although Figure 2 and Figure 3 depict full sized, 15 cm tall samples, for the above reasons the entire heat flux profile of a flame spreading across its surface cannot be measured in just one test. Instead, as seen here only one gauge is mounted at the top of the sample and it records the time dependent flame to surface heat flux at that sample height throughout each test.

By preparing samples with heights ranging from 2 to 15 cm, heat flux was effectively measured across the 15 cm sample's surface with the desired 1 cm resolution. Although this process required a significantly higher number of tests, it has provided repeatable data that can be combined to create an effective heat flux profile across the full sized sample as it burns.

To justify combining measurements in this fashion, one must consider the main assumption in doing so- measuring the heat flux at the top of a small sample of PMMA yields the same result as measuring the heat flux at that sample height in a larger (in this case, 15 cm tall) sample. This should be expected; conditions downstream of the measurement location (here, above the heat flux gauge) should have no effect on the reacting flow of interest.

It does not matter whether or not insulation or PMMA surrounds the top of the gauge as the hot boundary layer gases must already have crossed the face of the heat flux gauge before they encounter this region. Thus, the presence of virgin or burning sample material or a piece of insulation (possibly at elevated temperatures) should not change the measured incident heat flux to the gauge that results from the flame spreading across the sample surface.

As the front surfaces of the sample, heat flux gauge, and upper layer of insulation are each flush with one another, the insulation/polymer boundary should not cause a great physical disturbance in the reacting flow. Arguably, if this boundary layer is disturbed at this interface such that it thickens downstream of the gauge, then radiative heat transfer to the gauge could consequently be augmented.

This thickening of the boundary layer would have a comparatively greater impact when the reacting flow is thinnest and hence closest to the sample. However, heat transfer in such a system is primarily through convection, not radiation, and thus the net impact in such a system would be minimal. In larger, more turbulent wall fires where radiation is a significant mode of heat transfer, such a slight physical disturbance to the flow would be negligible with respect to the natural variations in and overall thickness of the flame.

Ultimately, direct measurements of purely radiant and convective heat flux (as provided by the cone calorimeter heater and a small, laminar propane flame, respectively) showed that, when mounted flush with the gauge face, the presence (or absence) of either Kaowool insulation or representative pieces of PMMA has a negligible effect on heat flux measurements. The assumption that small samples do in fact burn similarly as would the lower regions of a full sized sample is further validated by mass loss rate testing as will be explained in the experimental results section of this report.

2.2 Ignition Source

Collecting meaningful data required not only that test samples be prepared and set identically for each test, but also that each fire be started and allowed to grow in the same way. To do this, several ignition sources were tested including a premixed propane burner, 5 cm wide alcohol saturated wicks, and a 5 cm wide non-premixed propane burner. The premixed burner was used as a quick way to test for the ignitability of various polymers; however, as it introduced flow conditions that would otherwise be unseen during testing, it was not considered for actual experiments.

Small 'wicks'- 5 cm wide, 1-2 cm tall pieces of conditioned insulation- that were saturated with a liquid fuel and ignited at the sample's base were also tested. These wicks offered a simple, easy to set up ignition source that could be well characterized but ultimately did not produce uniform (with respect to time) heat flux profiles across the polymer's surface.

Ultimately, a 5 cm wide, flat, non-premixed propane burner was selected as the best available ignition source for these tests. When placed 1 cm beneath the sample, and with the aid of a horizontal shield, it preheats just the lower 3.5 cm of the plastic. This heat flux is consistent and very well defined as can be seen in Figure 4.

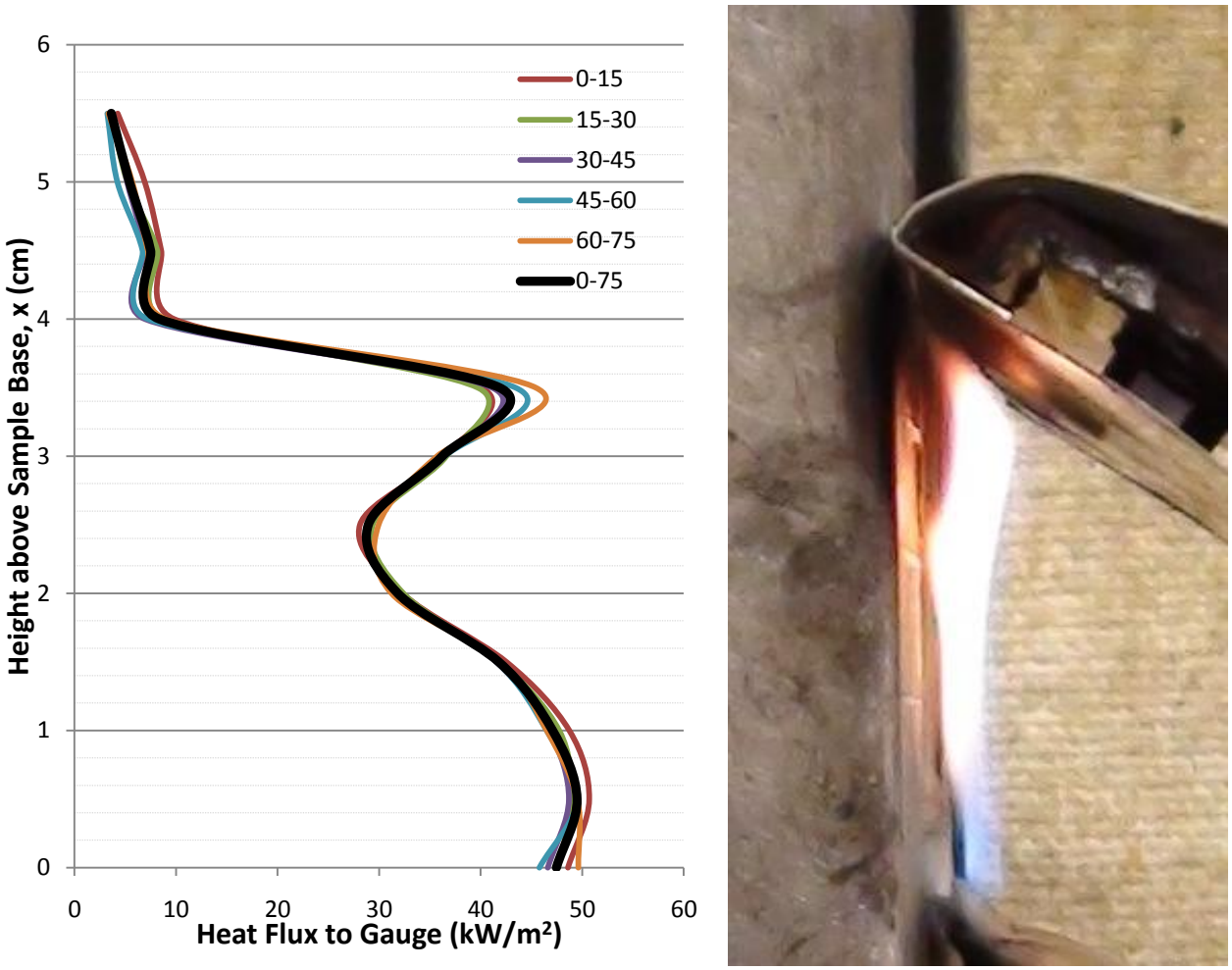

Figure 4. Measured propane burner heat flux profile as a function of time after ignition. A close up image of the propane burner above a sample has been included on the right to help visualize the physical conditions producing this heat flux distribution.

Here, we note that the heat flux decreases farther away from the base of the sample until the burner's flame is forced closer towards the sample's face (at 3.5 cm, right image of Figure 4) by the horizontal shield. Only at this height was the measured heat flux found to vary notably with respect to time after ignition. This increase, though subtle, is likely due to the burner shield itself heating up during its 75 s exposure. At all other heights, the full, 75 s, exposure average is sufficient to characterize the heat transfer of this ignition source.

2.3 Selection of Test Polymers

PMMA burns ideally and is therefore well studied; however, multiple other polymers were also considered before commencing final testing. In the future, after having studied PMMA so extensively, we intend to export our model to other polymers with the aid of additional experiments. Below are listed the polymers that were tested (the most promising first) to provide a potential outline for future work. Not only does this list introduce some common plastics upon which we would like to expand our research but it also presents some of the difficulties that will be faced when additional measurements are taken.

•Poly (methyl methacrylate), PMMA

Extruded sheets [39] were used in these experiments, rather than the commonly studied cell cast[C] samples, in order to better understand a material that is more representative of commonly used plastics. Cell cast plastics have a higher molecular weight and thus are much less prone to dripping than extruded plastics, but they also cost more and therefore are less often used. Similarly, clear PMMA was tested because it is more commonly used even though some studies use black samples so that in depth heat transfer can be better defined.

Testing of this material has been very successful. In these tests, PMMA has been non-charring, easily ignitable, non-dripping (mostly, samples are cut from extruded sheets) and has not formed too much soot.

[C] A method of in situ polymerization

•Polypropylene, PP

Likely the next polymer that would be tested in this configuration. Much like PMMA and several other plastics that were studied, it forms a thin film of soot that deposits on the downstream face of the sample. This coating is a little more obstructive than that produced by PMMA, but it fragments and slides down reasonably readily while leaving the rest of the sample in place, thus allowing for flame spread. Flame spread is slower than over PMMA and burnout is reached at the bottom of the sample before the top ignites, but polypropylene looks to be a promising material.

•Polyoxymethylene, POM

Flame spreads quickly, but sample dripping is also a significant issue. POM was very difficult to safely extinguish using a stream of compressed air as commonly done for other samples. This polymer shows promise as it presents a material on which rapid surface flame spread could be studied. A nitrogen extinguishing system would likely be needed; simply using water would complicate mass loss measurements.

•Polybutylene Terepthelate and High Impact Polystyrene, PBT and HIPS

Both PBT and HIPS produced soot deposits that would steadily grow (normal to the sample surface) downstream of the flame, effectively insulating the upper regions of the sample and inhibiting flame spread. These deposits were measured up to 1 cm thick and, despite extensive testing of HIPS at different orientations

(angling the sample away from vertical to allow soot to rise away from the surface) and longer and larger burner exposures, vertical flame spread could not be achieved. This is particularly interesting because in common flammability tests, e.g. UL94, one can easily ignite a sample of HIPS and it will readily drip and burn.

It is quite possible that flame spread could be induced on these materials given an external heat flux, such as that provided by a radiant heating panel. Such an approach was shown to be effective first for particle board [19] and later for other wall materials including plywood, cotton textiles and poplar [40].

•Poly ether ether ketone, PEEK-

Even with a premixed butane torch, sustained ignition could not be reached. Testing of this polymer would require an additional source of energy as provided by a radiant heating panel and possibly a new ignition source.

•Acrylonitrile Butadiene Styrene, ABS

ABS showed a similar sooting behavior as PBT and HIPS, but was found to be charring behind the soot as well; a behavior not consistent with traditional observations in a cone calorimeter. The combined insulating effect of these two processes meant that the surface flame spread was not truly established in the

traditional sense. Rather, full burnout of the preheated region was reached, and the flame would 'spread' upwards by burning the plastic directly below the protective layer that had formed.

•Nylon 6,6-

Nylon did not readily burn and supported a flame only when very thin; i.e. either in the preheat region or where it dripped down onto insulation flush with, but below, the sample. Furthermore, ignition was very challenging to obtain- nylon samples required more than three times as long of an exposure (5 minutes) to the propane burner as compared to PMMA. It is possible that, like HIPS, an external radiant panel would be able to successfully induce flame spread.

2.4 The Experimental Process

For each test, a 5 cm wide, 5 mm thick sample of PMMA is cut, weighed, and mounted onto a 0.6 cm thick piece of Kaowool PM insulation board[41]. Samples are also surrounded at the top/bottom and sides, respectively, by 2.0 cm and 2.5 cm wide strips of this same insulation (Figure 5a). Each of these pieces is attached to the back insulation board by a thin coating of 3M high temperature Locktite® epoxy. Along with the bottom strip of insulation, this epoxy successfully keeps the PMMA sample in place during the test. As the amount of epoxy needed for each sample is small (on average it is applied at 0.064 g/cm^2 to create a layer ~0.5 mm thick) and as it is essentially shielded from the flame by either insulation or plastic throughout the test, its presence should not have a measureable effect on sample burning behavior.

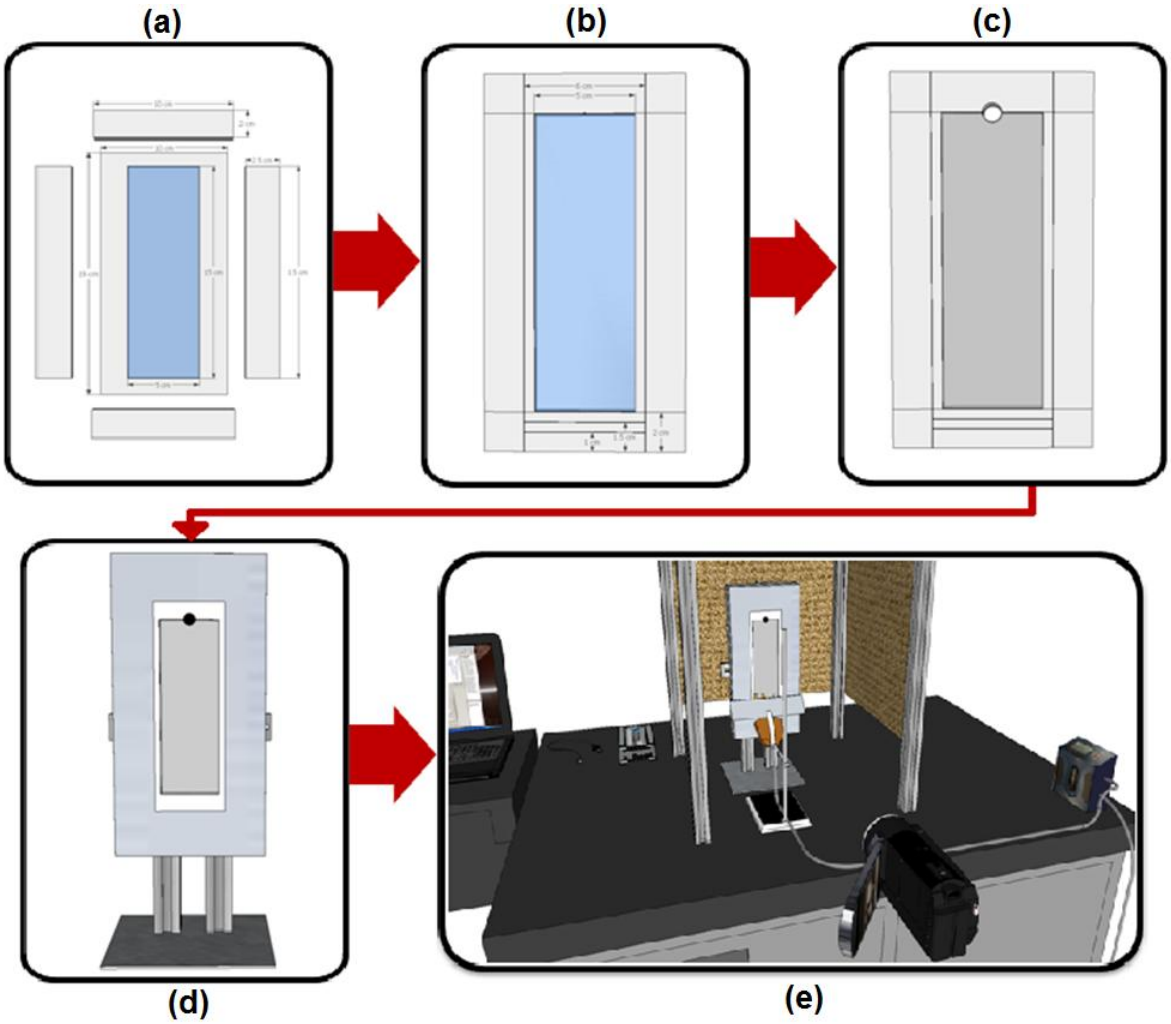

Figure 5. Depiction of test sample life cycle.
PMMA samples and insulation pieces are individually cut (a), set and marked (b), and conditioned (c) before being fitted in a sample holder (d) and set in the laboratory underneath an exhaust hood (e).

Once firmly supported in insulation, samples are marked for positioning in the holder (Figure 5b) and, unless used for mass loss rate testing, a hole is drilled at the top to allow for secure insertion of a heat flux gauge. When the sample is physically prepared, a protective film is removed from the plastic's exposed face and the sample is conditioned in a desiccator for a minimum of 12 hours before use in testing (Figure 5c).

Before each test, the heat flux gauge is cleaned and calibrated by placing it beneath a cone calorimeter heater, directly beside a reference gauge. Both gauges receive water at the same initial temperature and are exposed to incident radiant heat fluxes of $20, 35$ and 50 kW/m^2. A measured response of zero is assumed when the cone heater is off. The working gauge is thus provided a new calibration constant that is used to convert its measured readings (mV) to match the heat flux reported by the reference gauge (kW/m^2). The optical black coating—a spray applied paint that covers the face of working gauge to provide an average absorptance of 0.95—is carefully removed and reapplied after every three experiments.

For experiments that used 65°C or 87°C water to cool the heat flux gauge, gauges are calibrated beneath the cone calorimeter heater with water at the same elevated temperature used during testing versus a reference gauge that uses cold water. The reading of the experimental gauge using warmer water is determined with a calibration constant based on its unique response to the incident heat flux.

Tests begin by setting the flow rate of propane to the burner to 0.1502 L/min $\pm$ 0.18% (as measured by a Bios Defender 530 volumetric flow meter), weighing the sample, and setting it in the holder (Figure 5d). The heat flux gauge and propane burner are positioned at the top and base of the sample, respectively, and the entire apparatus is placed underneath an exhaust hood (Figure 5e), which provides adequate ventilation but fairly quiescent conditions (an induced vertical air velocity of ~3-5 cm/s).

During heat flux testing, an NI USB-9211A portable DAQ recording measurements to Labview™ at 2 Hz is then turned on and the burner is ignited and kept in place for 77 ± 2 seconds before being removed. During mass loss rate experiments, a

heat flux gauge is not used and the sample holder is instead placed on a Mettler Toledo XS4002S mass balance that continuously records total sample mass at 1 Hz. The sample mass loss rate at each time step is then calculated as the numerical derivative:

$$\frac{dm'}{dt} = \frac{1}{w} \bullet \frac{m_t - m_{t+1}}{\Delta t} \tag{7}$$

where $w = 5$ cm, the sample width and m_t is the total mass recorded at time t.

Samples are allowed to freely burn (Figure 6) for an additional 360 seconds, a time period that matches near complete burnout for the 2 cm samples and allows for quasi steady state[D] burning to be reached by the 15 cm samples. All tests are recorded on video and photographs of each sample are taken following extinction before their removal from the holder.

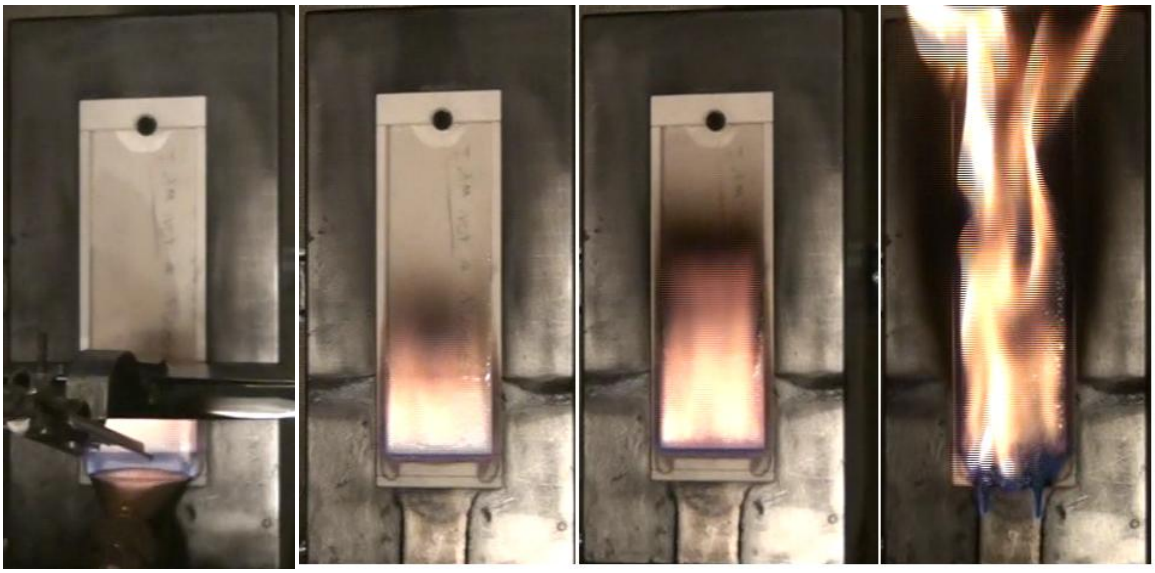

(a) (b) (c) (d)

Figure 6. Representative test of a 15 cm tall sample of PMMA.
This series of images shows a small, laminar flame propagating upwards shortly after burner removal. As more of the sample begins pyrolyzing and the flame grows, the flame begins to transition from purely laminar to turbulent. Images shown are taken (a) before, and (b) 15, (c) 50, and (d) 200 seconds after burner removal.

[D] Quasi-steady state is defined as the period during experiments at which measured heat flux remains relatively constant.

3. Experimental Results

3.1 Effects of Heat Flux Gauge Temperature

It has been noted that heat flux gauges used to measure flame to surface heat flux can collect water, soot, and other products of incomplete combustion when they are cooled with cold water. The accrual of these deposits throughout a test may limit the gauge's ability to accurately measure heat transfer. In order to mitigate this effect, it has been shown that that condensation on the heat flux gauge face can be prevented by cooling them with warm, 65°C, water [37] [42]. The possible effects of such deposits were a concern in these experiments, and so measurements were taken with a gauge connected to a Julabo F25 circulator that allowed the temperature of the water circulating through the gauge to be set between 10°C and 90°C.

These measurements were initially performed on 5 and 12 cm samples at 10°C and 65°C and then expanded to include tests at 87°C in an attempt to determine an effective heat transfer coefficient, h_{conv}, and boundary layer temperature, T_{fl}, for this system. To increase the spatial resolution of these measurements, and to better determine if these values have a clear dependence on sample height, testing was also extended to include 8 and 15 cm samples. A simple analysis of these results was performed, treating measured heat flux as purely convective, and classically describing it as per equation (3)-

$$q''_{conv} = h_{conv}(T_{fl} - T_{surf})$$

Using this model, a reduced incident heat flux can result either from a lower h_{conv} or from a smaller temperature difference. For the smaller samples, the supported flame is completely laminar, very thin, and fairly transparent so heat transfer is expected to be

primarily convective. Furthermore, for such a flame, T_{fl} should remain close to the adiabatic flame temperature of PMMA (~2,000°C) and thus varying the gauge temperature from 10°C to 87°C should have a minimal affect on measured heat flux. Across larger samples though, a transition to turbulence begins that might greatly reduce this effective boundary layer temperature. In this case, an elevated heat flux gauge temperature would more significantly reduce $\Delta T = T_{fl} - T_{surf}$ of equation (3) and thus have a more profound effect upon measured heat flux.

The result of these tests is shown in Figure 7 and Figure 8. The only notable feature of these tests (though it is difficult to say that this difference is statistically significant) is that for all samples, increasing the heat flux gauge temperature from 10°C to 87°C yields a slightly lower measured heat flux. There is no distinct trend showing that this difference, $\Delta q'' = \frac{q''_{cold\ gauge} - q''_{hot\ gauge}}{q''_{cold\ gauge}}$, is dependent on sample size. Therefore, as sample size increases from 3 to 15 cm, there does not appear to be a fundamental difference in T_{fl} (the temperature of the boundary layer above the pyrolysis zone) or the dominant heat transfer mechanism across the sample's surface.

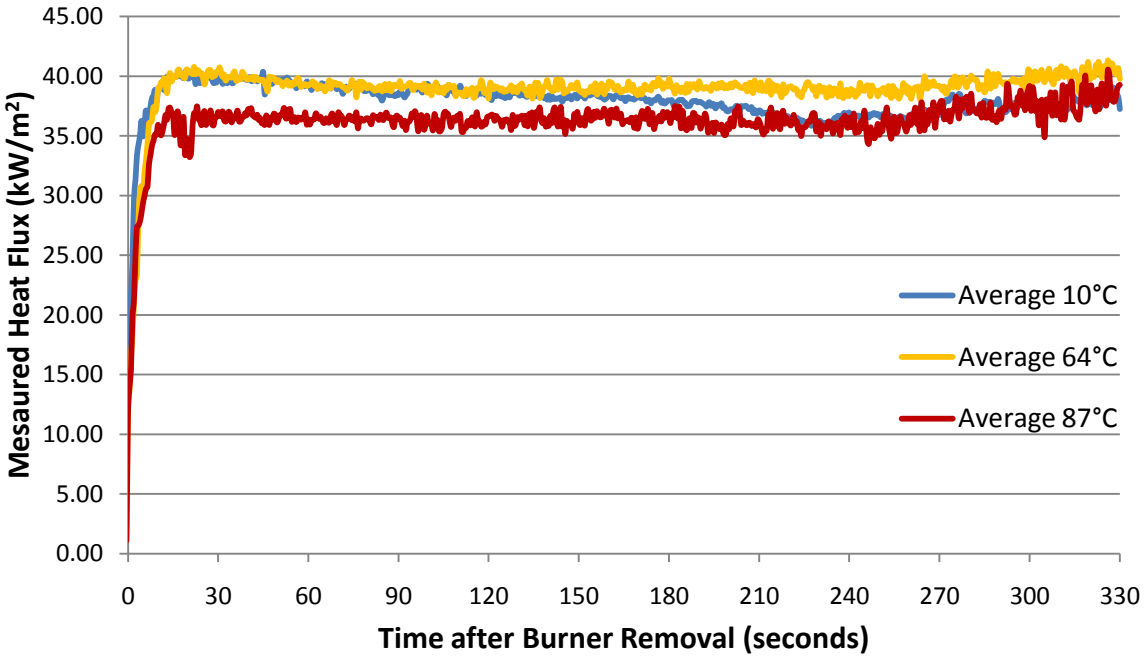

Figure 7. Measured incident heat flux as a function of heat flux gauge temperature (10°C, 65°C and 87°C) for 5 cm samples.

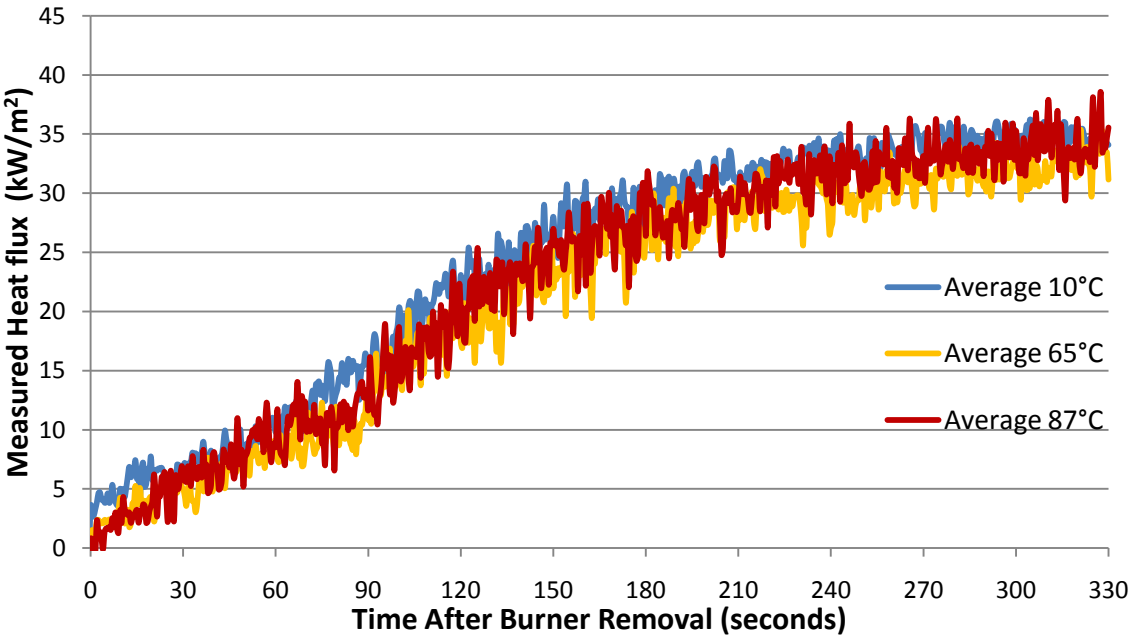

Figure 8. Measured incident heat flux as a function of heat flux gauge temperature (10°C, 65°C and 87°C) for 15 cm samples.

In addition to checking whether there was a noticeable difference in T_{fl} for larger samples, the data from these higher water temperature tests also allows us to determine the impact of depositions left on the heat flux gauge face during standard, 10°C tests. As suggested in the literature [37], increasing the heat flux gauge water temperature above 65°C effectively prevented condensation from forming on its face. While this improved the physical appearance of the gauge by the end of each test, it does not appear as if the water/soot mixture that deposits on the heat flux gauge face during testing has profound impacts on measurements.

Consider again Figure 7 and Figure 8, specifically the overall shape of curves throughout testing at either sample height. Although none of the tests provide perfectly constant measurements at the end of experiments, the heat flux recorded by gauges using cold water does not progressively differ during experiments as compared to that recorded by gauges using warm water. This suggests that while soot deposits on the gauge face may grow during testing, they do not have any significant impact on heat transfer into the gauge. Thus, as measurements taken by heat flux gauges using cold tap water are proven to be just as accurate, this simpler experimental setup was used for all further testing.

3.2 The Measured Heat Feedback Profile

Experiments were performed a minimum of three times for each sample size, though often five or more times each, in order to increase the signal to noise ratio in recorded data. Heat flux measurements were taken at 1 cm intervals for sample heights of 2-15 cm[E]. Mass loss rate measurements are similarly reported with confidence at 2 cm intervals for sample heights between 3 and 15 cm.

Data collection is performed as follows. First, an individual test is performed and the data is recorded and plotted such that burner removal corresponds to time, $t = 0s$. These tests are then repeated, creating a large data set that allows for the development of an average heat flux curve that shows both limited scatter and is an accurate representation of each individual test (Figure 9). This representative curve is then further smoothed and plotted as a five second running average (+/- 2.5s). Finally, this process is repeated for each of the sample heights of interest and the resulting representative curves can be plotted on a single graph (Figure 10).

[E] Test sample information (sample, insulation, and glue masses) can be found in the Appendix

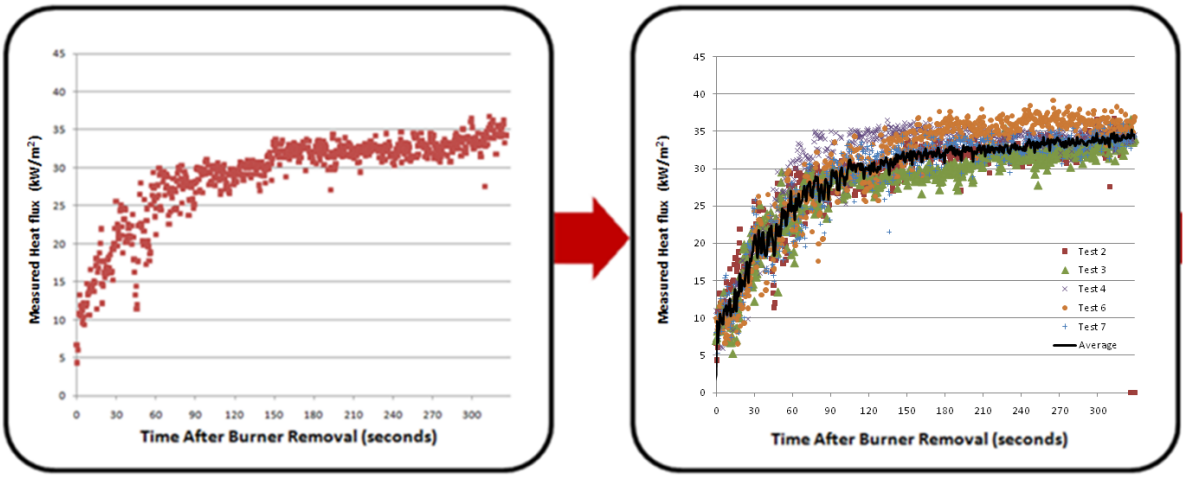

Figure 9. Developing representative curves for measured heat flux (kW/m^2) versus time after burner removal as a function of sample size.
Here, 10 cm samples are used to exemplify the data consolidation process performed at each sample height as follows. On the left, data from one individual test is shown. The same test is repeated and data from successful trials are combined studied together to produce an average data curve as seen in the image on the right.

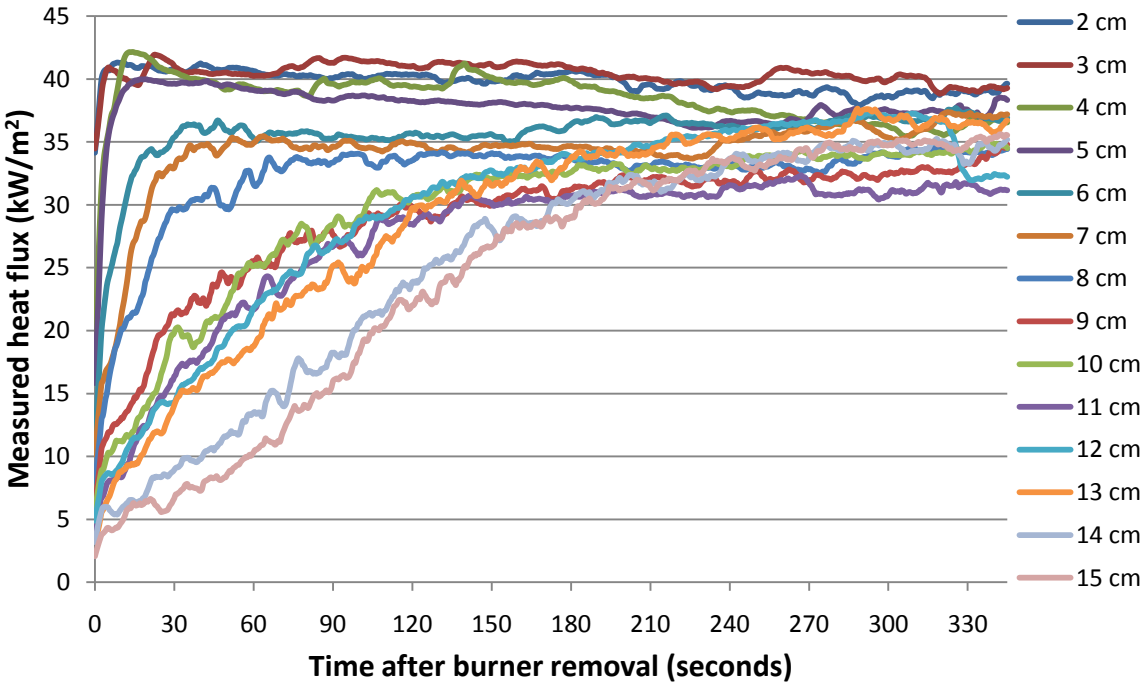

Figure 10. Average measured heat flux, $\dot{q}''_{HFg}$, versus time after burner removal as a function of sample height.

With more than 200 successful experiments complete, the results can now be analyzed. In Figure 10, measured heat flux, q''_{HFg}, has been plotted versus time after burner removal for all 15 sample sizes that have been tested. Following each set of data points from left to right yields the measured heat flux, at a specific sample height, with respect to time from sample ignition to fully involved burning.

When reviewing this figure, one must recognize that this is a measure of heat flux into a cold gauge and not the actual heat flux from the flame into the sample. These values differ because these tests measure heat transfer from the hot boundary layer to a water cooled heat flux gauge that is on the order of 300°C cooler than the surface temperature of pyrolyzing of PMMA.

As such, accounting for reradiation from and lower convective heat transfer to the burning sample's surface suggests that net heat flux should be roughly 35% lower than the measured q''_{HFg} values displayed here. This will be important later when incorporating these measurements into a well defined model of solid phase heat transfer. Net heat flux measurements of this magnitude are in the range of values reported from numerous reports as summarized by Consalvi et al.[24].

For clarity, the heat flux measured by the gauge, q''_{HFg}, and the net heat flux into the sample, q''_{net}, are defined once again as:

$$q''_{HFg} = h_{conv}(T_{fl} - T_{Surf}) + q''_{rad} \quad (8)$$

$$q''_{net} = h_{conv}(T_{fl} - T_{Surf}) + (1 - r)q''_{rad} - q''_{rerad} \quad (9)$$

It should be noted here that the convective components of equations (8) and (9), although identically expressed, can yield quite different values in absolute terms as T_{surf} is uniquely equal to $18℃$ in equation (8), and for equation (9) $T_\infty \leq T_{surf} < 360℃$ [33].

With this in mind, each of the curves in Figure 10 does converge to within 5 kW/m^2 of a single value, 36 kW/m^2, which is consistent with measured heat fluxes reported[F] by Beaulieu and Dembsey [37]. Qualitatively, this heat flux is determined as the average value recorded when measurements no longer increase (significantly) with respect to time. By this point in the experiment, the flame height has reached the heat flux gauge at the top of the sample.

For tests of the smallest samples (2-5 cm), this fairly constant heat flux is slightly higher than measured on taller samples, thus supporting the assumption that the thermal boundary layer is thinner near the sample's base. In Figure 10 it is also evident that the larger the sample, the longer the time delay before heat flux measurements reach their quasi steady state value; this makes sense of course, it takes progressively longer for the flame to reach the heat flux gauge in each of these tests.

With this accurately recorded heat flux data, mass loss rate tests were performed to ensure that smaller samples did in fact burn similarly as small sections of a full size

[F] Peak average heat flux measured at heights of 5.8 and 13.9 cm were reported as $33 \pm 3\ kW/m^2$ for for 10.2 cm tall samples of PMMA as it burned in a vertical configuration.

sample would so that these measurements can be combined to form a single heat flux profile across the height of the sample. These tests were performed on samples of heights from 3 to 15 cm in 2 cm intervals, and similarly repeated as was done for heat flux measurements.

Figure 11 illustrates this process as exemplified with data from 13 cm experiments. Here, data from individual tests are collected and combined to produce an average, representative curve for that height. After extensive testing, these curves are plotted together on one graph as seen in Figure 12.

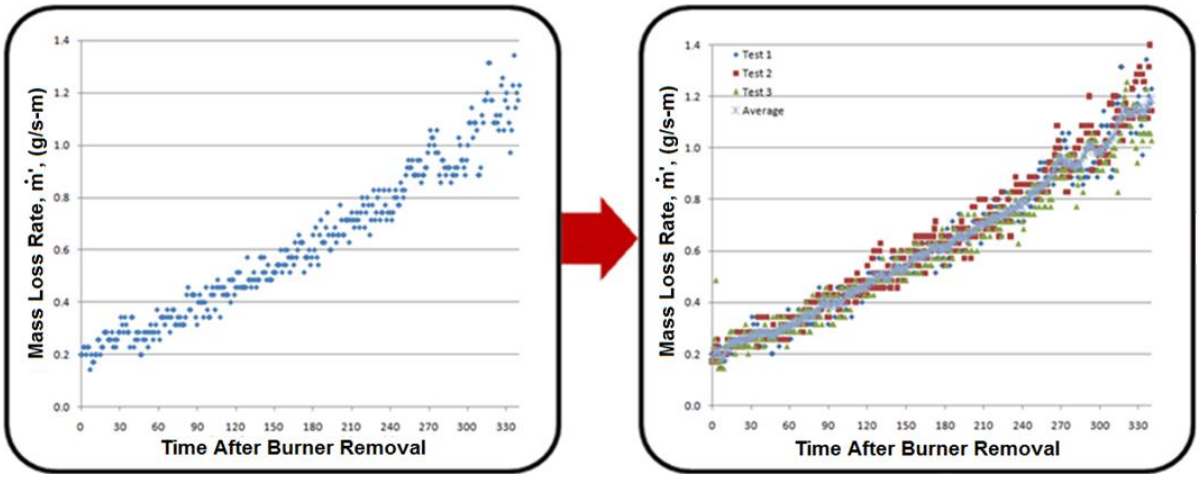

Figure 11. Developing average sample mass loss rate versus time as a function of sample height. On the left, data from one 13 cm mass loss test is shown. The same test is repeated and data from successful trials are combined studied together to produce an average mass loss curve as seen in the image on the right.

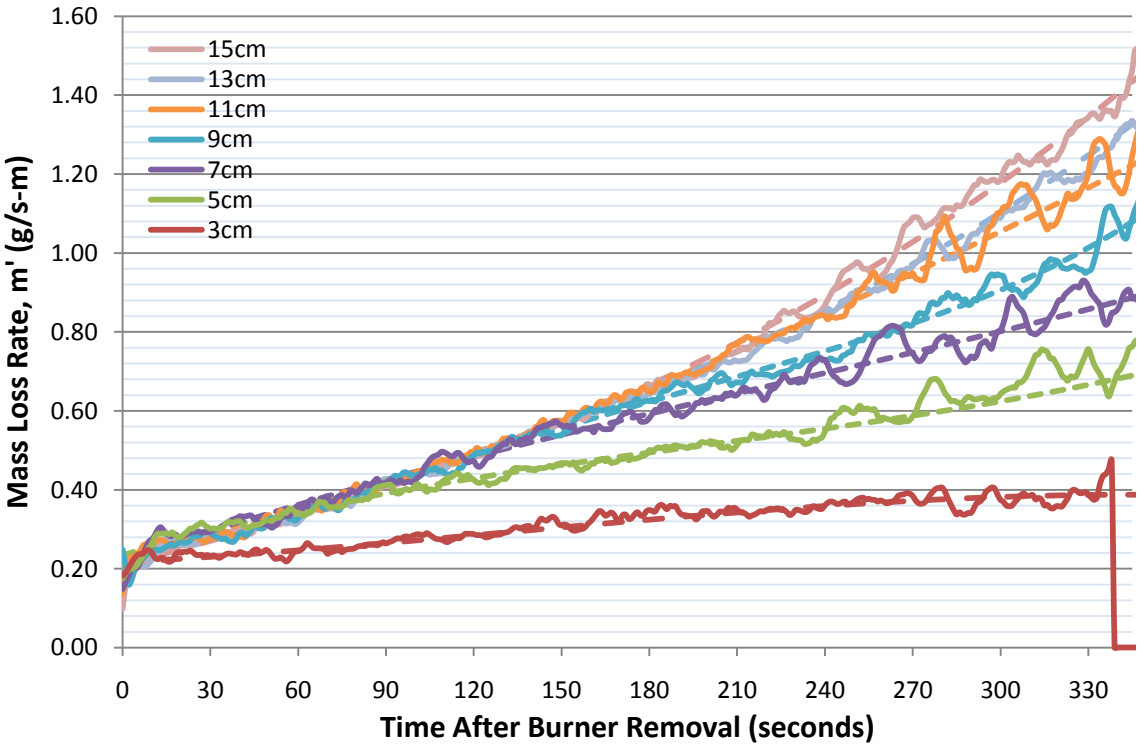

Figure 12. Measured sample mass loss rate vs. time after burner removal as a function of sample height.
Here, solid lines represent average test data while the dotted curves are third order polynomial fits of the data. These curve fits are highly accurate and allow for the prediction of $\boldsymbol{dm'/dt}$ versus time without persistent scatter in readings with respect to time.

As seen in Figure 12, measured mass loss rates for all sample heights between 5 and 15 cm are nearly identical during the first 80 s of free burning. Until this time, it is apparent that only the lower 5cm of any sample is undergoing significant pyrolysis and thus any sample of at least 5 cm in height should (and does) maintain the same net burning rate. One notes that the 3 cm curve quickly breaks away from the others; this is expected, however, as the whole surface of samples this small is entirely exposed to, and heated by, the propane burner during sample ignition resulting in flame spread across its entire surface within 12 to 14 seconds.

For successively larger samples, the same trend holds progressively longer. That is, the net burning rates of all samples are equivalent until the pyrolysis height equals the sample height and its mass loss rate can no longer continue increasing at the same rate as larger samples. Thus, the measured net burning rates of all smaller samples are equivalent to that of the full sized sample until a certain time in the experiment. As expected, this time period of equivalent burning is longer and longer for successively larger samples and so, based on these results, it is apparent that the predicted burning behavior is in fact observed.

Also plotted in Figure 12 are fitted (third to fourth order polynomial) curves[G] to match each measured data set. These fitted values eliminate the minor fluctuations seen in raw data and allow for a more concise description of sample mass loss rate versus experimental time. The accuracy with which these curves represent measured data can be seen qualitatively in Figure 12 and has been calculated more formally in the appendix.

[G] These curves are of the form, $\frac{dm'}{dt} = a_0 + a_1 t + a_2 t^2 + a_3 t^3 + a_4 t^4$. The coefficients needed for their reproduction can be found in the appendix (Table 4). Reporting sample mass loss rate in this manner allows $\frac{dm'}{dt}$ to be expressed at each measured height by no more than 5 coefficients, rather than as a collection of numerous experimental data points.

It is interesting to recognize that the data displayed in Figure 10 and Figure 12 allow for the measurement of flame spread rate (or, more specifically, the location of the pyrolysis and flame fronts.) By noting when each sample height sees quasi steady state heat flux measurements and mass loss rates that begin to differ from that of the 15 cm sample, the time at which the flame and pyrolysis fronts, respectively, have reached that height in the sample can be determined.

Although this is not the focus of this research, the ability to measure these fronts exemplifies the wealth of information collected from these experiments. Additionally, it allows for the evaluation and comparison of these measurements to correlations for pyrolysis and flame heights of PMMA as functions of mass loss rate or time. Measuring these heights in this way also provides a quantitative method to track pyrolysis and flame fronts that does not rely on qualitative or visual analysis as is typically the case [8].

3.3 Resolving Radiation and Convection from Total Heat Flux Measurements

To further improve the value of measurements taken during this series of experiments, additional work was performed to allow the total measured heat flux to be presented as the sum of its radiative and convective components as seen earlier in equation (4):

$$q_{HFg} = q_{rad} + q_{conv}$$

One of the most thorough works to have reported such measurements is that of Beaulieu and Dembsey [37] who measured both the total and radiative components of flames on PMMA, PP, and POM in both vertical and horizontal configurations. Heat transfer by radiation was determined in three distinct ways—using a gauge with individual sensors for radiation and total heat flux, recessing a total heat flux gauge so as to protect from hot flow gases and thus the convective component of heat flux, and predicting radiation by measurements of flame emissivity and temperature—each of which was reported as consistent with the other two.

Recessing a total heat flux gauge was deemed the simplest and most effective approach that could be extended to experiments performed in this study and so additional testing was repeated on samples 3, 5, 8, 10, 12, and 15 cm in height with the heat flux gauge similarly recessed 0.64 cm into the sample's surface. When recessed, the heat flux gauge is initially shielded to prevent the accrual of deposits on its face by a small, snuggly fit, conical section of Kaowool PM board. When enough time has passed in the experiment such that the heat flux readings would reach a plateau in standard heat flux

testing, the plug is removed, the sample is allowed to burn for an additional ten seconds and then the flame is extinguished.

To remove the contribution of hot insulation and PMMA that surround the heat flux gauge to its measurements, the reported heat flux from these tests is calculated as Δq": the value obtained just before flame extinction minus the value obtained after extinction when the rate of change of measured heat flux, $\frac{dq"}{dt}$, begins decreasing by less than 1 kW/m^2-s (Figure 13).

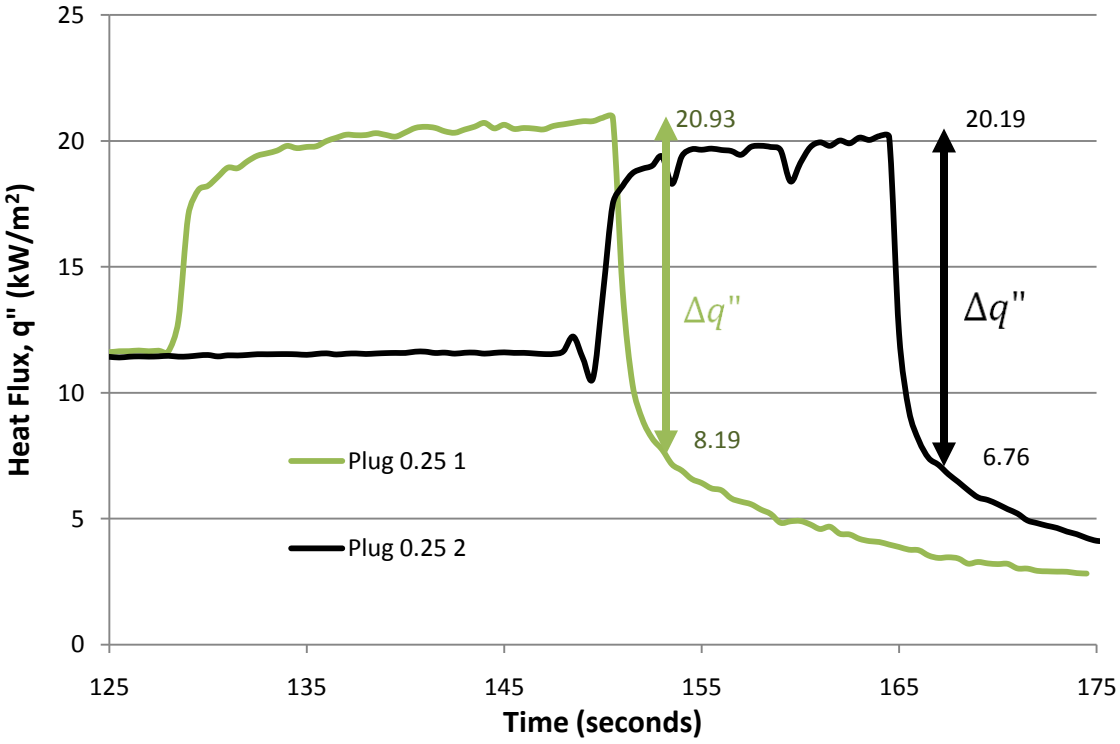

Figure 13. Recessed gauge heat flux measurements taken at flame extinction.

A representative calculation for this process can be found in the appendix where it is also shown that this method effectively eliminates any influence that the hot surrounding insulation that forms the heat flux gauge cavity walls may have on readings, thus providing a measurement that is reliably equal to only the flame to surface heat flux.

Treating this measurement as purely radiation and dividing it by its view factor, φ, would then yield an estimate of the radiative heat flux, q''_{rad}, incident upon the sample's surface. Given that the flame to surface heat flux profile had already been carefully measured, this then provides an upper bound for the percentage of flame to surface heat transfer that can be attributed to radiation.

A radiative view factor was therefore determined both analytically and experimentally[H] with the experimentally determined value, $= 0.77 \pm 0.05$, selected as more representative of actual test conditions[I]. Listed uncertainties here are derived from a propagation of error based on errors arising from variations in flush and recessed measurements of radiative heat flux underneath the cone calorimeter.

The results of this process can be seen in the first row of Table 1, which lists the calculated radiative fraction of total heat flux ($q_{rad}(\%) = 100 \bullet \frac{q''_{rad}}{q''_{HFg}}$) at each sample height tested along with their respective uncertainties. The radiative fractions listed in this row are effectively maximum values because their development rests upon the assumption that recessing the heat flux gauge allows for solely the radiative component of flame to surface heat transfer to be measured[37].

Current experimental observations suggest, however, that, although limited, there is a residual conductive or convective component of heat transfer to the heat flux gauge that occurs even when it is recessed. In the second row of this table are calculated values of $q_{rad}(\%)$ that have been adjusted to take into account this non radiative component of heat transfer. Their development is further discussed below.

[H] See appendix for a description of view factor calculations.

[I] Theoretical predictions of ϕ, when coupled with measurements of incident heat flux to the gauge when both flush and recessed suggested a maximum possible radiative component that exceeded 80% of the total incident heat flux, the value predicted for large scale, wholly turbulent flames. [16]

Table 1. Calculated Radiative Fraction of Total Flame to Surface Heat Flux, $q_{rad}(\%)$

	3 cm	5 cm	8 cm	10 cm	12 cm	15 cm
Uncorrected for convection	$27 \pm 6\ \%$	$28 \pm 2\ \%$	$34 \pm 3\ \%$	$34 \pm 8\ \%$	$27 \pm 4\ \%$	$38 \pm 9\ \%$
Corrected for convection	$5 \pm 15\%$	$5 \pm 13\%$	$14 \pm 28\%$	$14 \pm 32\%$	$5 \pm 13\%$	$17 \pm 38\%$

Both the first and second rows of this table list calculated fractions of total flame heat flux that is attributed to radiation. In the first row, values were obtained assuming hot flow gasses could not reach the heat flux gauge, hence the convective component of measurements was zero; effectively this yields an upper limit for $q_{rad}(\%)$. The second row lists more likely values of $q_{rad}(\%)$ that were determined based on calculations that accounted for limited convective heat transfer at the face of the recessed heat flux gauge. Uncertainties listed in this table are calculated at each height, individually, using a propagation of error in measurements of q'', and φ.

Although it was previously assumed that recessing the heat flux gauge by 0.64 cm was enough to prevent conductive and convective heat transfer into the gauge, it became clear in our radiation measurements that this was not the case. During testing, despite the greater distance separating the heat flux gauge from the flame sheet, deposits were still found on its surface; hence the presence of a shielding plug in front of the recessed gauge until just prior to measuring heat flux. It is possible that this was overlooked in earlier works[37][38] because heat flux gauges used in those tests were cooled with 65°C water in order to prevent condensation from forming at all.

This suggested that, even when recessed, the gauge measured a non radiative component of heat transfer (arising either from diffusion or limited convection from the fire induced flow), a fact that is reinforced by the maximum radiative heat flux calculated for 3 and 5 cm samples (Table 1, row 1). At this length scale, the flame remains fairly thin and transparent and thus it is highly unlikely that radiation accounts for close to 30% of flame to surface heat transfer.

With this in mind, further work was performed to develop an effective parameter that indicates what fraction of a non radiative heat flux would be transmitted to the gauge

when it is recessed into a sample. This parameter, φ_{conv}, was determined experimentally for this report by measuring the heat transfer from the thermal plume above a steady, well defined propane flame with a heat flux gauge mounted flush and 0.64 cm into a layer of Kaowool PM board. Specifically, this value was calculated as:

$$\varphi_{conv} = \frac{\sum_{i=1}^{N}\left(\frac{\dot{q}''_{recessed,i}}{\dot{q}''_{flush,i}}\right)}{N} = 0.18 \pm 0.07 \tag{10}$$

Here, the subscripts *recessed* and *flush* denote the gauge's position, i indicates the heat flux gauge reading at time $t = t_i$ seconds after burner removal, and N is a large enough number such that inherent variations in $\frac{\dot{q}''_{recessed,i}}{\dot{q}''_{flush,i}}$ are smoothed out but still small enough that secondary convective effects induced by the steadily warming insulation that surrounds the gauge remain negligible.

Using φ_{conv} and the radiative view factor, φ, described earlier, the conductive/convective and radiative components of heat flux measured by the recessed gauge can be calculated as a function of $\dot{q}''_{steady}$ and $q_{rad}(\%)$ using the following:

$$\dot{q}''_{conv,recessed} = \varphi_{conv}\left(1 - q_{rad}(\%)\right)\left(\dot{q}''_{steady}\right) \tag{11}$$

$$\dot{q}''_{rad,recessed} = \varphi\left(q_{rad}(\%)\right)\left(\dot{q}''_{steady}\right) \tag{12}$$

The corresponding $q_{rad}(\%)$ at each position in the sample is determined as the value which satisfies the energy balance:

$$\dot{q}''_{recessed} = \dot{q}''_{conv,recessed} + \dot{q}''_{rad,recessed} \tag{13}$$

where $\dot{q}''_{recessed}$ is the total heat flux measured by a recessed gauge.

The results of this series of calculations are presented in the second for of Table 1 and shown in Figure 14. A relationship between $q_{rad}(\%)$ and distance from the base of the flame has been developed by coupling experimental data with that reported by Tewarson and Ogden [16] for large PMMA slabs. As seen in Figure 14, this fit suggests that flame to surface radiation is weakly dependent upon sample height. This regression, which not only includes the results of previous studies, but matches experiment data taken in this work quite well, allows $q_{rad}(\%)$ to be determined as:

$$q_{rad}(\%) = \begin{cases} cx + d & ; \quad x \leq 1m \\ e & ; \quad x > 1m \end{cases} \tag{14}$$

With $c = 0.77cm^{-1}$ $d = 3.2$ $e = 80$

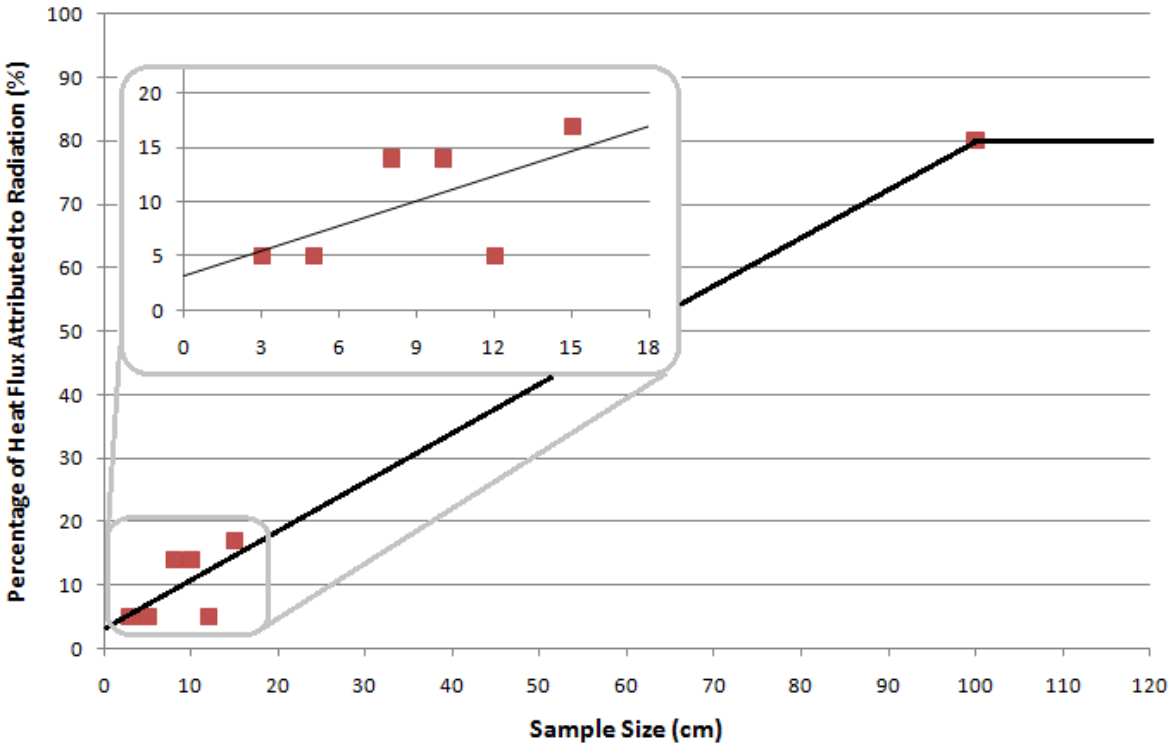

Figure 14. Radiative fraction, $q_{rad}(\%)$ as a function of sample height.

Included in this data set, and used to produce a linear regression to predict $q_{rad}(\%)$ as a function of sample height, is the point (100 cm, 80%). This value is derived based on Tewarson and Ogden's [16] suggestion that for upward flame spread on thick PMMA slabs, at heights above 1 m, radiation accounts for 80% of flame to surface heat transfer. Beyond this height, $\boldsymbol{q_{rad}}(\%)$ is estimated as a constant value.

4. Analysis

4.1 Determining the Heat Feedback of a Flame Spreading on PMMA as a Function of Mass Loss Rate

The ultimate objective of this work is to predict how the flame to surface heat flux over a burning sample evolves as the flame spreads, solely as a function of sample burning rate, $\frac{dm'}{dt}$. Such a heat flux profile is expected to be of the form[8]:

$$q''_{HFg} = f\left(x, \frac{dm'}{dt}\right) = \begin{cases} q''_{flame}, & 0 \le x \le x_f \\ \alpha \bullet q''_{flame}\left(\frac{x}{x_f}\right)^{\beta}, & x > x_f \end{cases} \tag{15}$$

with

$$\alpha, \beta, x_f = f\left(\frac{dm'}{dt}\right) \tag{16}$$

Here, x_f is a measure of flame height and q''_{flame} is a reference heat flux value that will be more precisely defined later in this analysis. This provides for a constant heat flux value in the flaming region ($0 \le x \le x_f$) and a decaying value farther downstream in the flow.

To parameterize the heat flux model presented above, each of the measured heat flux data sets seen in Figure 10 was further smoothed by fitting them with between one and three polynomial regressions (up to fifth order) that accurately captured its form.[J] This created 15 "fitted" curves, each representing the measured heat flux at a particular height in the sample without the scatter resulting from natural variations in the heat flux produced by a constantly changing flame (Figure 15).

[J] These curves have the form: $q''_{HFg} = a_0 + a_1 t + a_2 t^2 + a_3 t^3 + a_4 t^4 + a_5 t^5$. In the appendix (Table 5) the coefficients $a_0, .., a_5$ are listed and these fitted curves are plotted along with the original average heat flux measurements to provide the reader a qualitative comparison of the two data sets.

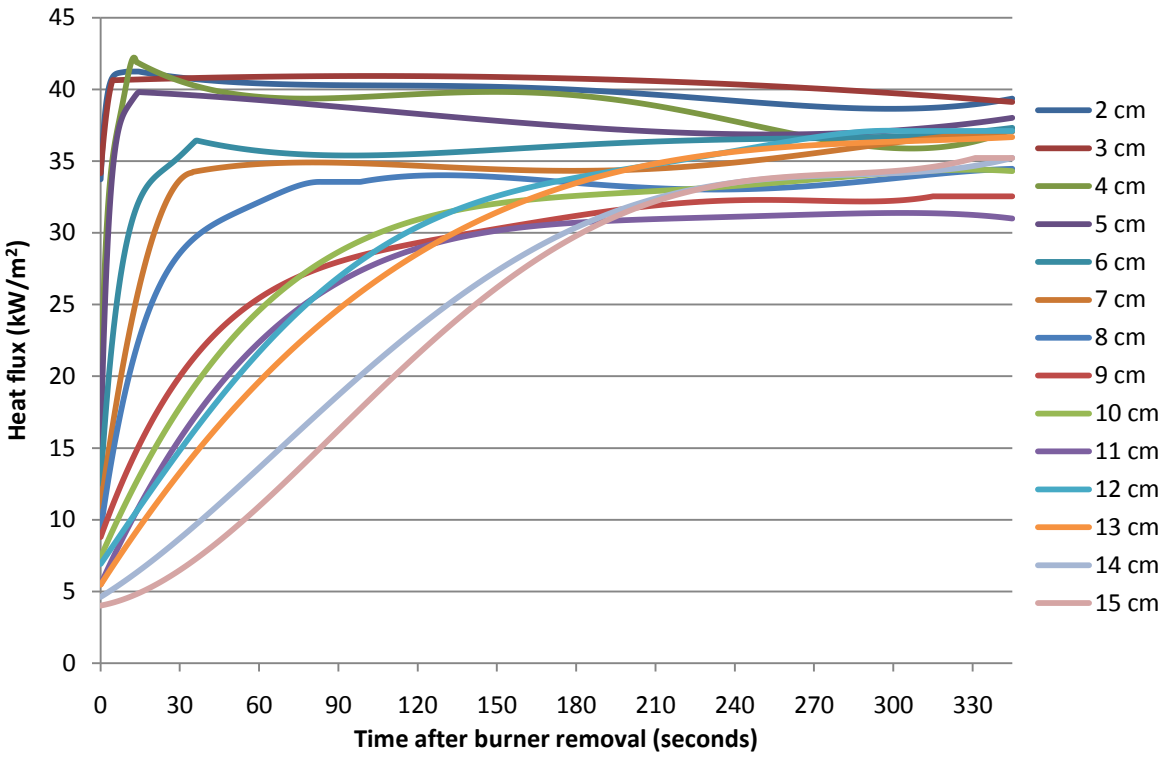

Figure 15. Fitted heat flux data versus time after burner removal as a function of sample height.

It is critical that these fitted values of heat flux, $\dot{q}''_{steady}$, accurately represent original data and so a formal statistical analysis was used to calculate the standard deviation of the mean, σ_{mean}, at each time step along these curves as:

$$\sigma_{mean} = \sqrt{\frac{\sum_i^N \left(\dot{q}''_{fitted} - \dot{q}''_i\right)^2}{N(N-1)}} \qquad (17)$$

Here, $\dot{q}''_i$ is the measured heat flux recorded from individual experiments and N is the total number of data points recorded during the time interval, $t = t \pm 2.5\ s$[K].

This calculation is repeated for each sample height for the duration of experiments and plotted in Figure 16 as $2\frac{\sigma_{mean}}{\dot{q}''_{fitted}}$ [%]. As seen in this figure, the fitted curves match experimental measurements very well, with scatter in measured readings causing the two

[K] N=11•(number of successful tests performed at that height). 11 is used here because the average heat flux profile has been smoothed with a 2.5s running average of data and measurements are taken at 2Hz.

to vary, on average, by just 5 to 8% in the first 15 s of experiments with this error decreasing to ~2% for the remainder of the test.

Due to the accrual of soot, water, and other deposits over the course of each test, it was found that the heat flux gauge's calibration constant could vary by between 2 and 3% from the beginning to the end of each test. Although experiments with hot water, which limited the appearance of such deposits (Figure 7 and Figure 8), showed that condensation on the face of the gauge has a negligible effect on readings, this systematic error will be considered here as well. Additional (minor and more difficult to precisely quantify) sources of error are also accounted for by reporting the fitted curves as representative of true conditions with an uncertainty of $\pm 5\%$.

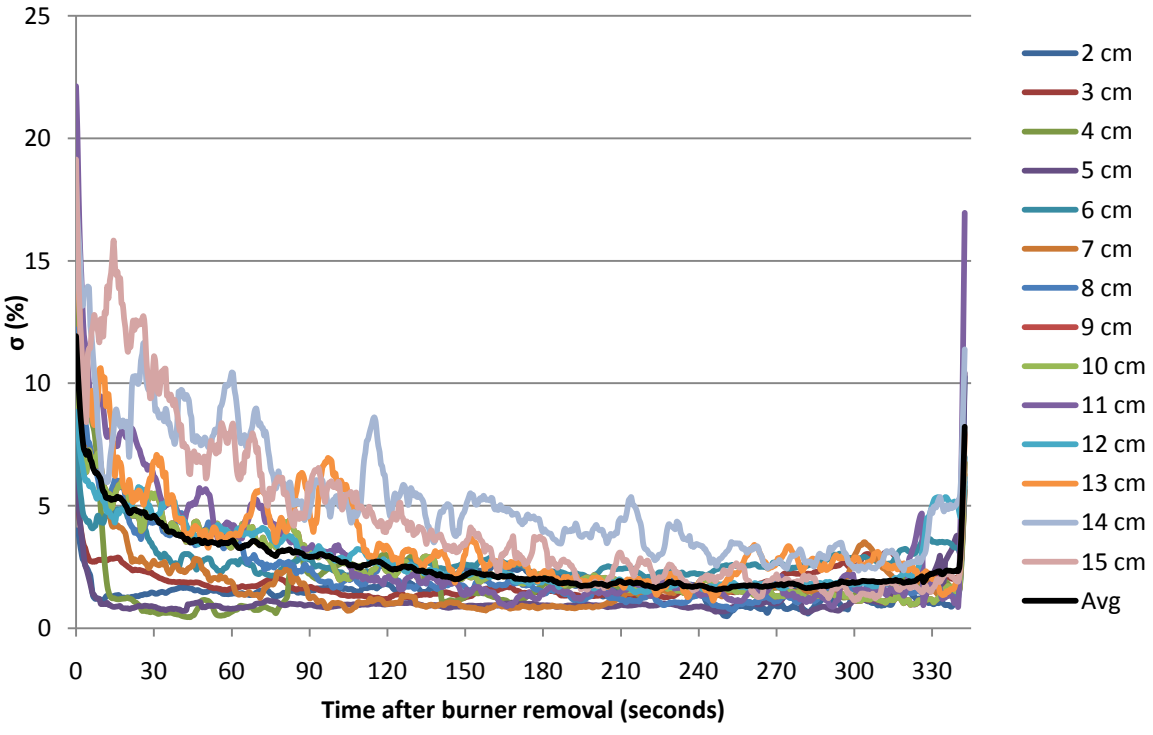

Figure 16. Uncertainty of fitted q" curves versus experimental data.
Here the uncertainty is reported as $\mathbf{2}\frac{\sigma_{\mathbf{mean}}}{\mathbf{q''_{fitted}}}$ to provide, ideally, $\boldsymbol{q''}$ with 95% confidence.

The heat flux profile is better visualized as a function of sample height by normalizing $\boldsymbol{q''_{fitted}}$ data by the quasi-steady heat flux measured at each height in the sample. This highlights the general form of the evolving heat flux profile by better depicting both the flame height and the shape of the region of decaying heat flux beyond $\boldsymbol{x_f}$. This quasi-steady heat flux, henceforth known as $\boldsymbol{q''_{steady}}$, is an integral part of further analysis, and so a more detailed description its determination is warranted here.

Plotted in Figure 17 are measured and fitted representations of the time dependant heat flux readings taken at the top of a 13 cm sample along with the time derivative of this fitted heat flux curve, $\frac{dq''}{dt}$. Qualitatively, q''_{steady} represents measured heat flux once it remains relatively constant with respect to time (quasi-steady state). When this value is reached, the flame height is reported as equal to the gauge position and the heat flux from $0 \leq x \leq x_f$ is assumed to be constant and defined by q''_{steady}.

In order to calculate q''_{steady} for each sample height, the following process is used. After having fitted each of the measured data sets by a polynomial regression as in Figure 15, the first derivative (with respect to time) of each fitted curve is computed and the earliest time at which $\frac{dq''}{dt} < 0.02 \frac{kW}{m^2 s}$ is noted. In Figure 17, this is shown to occur just after $t = 240$ s for 13 cm samples. Experimental measurements recorded over the subsequent 30 s interval (darkened data points highlighted in Figure 17) are then averaged to produce a representative value of this quasi-steady state heat flux. For 13 cm samples, this yields the result: $q''_{steady} = 35.7 \frac{kW}{m^2}$.

Also calculated from this data is the maximum heat flux recorded during the full length of experiments, q''_{max}. Qualitatively, checking that $q''_{steady} \approx q''_{max}$ ensures that

this steady state value is not calculated from a point too early in the experiments, before the flame was fully established above the heat flux gauge.

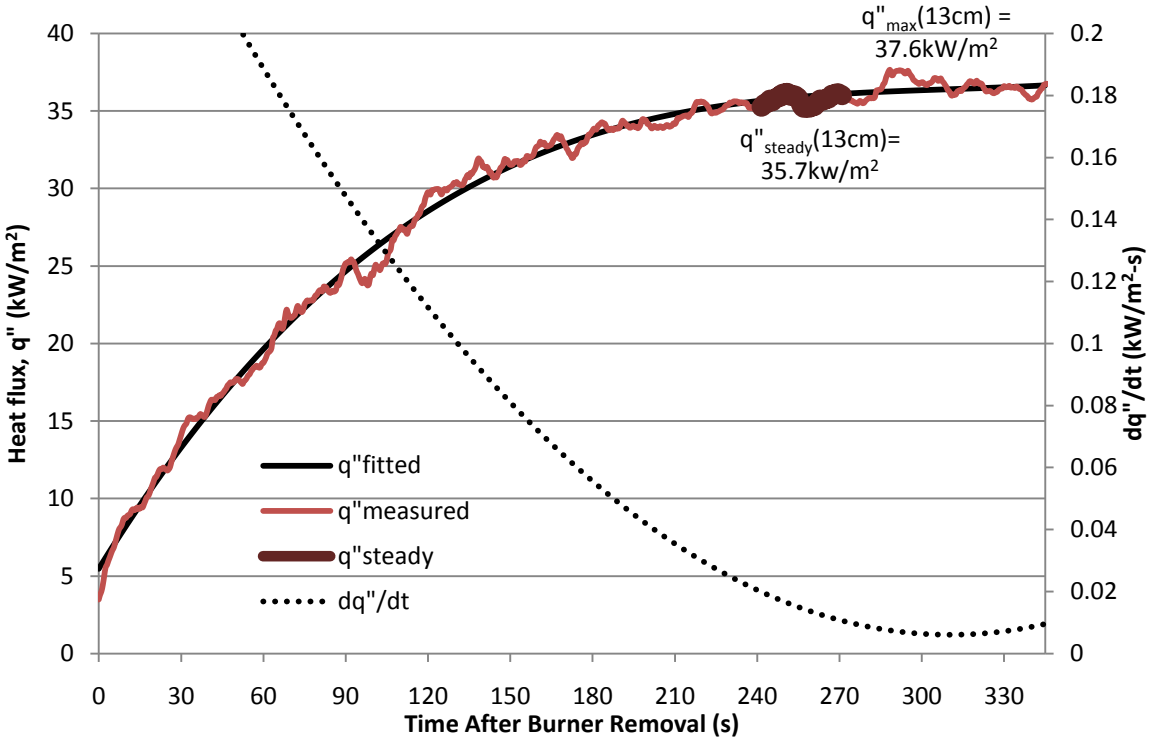

Figure 17. Determining q''_{steady}.
Shown in this figure are measured and fitted curves representing the time dependant heat flux recorded at the top of a 13 cm sample. Quasi steady state heat flux at this height, q''_{steady}, is calculated as the average heat flux recorded in the 30 s interval following the first time at which dq"/dt is less than 0.02 kW/m^2-s. This time interval is highlighted here and the calculated q''_{steady} is shown as well.

This process is repeated for all measured sample heights and, as seen in Figure 18, $\boldsymbol{q''_{steady}}$ has a spatial dependence. Steady state heat flux readings are shown to be highest near the sample's base, decrease slightly farther downstream, and then begin to average to a single representative value at larger heights. As seen here, reported values of $\boldsymbol{q''_{steady}}$ for each height closely follow the maximum heat flux recorded at the same position.

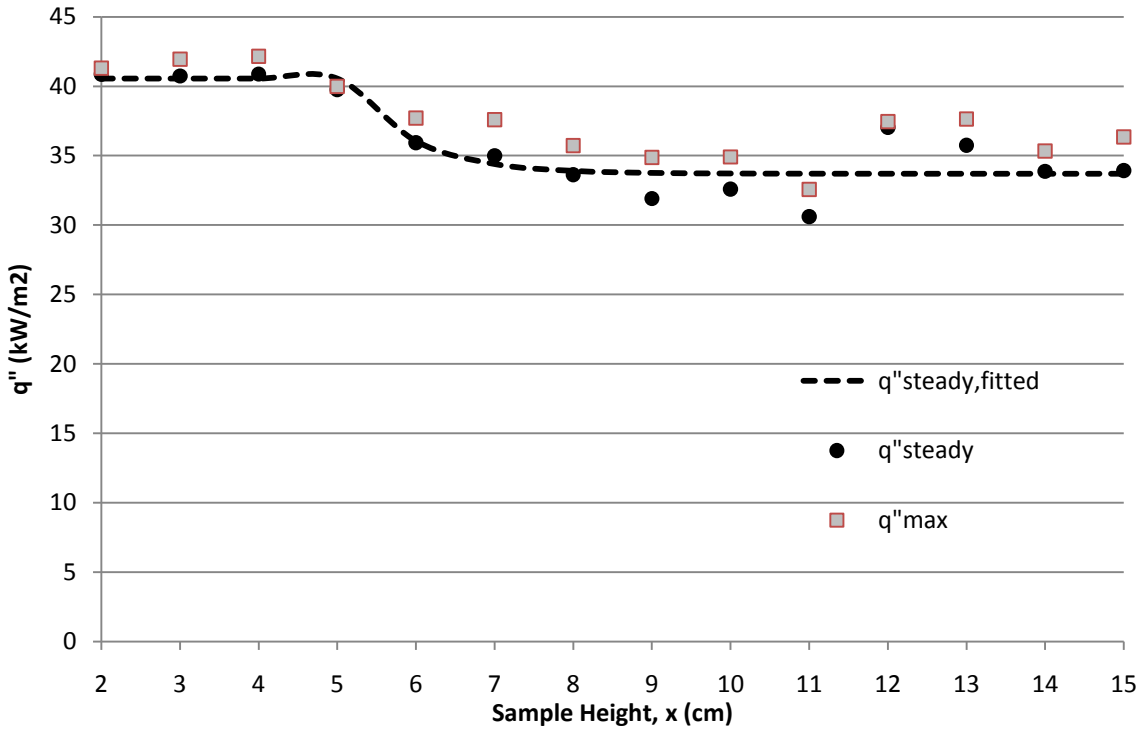

Figure 18. Measured steady state and peak heat flux readings versus sample height.

Also shown in Figure 18 are fitted values of $\boldsymbol{q}''_{\boldsymbol{steady}}$, which will be needed later in this analysis. The value of $\boldsymbol{q}''_{\boldsymbol{steady}}$ was fitted by the following function:

$$q''_{steady}\left[\frac{\mathrm{kW}}{\mathrm{m}^2}\right] = \begin{cases} f & ; \quad 2cm \le x \le 5cm \\ f - \left[y_0 + \dfrac{a_0}{\left(1 + e^{\left(-\frac{x-x_0}{b_0}\right)}\right)^{c_0}} \right] & ; \quad 6cm \le x \le 9cm \\ g & ; \quad 10cm \le x \end{cases} \tag{18}$$

With $a_0 = 6.88, \quad b_0 = -0.021cm, \quad c_0 = 0.026,$

$x_0 = 5.12cm, \; y_0 = -6.88 \qquad f = 40.6 \qquad g = 33.7$

This definition, equation (18), provides a constant heat flux to represent q''_{steady} from 2-5 cm and then uses a sigmoidal fit to capture the decrease in q''_{steady} as sample height increases from 6-9 cm. Beyond this region, this fitted value is defined as a constant, $q''_{steady} = 33.7 \frac{kW}{m^2}$ to provide a single representative value for $x > 10$ cm. This representation is consistent with the data seen in Figure 18 and it also matches Brehob et al.'s [9] observation that flame to surface heat flux remains constant for slabs up to 1.2 m in height.

Using the calculated $\boldsymbol{q''_{steady}}$ values seen in Figure 18, and the smoothed heat flux measurements, $\boldsymbol{q''_{fitted}}$, plotted in Figure 15, heat flux data taken across the height of the sample can be normalized as seen in Figure 19a, which plots $\boldsymbol{q^*} = \frac{\boldsymbol{q''_{fitted}}}{\boldsymbol{q''_{steady}}}$ versus time. This figure also presents the process by which these curves are converted to produce heat flux profiles across the height of the sample. Here, normalized heat flux ($\boldsymbol{q^*}$) profiles are resolved across the sample's surface at 30s intervals from 0-150 s after burner removal. This is done by taking heat flux readings from all heights at a specific time (vertical strips in Figure 19a) and then plotting these measurements versus sample height (individual curves in Figure 19b).

As sample mass loss rate is known at all times throughout the experiment, these $\boldsymbol{q^* \, vs. \, x}$ profiles can be expressed as a function of not only experimental time, but by sample mass loss rate at that moment as well. Several iterations of this process are displayed here for clarification; in practice, and for further detailed analysis, this process is repeated at 5 s intervals throughout the length of the experiment.

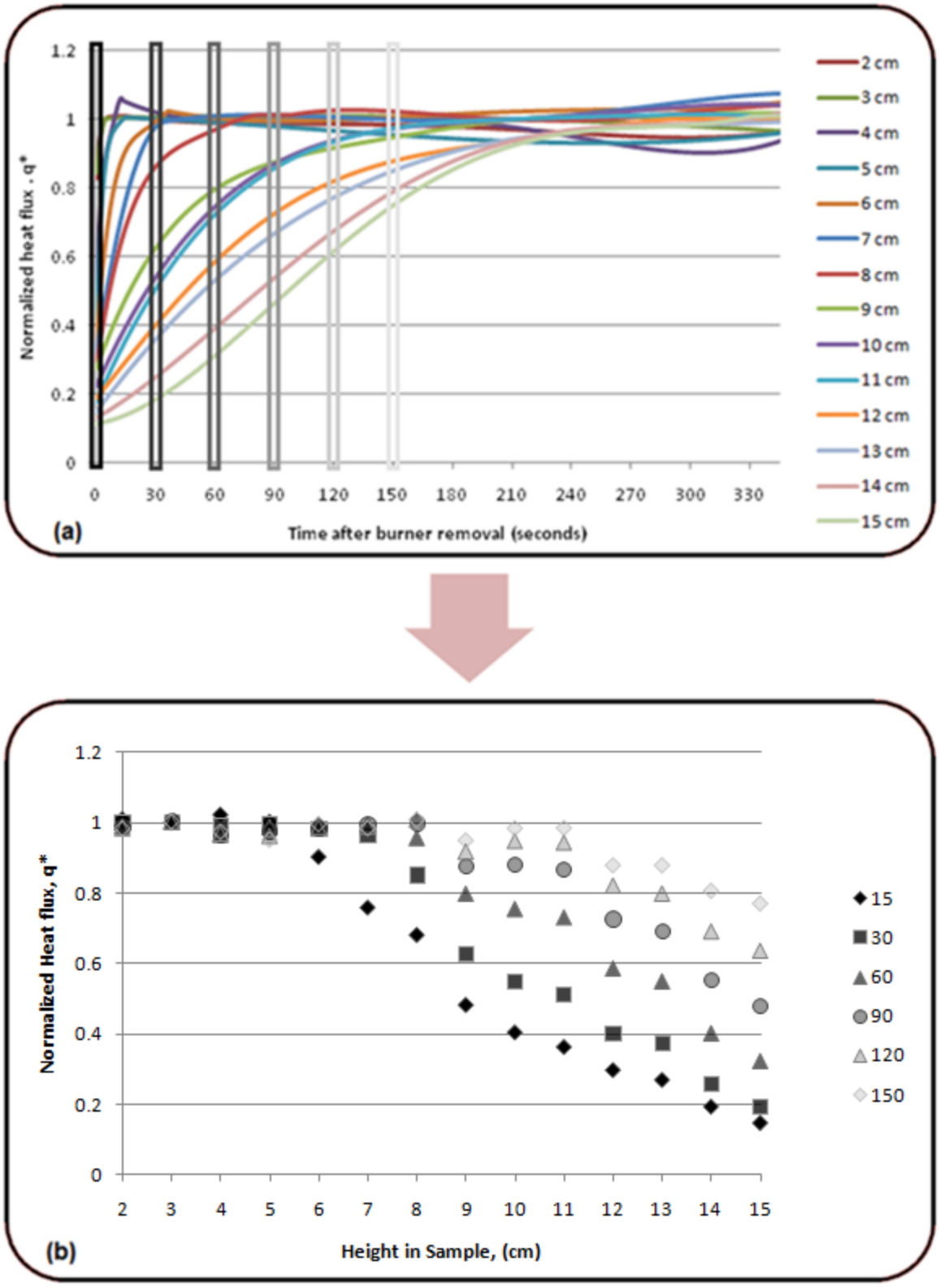

Figure 19. A visual depiction of how heat flux measurements taken at different sample heights are reformatted to produce spatially varying heat flux profiles as a function of time.

4.2 Calculating flame height as a function of sample burning rate

A common parameter needed to define the steady and decay regions of the heat flux profile predicted by equation (15) is the flame height, x_f. Here, x_f is defined as the highest position along the sample at which measured heat flux approaches close to its local quasi-steady state value; specifically where $\dot{q}''_{fitted} \geq (0.975)\left(\dot{q}''_{steady}\right)$. This flame height can be plotted versus experimental time as in Figure 20 or, by using mass loss rate measurements first presented in Figure 12, x_f can be expressed as a function of normalized mass loss rate as in Figure 21.

A linear regression of the measurements presented in Figure 21 is used to predict flame height at $x_f \geq 6$ cm as a function of sample mass loss rate, $\frac{dm'}{dt}$. This fit will be described in greater detail later in this report.

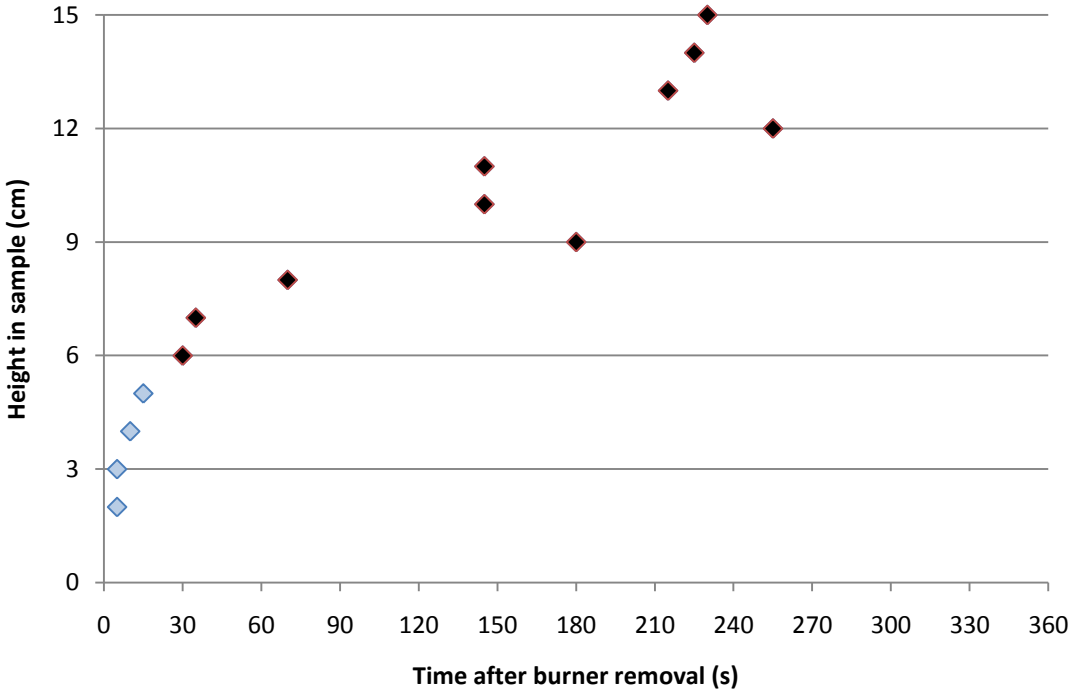

Figure 20. Flame height versus time after burner removal.

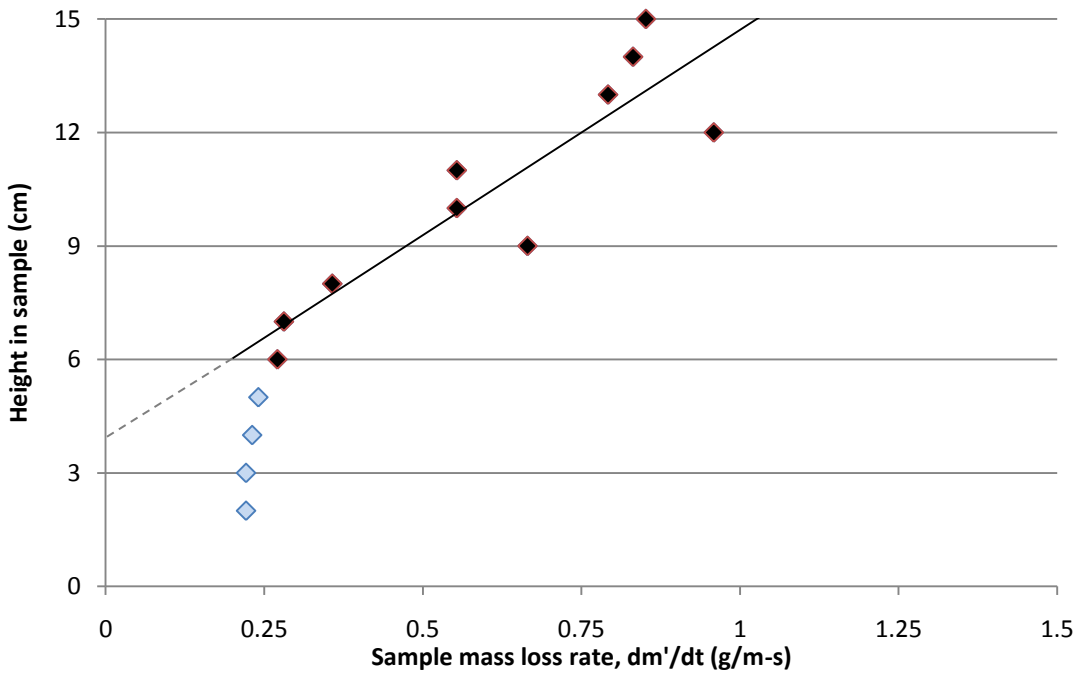

Figure 21. Flame height versus sample mass loss rate.

A cursory review of Figure 20 indicates that flame spread rate decreases from ignition until extinction. This result counters the vertical flame spread behavior expected for PMMA and so a closer review of this trend was warranted. The data presented in Figure 20 has been separated into two groups with flame heights from 6 to 15 cm highlighted as distinct from the four lowest measured heights. In effect, this separates flame spread (in this experiment) into two distinct phases- rapid initial spread and a spread that shows a linear correlation with $\frac{dm'}{dt}$.

This separation can be explained by sample burning behavior at ignition. Returning to the propane burner heat flux profile in Figure 4, consider once again the elevated heat flux at 3-3.5 cm that arises due to the burner shield's proximity to the sample. During the initial burner exposure, as the sample heats up prior to ignition, the strip closest to this shield begins heating up more rapidly than the region between 1 and 3 cm above the sample's base (Figure 22).

This second region does not ignite immediately but does begin pyrolyzing shortly after the burner is removed, briefly creating a dual flame system- one anchored to the base of the sample and another tied to this forward region. As the sample continues to burn, the two pyrolysis fronts combine into one and then, as this unified front advances, changes in flame height can be attributed directly to the sample's increasing mass loss rate. Additional analysis, presented later in this report, confirms that the shape of this heat flux profile is significantly different during this brief period after ignition as well.

Figure 22. 13 cm sample following burner exposure in a test that did not produce ignition. Note the two regions of elevated pyrolysis- one directly at the sample's base and the second, smaller region, at 3.5 cm (closest to the burner shield)

Further support for this short lived dual flame system comes from a closer review of the mass loss rate curves first presented in Figure 12. Focusing in on these measurements at sample ignition, as highlighted in Figure 23, one sees that the entire 3 cm region is pyrolyzing within 12 to 14 seconds after burner removal; after this point the mass loss rate curve of a 3 cm sample begins to deviate from those of larger samples.

For this brief period, there is rapid spread across the lowest 3 cm of the sample. It then takes 70 s longer before the unified pyrolysis front advances 2 cm as indicated by when the 5 cm $\frac{dm'}{dt}$ curve deviates from those of larger samples. The period 20 s prior to burner removal is included in this figure as well to highlight the magnitude of the sudden increase in sample mass loss rate once the region heated by the burner begins pyrolyzing.

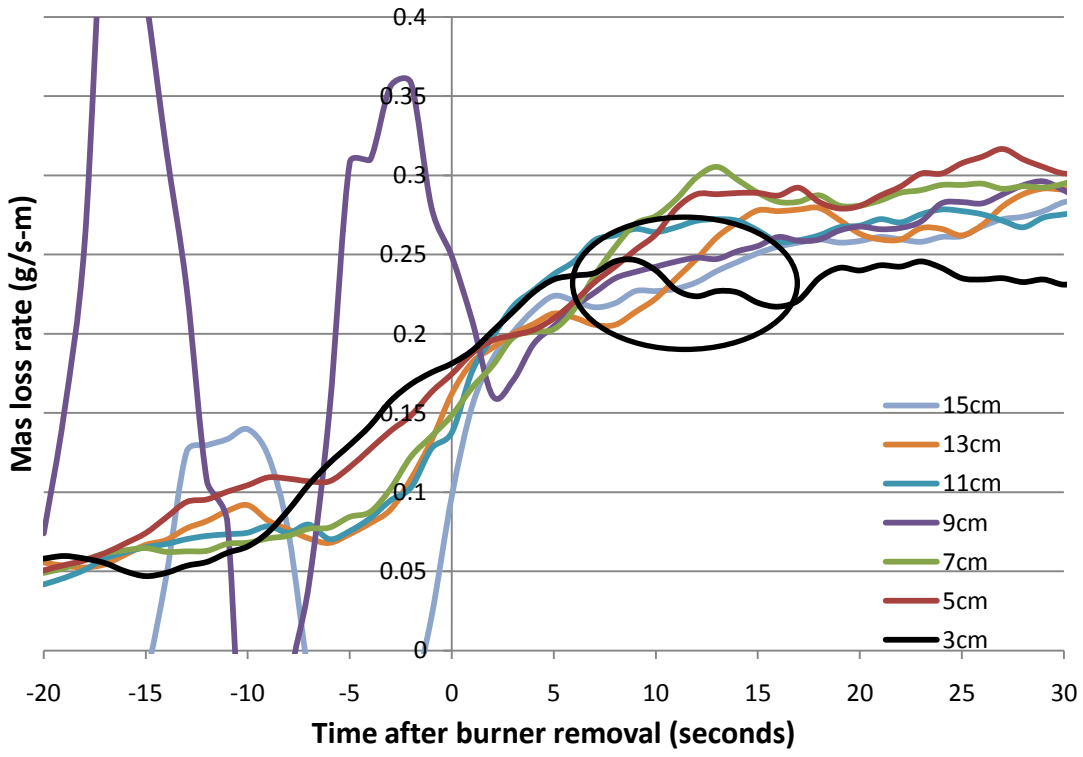

Figure 23. Sample mass loss rate at ignition.

The separation of the 3 cm $\frac{dm'}{dt}$ curve from those measured at larger heights is circled here for emphasis.

Returning to Figure 21, one notes that the first four data points, which denote very rapid flame spread, all occur at $t < 15s$; correspondingly, they should not be used in a correlation predicting flame height as a function of mass loss rate. As such, only the flame height data highlighted in Figure 21 (heights 6-15 cm, each measured at $t > 15$ s) was used to develop a correlation between x_f and $\frac{dm'}{dt}$. This correlation was linear[L] in character and is expressed below:

$$x_f = a\left(\frac{dm'}{dt}\right) + b \tag{19}$$

with $a = 1090\,\frac{cm^2 s}{g}$ and $b = 3.9cm$

A linear relation of this form is similarly presented in the literature for flames that are more laminar than turbulent in character [7][8]. As seen in Figure 24, a transition from purely laminar flow begins in this system between 7 and 10 cm above the base of the sample. The absence of extensive wrinkling and turbulent eddies suggests that this flame can be treated as primarily laminar.

[L] Figure A 18 in the appendix shows this regression alongside experimental data to provide a qualitative representation of how it fits measured values of x_f. As these individual data points did not present an overwhelmingly non-linear trend with respect to mass loss rate, a linear fit was deemed most appropriate as it is the simplest possible representation of the behavior.

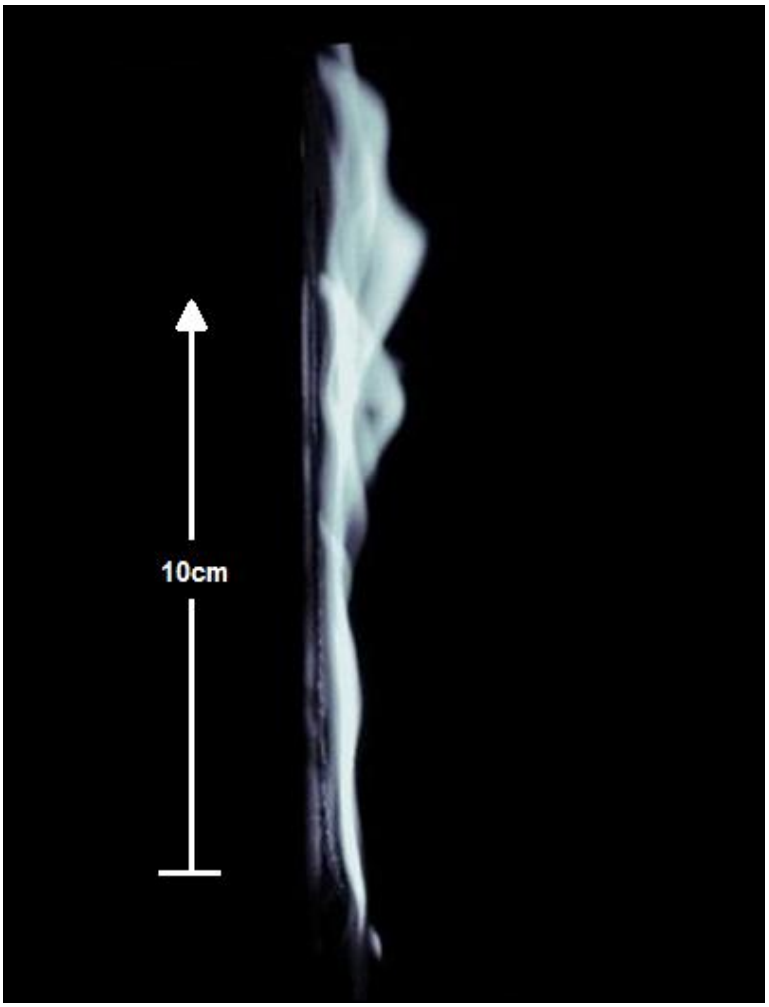

Figure 24. Composite image of four pictures taken at 1/3 s intervals, 250 s after burner removal. Note that while flamelets begin to form 7 to 10 cm above the base of the sample, the flame sheet remains fairly continuous and can be characterized as primarily laminar in nature.

Using the correlation for flame height versus mass loss rate presented as equation (19), flame to surface heat flux can be predicted for $x \leq x_f$ as equal to the local fitted values of q''_{steady}[M] . To complete the description of the heat feedback profile, an appropriate correlation describing how flame to surface heat flux varies for $x > x_f$ was developed. Again, this profile is expected to be of the form: $q'' = \alpha \left(\frac{x}{x_f}\right)^{\beta}$

[M] See appendix (Figure A5) for a description of how $q''_{steady,fitted}$ is used here.

Power law regressions were used to fit the measured decay region curves at 5 s intervals throughout the test and it became apparent that the exponential parameter of equation (15), β, showed a strong dependence on burning rate whereas as the scaling parameter, α, was nearly invariant and in fact stayed near unity (red squares and blue circles of Figure 25, respectively).

To reduce the number of parameters used to describe this system, the same analysis was repeated with a new set of power law regressions in which α was forced to remain a constant value and its minor variations with respect to $\frac{dm'}{dt}$ were accounted for by changes in β. This yielded the black data set seen in Figure 24 and ultimately the following expressions:

$$\beta = \tau + \omega\left(1 - e^{\gamma\left(\frac{dm'}{dt}\right)}\right) \tag{20}$$

with

$$\alpha = 1 \qquad \tau = -8.05 \qquad \omega = 7.8 \qquad \text{and} \qquad \gamma = -5.8\left(\frac{g}{s-m}\right)^{-1}$$

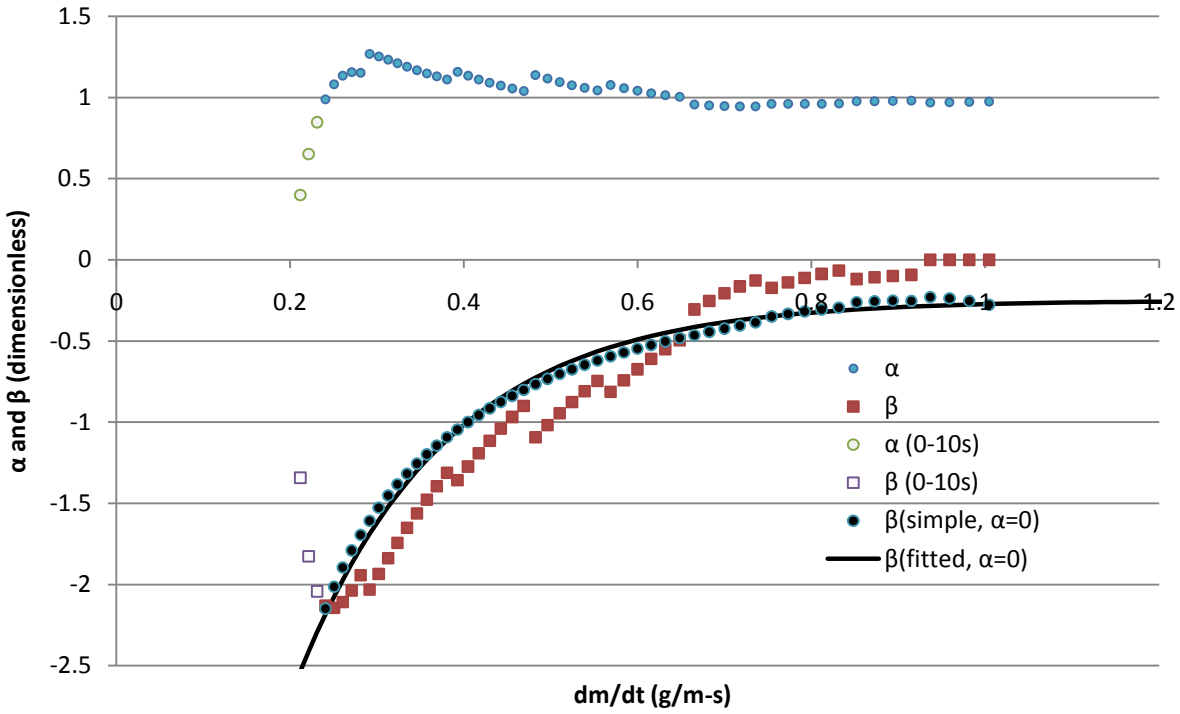

Figure 25. Dependence upon mass loss rate of parameters used to predict q^* as a function of x/x_f.

Note that α and β values calculated with data taken within the first ten seconds after burner removal are included here for completeness but not actually used for the final analysis used to predict α and β at different mass loss rates.

4.3 Calculated Heat Feedback Profile vs. Experimental Measurements

A final collection of the correlations developed during this analysis yields the following relationships[N] predicting the evolution of flame to surface heat feedback of a vertically spreading flame on PMMA as a function of sample mass loss rate:

$$q''_{HFg} = f(x, \dot{m}') = \begin{cases} q''_{steady,} \; ; & 0 \le x \le x_f \\ q''_{steady} \left(\frac{x}{x_f}\right)^{\beta} \; ; & x > x_f \end{cases} \tag{21}$$

with

$$x_f = a\left(\frac{dm'}{dt}\right) + b \tag{22}$$

$$\beta = \tau + \omega\left(1 - e^{\gamma\left(\frac{dm'}{dt}\right)}\right) \tag{23}$$

and

$$a = 1090\,\frac{cm^2 s}{g} \qquad b = 3.9cm$$

$$\tau = -8.05 \qquad \omega = 7.8 \qquad \gamma = -5.8\left(\frac{g}{s-m}\right)^{-1}$$

Using these correlations, the heat flux profile produced by a flame spreading over a 5 cm wide slab of PMMA can be predicted at a range of mass loss rates. As seen in Figure 26, these predicted values closely match measured values (smoothed +/-2.5 s running averages of all tests) obtained directly from experimental data. The predicted flame height, as indicated by the portion of each curve at which q''_{steady} has been reached,

[N]Here, q''_{steady} are fitted values of steady state heat flux that have been smoothed to reduce the scatter in q''_{steady} with respect to sample height. Refer to Figure A 5 and the subsequent discussion in the appendix for a more detailed description of how they are calculated.

corresponds with that of measured data and the shape of the decaying heat flux profile beyond x_f is well predicted too. Predicted heat fluxes in the decay region may not perfectly match those from experiments, but they are very similar. There does not appear to be any systematic error in these correlations that leads to consistent over- or under-prediction of incident heat flux.

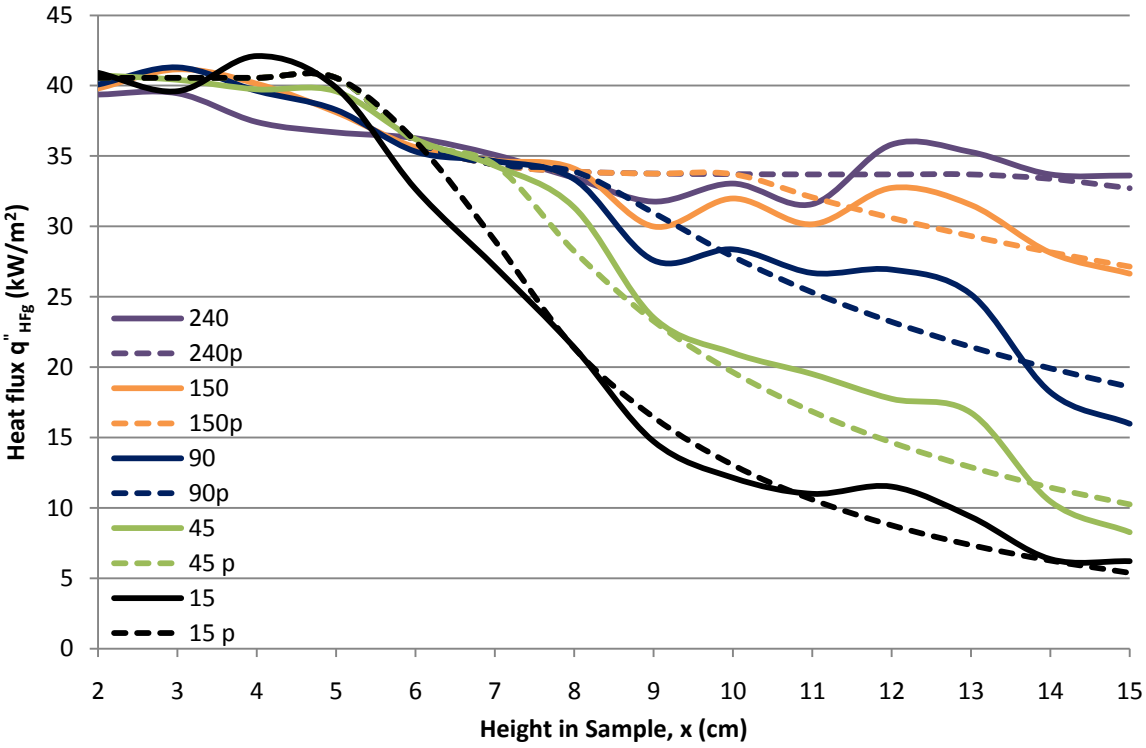

Figure 26. Measured (five second running average of experimental data, solid lines) versus predicted (calculated with equations (21**)** - (23**)**, dashed lines) heat flux profiles as a function of time after burner removal.

4.4 Predicting Flame to Polymer Heat Flux

The true benefit of this work is not only the ability to predict the cold water gauge heat flux $\left(q''_{HFg}\right)$ profile of a burning material based on its mass loss rate; while this heat flux profile is useful, predicting net heat flux into the material itself is even more valuable. To this end, predicting the dependence of parameters that accurately describe the convective and radiative components of flame to surface heat flux on mass loss rate, $\frac{dm\prime}{dt}$, is essential. Such a correlation will be of the same format as equation (21) and will allow for a more accurate description of flame to surface heat feedback regardless of the material's surface temperature. These dependencies are formulated below.

4.4.1 Radiation

Because incident radiative heat transfer to a material's surface is invariant with respect to its temperature, the radiative heat flux measured by a water cooled gauge in these experiments is equivalent to that incident upon the surrounding PMMA. For $x \leq x_f$, $q_{rad}(\%)$ and q''_{steady}, can be determined by equations (14) and (18), respectively, and combined to yield an absolute measure of the radiative heat flux at different heights in the sample equal to:

$$q''_{rad} = \left(q_{rad}(\%)\right) \bullet \left(q''_{HFg}\right) \tag{24}$$

In the absence of further knowledge, this description of q''_{rad} is extended beyond x_f accepting that it may over predict radiative heat transfer because at large x, heat transfer into the material arises solely from the thermal plume and not due to the presence of a flame directly above the material's surface. At this point, arguably, $q_{rad}(\%)$ could

be defined as zero but such a condition is not enforced. It is important to understand this concept; however, it should not have a remarkable affect on predicted net heat flux into the material as will be further discussed in the next section.

4.4.2 Convection

By quantifying radiative heat transfer in absolute terms, rather than just as a percent of total heat transfer, $\dot{q}''_{conv}$ can determined for $x < x_f$ by rearranging equation (4) into the form:

$$\dot{q}''_{conv} = \dot{q}''_{HFg} - \dot{q}''_{rad}$$

With this definition and the relationship for $\dot{q}''_{rad}$ presented as equation (24), convective heat transfer can be expressed as:

$$\dot{q}''_{conv} = \left(1 - q_{rad}(\%)\right)\dot{q}''_{steady} \tag{25}$$

This allows total steady state heat flux (where $x \leq x_f$) to be separated into its radiative and convective components and expressed in absolute terms as in Figure 27.

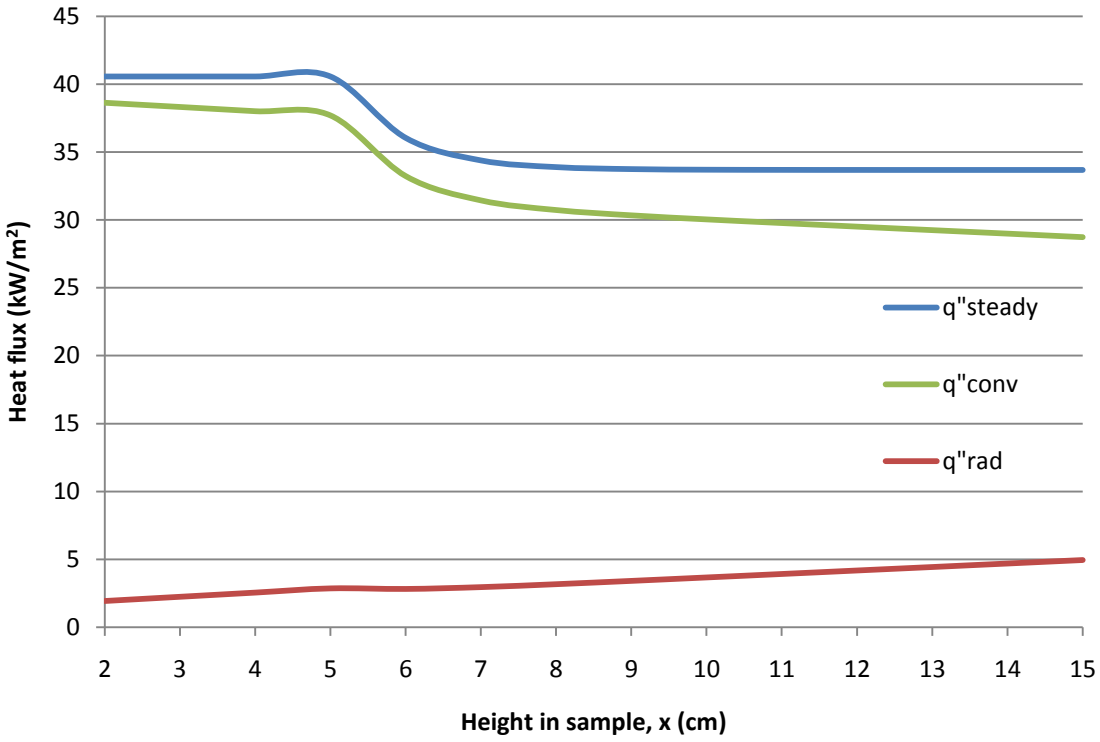

Figure 27. Quasi-steady state convective, radiative, and total heat flux versus height in sample.

The next step in this analysis is to capture this predicted convective heat flux in terms of an effective surface temperature, convective heat transfer coefficient, and a corresponding temperature profile of the boundary layer flow above the material's surface in accordance with equation (3):

$$q"_{conv} = h_{conv}(T_{fl} - T_{surf})$$

To do this, T_{fl} is needed. We are justified in choosing from a range of temperatures for this boundary layer [43] including the maximum temperature, which can be approximated for laminar diffusion flames as the stoichiometric adiabatic flame temperature[44]. A formal calculation of this temperature, $T_{fl,adiabatic}$ = 2,220°C, for Methyl Methacrylate can be found in the appendix.

This temperature is a fair approximation as it has a physical significance to this specific system and it meets the previously discussed criteria that T_{fl} must be high enough to account for the observed independence of net heat flux measurements on heat flux gauge temperature. Using the adiabatic flame temperature in this manner is further justified as it has been noted by De Ris [12] to strongly influence flame spread rate.

The convective heat transfer coefficient for this system can be calculated by reorganizing equation (3), as suggested by Diller [45] for non reacting systems, into:

$$h = \frac{q''_{conv}}{T_{fl} - T_{surf}} \tag{26}$$

Here, using $T_{fl} = 2{,}220℃$, q''_{conv} as determined from equation (25), and $T_{surf} = T_{HFg} = 18℃$ (average heat flux gauge temperature during testing) the resulting heat transfer coefficient is found at each sample height.[O] Figure 28 plots the results of this calculation at each height in the sample that was tested along with theoretical results calculated based on the thermal boundary layer approximation[23]. One immediately notes how similar these two approximations are, a trend that helps to further support the method used here for the deconvolution of total heat flux measurements into its convective and radiative components.

[O] See Appendix for representative calculations and the explicit formulas used here to calculate experimental and theoretical values of h.

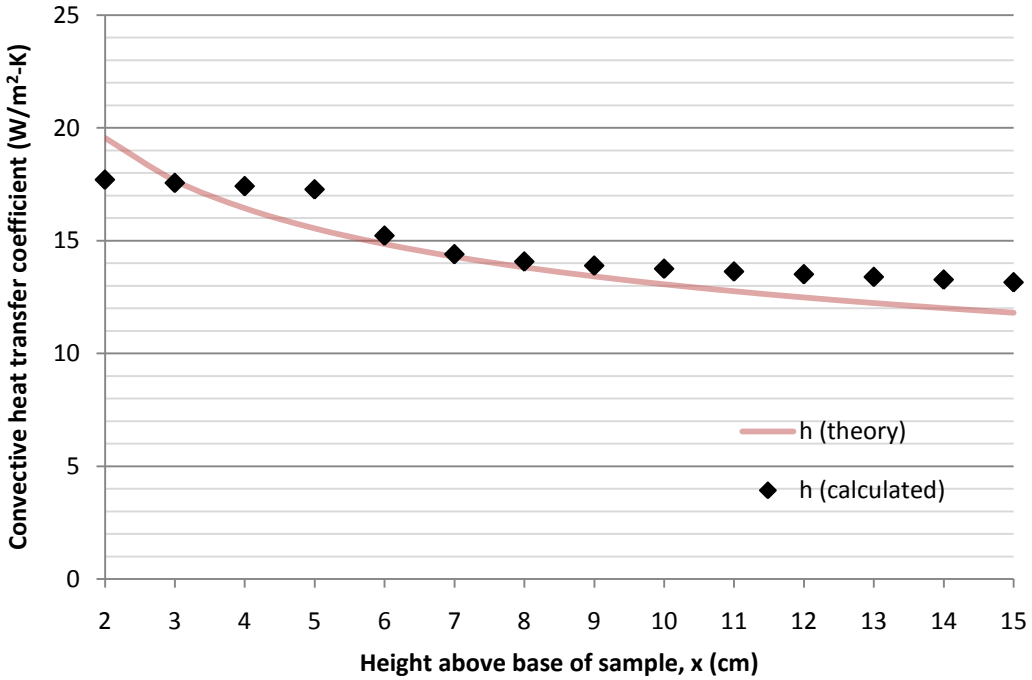

Figure 28. Calculated convective heat transfer coefficient across the sample.

It is clear that both the calculated and theoretical predictions of the convective heat transfer coefficient decrease at larger sample heights. Returning to the thermal boundary layer approximation[23], the convective heat transfer coefficient is inversely proportional to flame standoff distance $\left(h = \frac{2k}{\delta}\right)$ which itself increases with height along the sample $\left(\delta_{fl} \propto x^{1/4}\right)$ so h in turn is predicted to decrease slightly with larger x. In Figure 29, a side view of this flame system, this increasing standoff distance (as indicated by the flame thickness) is clearly visible.

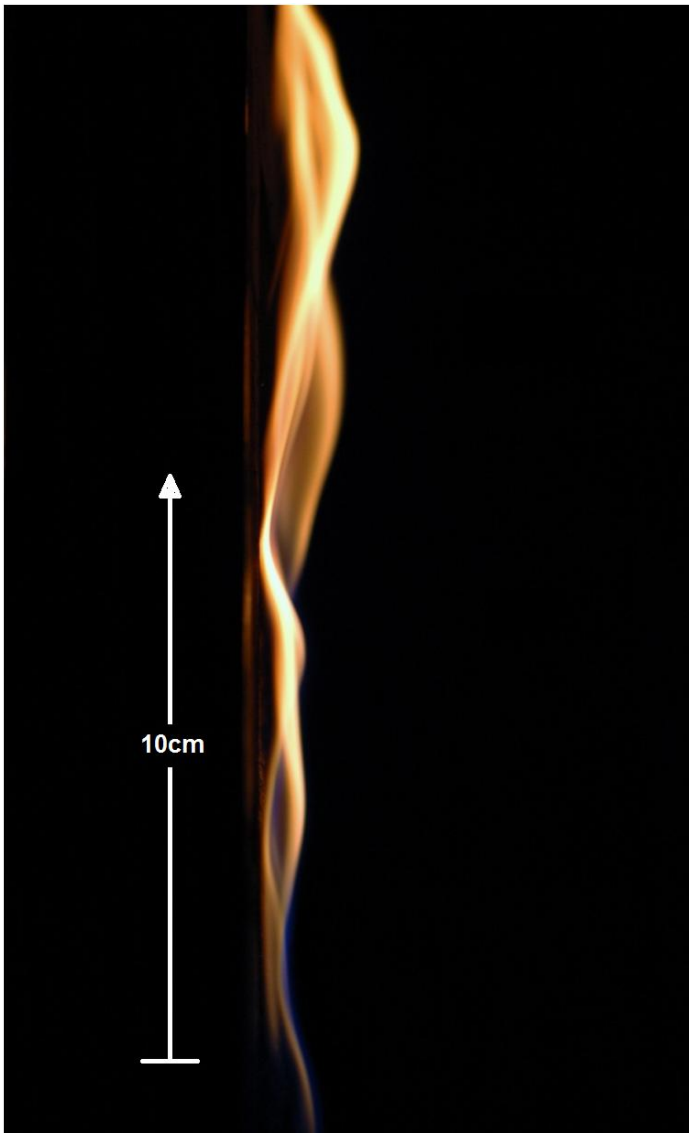

Figure 29. Side view of a 10 cm sample 300 s after burner removal showing full flame spread above the height of the sample.
Note how flame standoff distance increases with height and how luminous intensity is augmented as well. At its base, the flame is nearly transparent and shades of blue become clearly visible whereas the top of the sample (where $\boldsymbol{q_{rad}}(\%)$ is greatest) the flame is brightest.

Qualitatively, experimentally derived values of h decrease with larger x similarly as theoretical predictions. Returning to equation (26), it should be noted that at steady state, T_{fl} and T_{surf} are treated as constant and independent of x. Heat flux, $\dot{q}''_{steady}$, at heights greater than 10 cm is also treated as constant [9]; however, because $q_{rad}(\%)$

increases linearly with respect to x (equation (14)), q''_{conv} (and hence h) is predicted to decrease linearly with sample height.

Using these formulas, experimental results can be extrapolated to predict the convective heat transfer coefficient beyond $x = 15$ cm as seen in Figure 30 . Also plotted in this figure is the heat transfer coefficient predicted by the TBL approximation [23]. As seen here, the heat transfer coefficients predicted by each of the two methods remain within ten percent of one another for 2 cm $< x <$ 70 cm; beyond this height, the two predicted values begin to notably diverge.

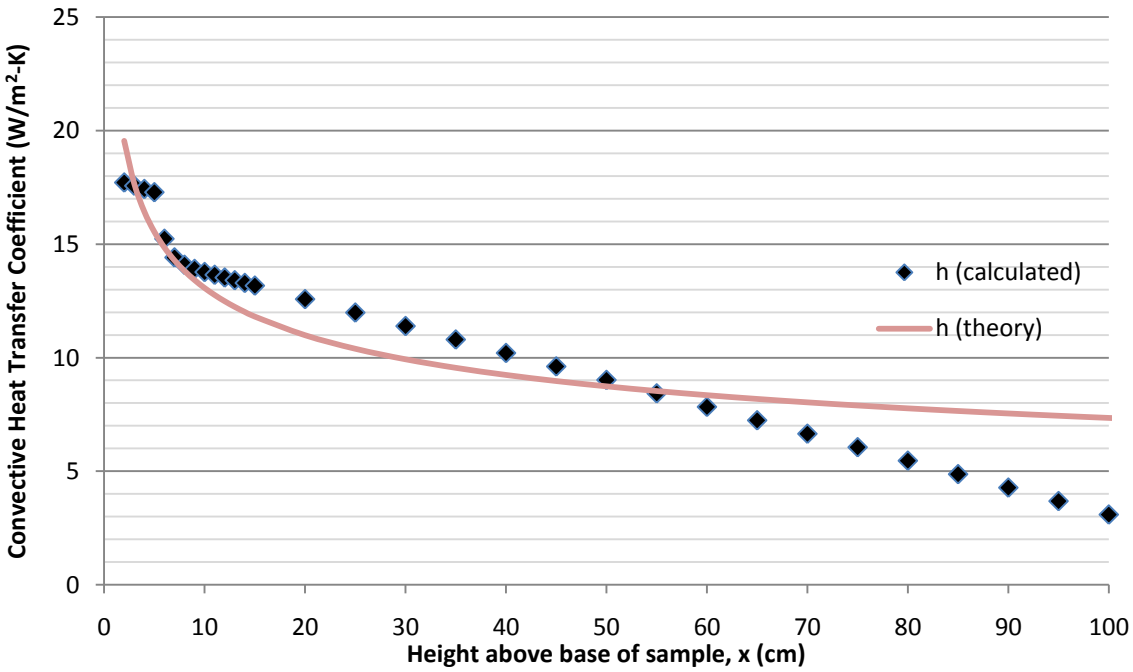

Figure 30. Calculated convective heat transfer coefficient from 0 to 1 m above the base of the sample.

A likely source for the discrepancy between the two predictions is the assumption (used to determine h experimentally) that T_{fl} remains constant and equal to $T_{fl,adiabatic}$ at all heights, x, where q''_{steady} is reached. With large, turbulent flames, greater volumes of (comparatively cooler) air are entrained into the plume and thus

forcing $T_{fl} = 2{,}220℃$ could overestimate the temperature gradient, $\Delta T = T_{fl} - T_{surf}$. As this temperature gradient drives convective heat transfer, this would in turn result in an over prediction of q''_{conv} to warmer regions of the sample, an error that must be mitigated by allowing h (experimental) to rapidly decrease with increasing x.

It should also be noted that formulas used to calculate h from experimental data are determined from measurements associated with quasi-steady state burning, when the flame is fully established above the heat flux gauge, 2 - 15 cm above the sample's base. These formulas are treated as valid for larger x because of how well they match theoretical predictions (Figure 30).

Farther downstream in the system, well beyond x_f, heat transfer into the material arises solely from the thermal plume and not due to the presence of a flame directly above the material's surface. The experimentally determined heat transfer coefficient is assumed valid in this region as well because, once again, it is comparable to the value predicted by the thermal boundary layer theory, a similarly non-reacting flow.

Ultimately, such minor discrepancies will not have a profound impact on predicting net heat transfer to higher regions of the sample. Consider, for example, the absolute value of flame to surface heat flux far downstream of $x_f -$ at this large x/x_f, q''_{HFg} is significantly below its steady state value. As such, on an absolute scale, perfectly separating this heat flux into its radiative and convective components is not essential to acceptably predicting q''_{net}.

Moreover, at large x/x_f, both the sample and the heat flux gauge temperatures are near ambient $\left(T_{surf} \approx T_{HFg} \approx T_\infty\right)$ so how total heat flux is separated into its convective and radiative components is not critical- the accuracy of this deconvolution is crucial

only when the material's surface temperature is significantly greater than that of the heat flux gauge, or ambient, temperature.

Ultimately, coupling the definitions of q''_{conv} (equation (25)) and h (equation (26)) allows for the calculation of the effective flame temperature, T_{fl}, at different heights above the sample base, as a function of burning rate:

$$\boldsymbol{T_{fl} = \left(\frac{q''_{HFg}}{q''_{steady}}\right)\left(T_{fl,adiabatic} - T_{HFg}\right) + T_{HFg}} \tag{27}$$

The result of the above definition of T_{fl} in this system is shown in Figure 31.

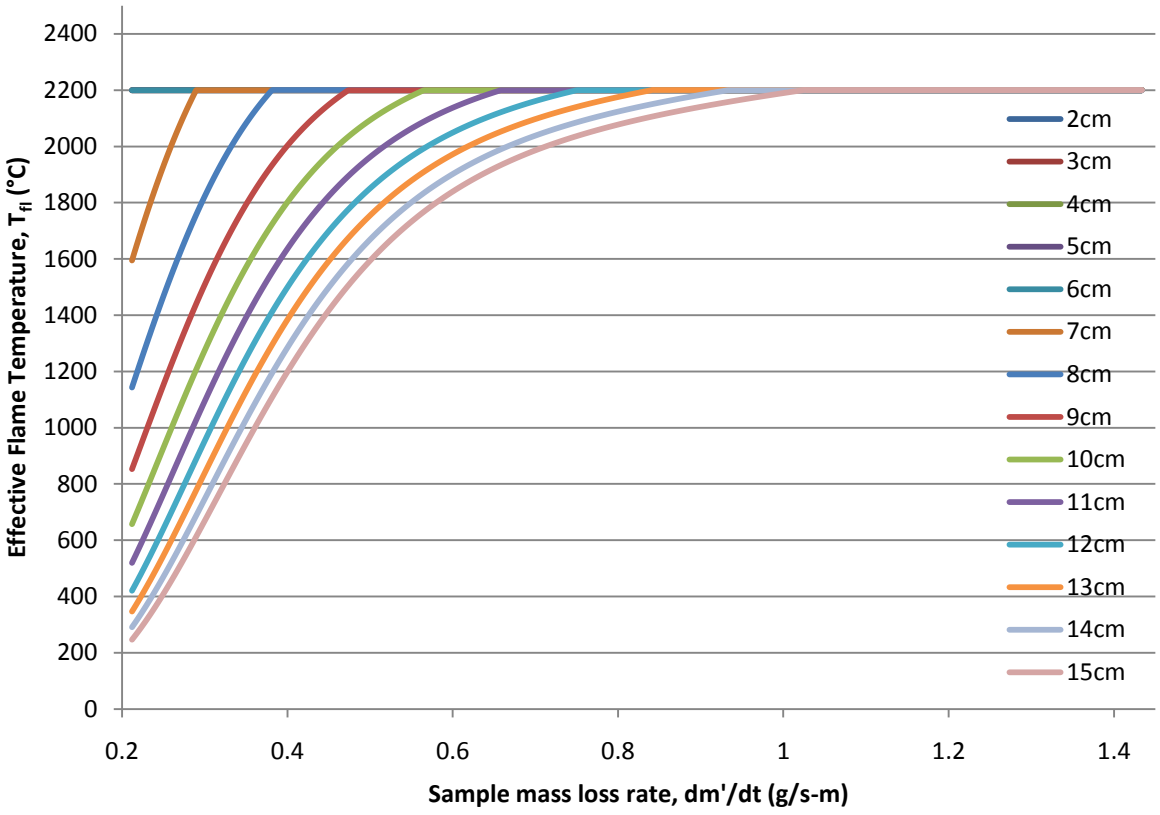

Figure 31. Predicted flame temperature versus sample burning rate as a function of height above sample base.

5. Secondary Effects

5.1 Blowing Effect

It could be argued that the results in Figure 28 suggest that this system could be simplified such that flame heat flux is entirely described by the thermal boundary layer approximation. While this is a useful way to simply visualize the system, it clearly neglects the effects of radiative heat transfer, which, while small, are not negligible. Additionally, with this simplified theory, there is no impetus for the horizontal (normal to the sample's face) component of flow velocity that is induced when products of pyrolysis are expelled outward from the sample as it burns.

Near the sample's base, the flame standoff distance, δ_f, grows noticeably larger from ignition to extinction. The change in δ_f is indicated by the thickening of the flame at the bottom of samples during experiments (Figure 32). Correspondingly, local burning rate, $\frac{dm"}{dt}$, increases during this period as well, which suggests that the horizontal expulsion of products of pyrolysis causes a blowing effect that alters the flame behavior.

At low local burning rates, this blowing effect is minor; however, as the sample continues to burn during the experiment, $\frac{dm"}{dt}$ from $0 \leq x \leq x_p$ continuously increases resulting in a correspondingly higher horizontal, or blowing, velocity. This effect is small in higher regions of the sample where $\frac{dm"}{dt}$ remains reasonably low throughout the test and its impacts are harder to distinguish from (and are effectively masked by) the turbulent characteristics of the flame.

A closer review of the heat flux measurements obtained in this study reveals that this thickening of the flame has a quantifiable impact on flame to surface heat feedback. Specifically, 300-345 s after burner removal, average heat flux measurements at 2-5 cm above the base of the sample decrease by 6% as compared to their reported quasi steady state values. This decrease occurs as average mass flux for that region roughly doubles from ~7 to 13 g/s-m^2. This effect will be accounted for in future work; however, for this report, it is simply mentioned to explain why, near the base of the sample (at large $\frac{dm'}{dt}$), measured heat flux may be lower than predicted values.

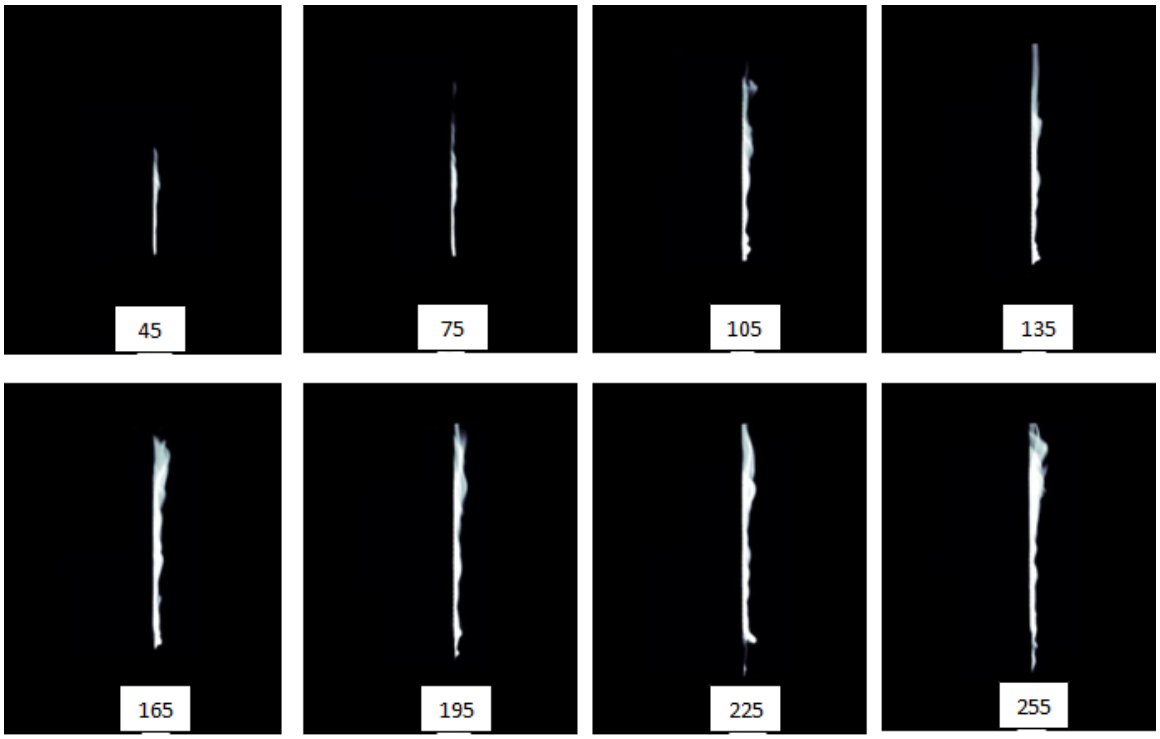

Figure 32. Side view images of flame spread along a 10 cm sample taken at 30 s intervals from 45 s until 255 s after sample ignition.
These images (tagged with time, s, after burner removal) are created as composites of multiple (4-5) images taken at 1/3s intervals around each time shown. Individual pictures are converted to grayscale and averaged together to produce a more representative image of the flame's profile at each time. When the flame is fully established across the sample, the flame standoff distance increases farther downstream in the flow (from the base to the top of the sample). Note that as time progresses, not only does the flame grow in length but the flame to surface standoff distance increases as well.

5.2 Effect of Finite Sample width

In the literature review presented earlier in this report, it was shown that narrow sample width can reduce the rate of flame spread across a material's surface. While these effects become recognizable for sample widths below 20-30 cm, Pizzo et al.[20] showed that for 30 cm tall samples, burning rate, when normalized by sample width, is nearly identical for samples of widths between 5 and 20 cm. Their findings indicate that the correlations produced here predicting flame heat flux as a function of mass loss rate, $\frac{dm'}{dt}$, are applicable not only for 5 cm wide samples, but for wider slabs as well.

At narrower widths (specifically, $w = 2.5cm$) however, Pizzo et al. [20] reported a distinctly different burning behavior as measured by $\frac{dm'}{dt}$. On such narrow samples, it took roughly twice as long as 5-20 cm wide slabs for $\frac{dm'}{dt}$ to reach a peak, quasi steady value. Furthermore this quasi-steady normalized mass loss rate was ~40% lower for 2.5 cm wide samples than the value recorded during tests of their wider counterparts. Together, these results suggest that flame spread rate and normalized burning rate decrease on sufficiently narrow slabs.

In our experiments, the evolution of heat feedback at the tops of 5, 10, and 15 cm tall, 2.5 cm wide samples was studied, the results of which can be seen in Figures 32-34). These measurements indicate that there is not a significant decrease in $\dot{q}''_{steady}$ as slab width decreases to 2.5 cm. Nonetheless, there is an increasing delay time before quasi-steady state heat fluxes were measured at the tops of taller narrow samples (as compared

to the delay needed for their 5 cm wide counterparts)- a clear indication of a lower flame spread rate.

Given the similarity in the peak heat flux values measured during tests on samples of both widths, this suggests that, similarly as reported in the literature [20] for 30 cm tall samples, the flame (or perhaps the thermal plume) structure is shortened or altered in some way in flame spread across very narrow polymer slabs.

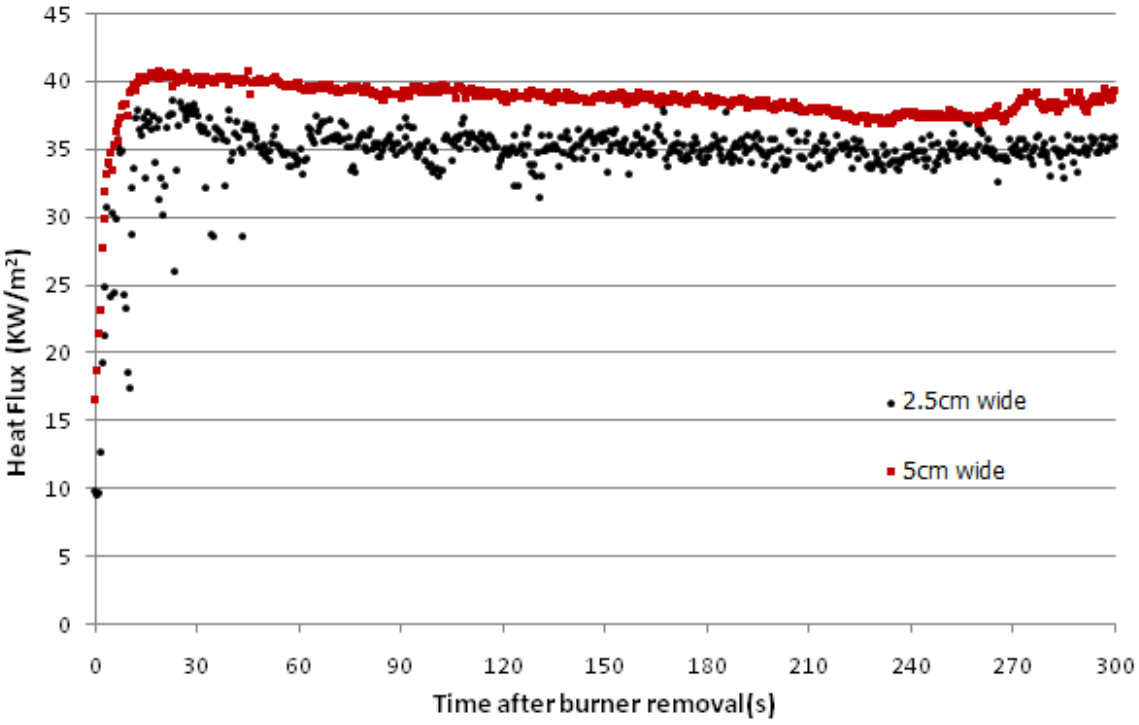

Figure 33. Comparison of 2.5 cm and 5 cm wide heat flux measurements on 5 cm tall samples.

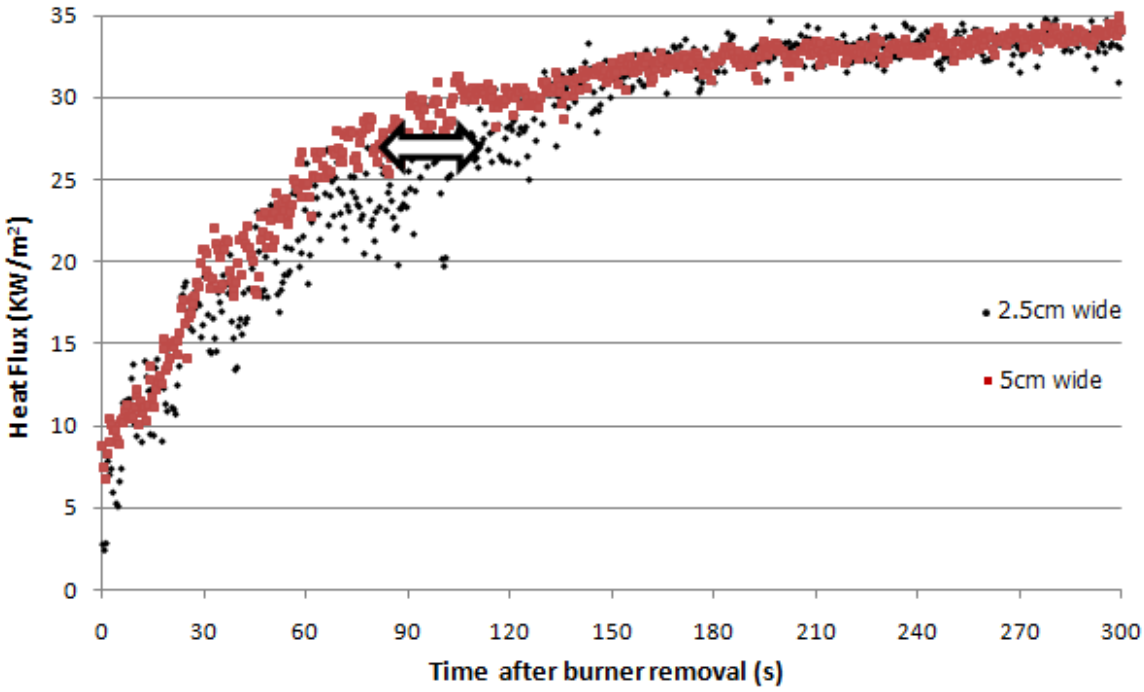

Figure 34. Comparison of 2.5 cm and 5 cm wide heat flux measurements on 10 cm tall samples.

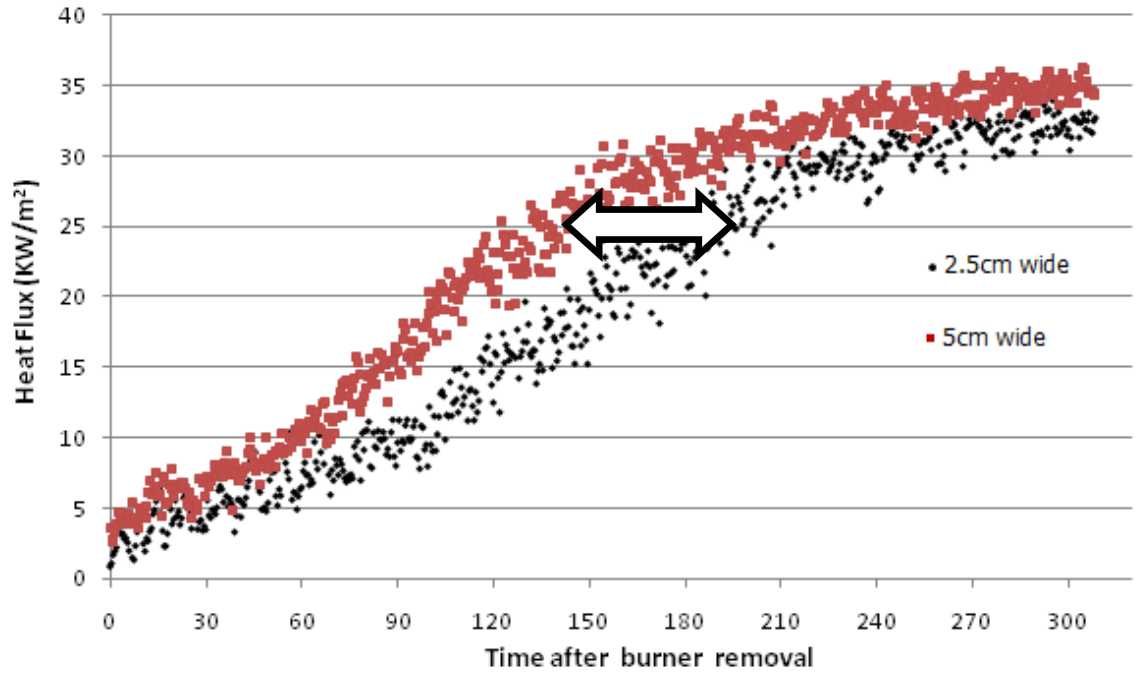

Figure 35. Comparison of 2.5 cm and 5 cm wide heat flux measurements on 15 cm tall samples.

6. Conclusions

- A test apparatus capable of supporting samples in the necessary orientation for repeatable studies of unrestricted, 1-dimensional vertical flame spread with limited heat losses has been designed and built.

- A well defined test method has been developed to study the evolving heat feedback profile across small (<5 cm wide, 15 cm tall) pyrolyzable solids during vertical flame spread; incident heat flux has been well measured at 1 cm intervals between 2 and 15 cm.

- Sample mass loss rate, $\frac{dm'}{dt}$, has been well characterized for 5 cm wide samples of heights in 2 cm intervals from 3 to 15 cm.

- An effective heat feedback profile (from flame to cold gauge) has been measured for 15 cm tall PMMA samples.

- Correlations expressed solely as a function of mass loss rate, $\frac{dm\prime}{dt}$, and above the sample base have been developed to predict the flame height and heat feedback profile of a flame spreading vertically across small slabs of PMMA.

- Flame to surface heat transfer is mostly convective across the full length of 15 cm samples. Radiative fraction $\left(q_{rad}(\%) = \frac{q''_{rad}}{q''_{tot}}\right)$was measured to increase from 5% at the sample's base to 18% percent at its top.

- Flame heat flux was found to increase $(\sim 10\%)$ near the base of the flame where it is thinnest and more purely laminar in nature. As local mass loss rate increases, however, flame standoff distance increases resulting in a slightly lower total heat flux; this effect was distinguishable closest to the base of the sample where δ_f is thinnest, ~0.8–1.2 cm.

- Flame spread rate was found to decrease for narrower (2.5 cm wide) samples. Total heat flux measured in these experiments was unchanged suggesting that this was a result of changes in the flame or plume structure.

- Multiple plastics have been tested to determine which ones are directly suitable for similar testing and how to overcome the various impediments to flame spread that others can pose in order to further this research.

- Flame to surface heat feedback, q''_{net}, can be predicted solely as a function of sample burning rate with the following correlations by the process outlined below.

$$q''_{net} = h_{conv}(T_{fl} - T_{Surf}) + (1 - r)q''_{rad} - q''_{rerad} \tag{9}$$

$$q''_{HFg} = h_{conv}(T_{fl} - T_{Surf}) + q''_{rad} \tag{8}$$

$$q''_{HFg} = f\left(x, \frac{dm'}{dt}\right) = \begin{cases} q''_{steady}; & 0 \le x \le x_f \\ q''_{steady}\left(\frac{x}{x_f}\right)^{\beta}; & x > x_f \end{cases} \tag{21}$$

$$q''_{rerad} = \sigma(1 - r)\left(T^4_{surf}\right) \tag{6}$$

$$q''_{steady}\left[\frac{kW}{m^2}\right]\begin{cases} f & ; \quad 2cm \le x \le 5cm \\ f - \left[y_0 + \frac{a_0}{\left(1 + e^{\left(-\frac{x - x_0}{b_0}\right)}\right)^{c_0}}\right] & ; \quad 6cm \le x \le 9cm \\ g & ; \quad 10cm \le x \end{cases} \tag{18}$$

$$x_f = a\left(\frac{d\dot{m}'}{dt}\right) + b \tag{19}$$

$$\beta = \tau + \omega\left(1 - e^{\gamma\left(\frac{dm'}{dt}\right)}\right) \tag{20}$$

$$q_{rad}(\%)\begin{cases} cx + d & ; \quad x \le 1m \\ e & ; \quad x > 1m \end{cases} \tag{14}$$

$$h = \frac{q''_{steady}\left(1 - q_{rad}(\%)\right)}{T_{fl,adibatic} - T_{HFg}} \tag{26}$$

Table 2. Values of experimental parameters used to predict flame to surface heat flux.

Parameter	alue	Units
a	1090	$\frac{cm^2 s}{g}$
b	3.9	cm
c	0.77	cm^{-1}
d	3.2	-
e	80	-
f	40.6	$\frac{kW}{m^2}$
g	33.7	$\frac{kW}{m^2}$
$T_{fl,adiabatic}$	2,220	℃
T_{HFg}	18	℃
a_0	6.88	-
b_0	-0.021	cm
c_0	0.026	-
x_0	5.12	cm
y_0	-6.88	-
γ	-5.8	$\left(\frac{g}{s-m}\right)^{-1}$
τ	-8.05	-
ω	7.8	-

The ultimate goal of this study is to be able to predict the net heat flux to a flaming sample's surface (q''_{net}) solely as a function of sample mass loss rate, $\frac{dm'}{dt}$. In the future, this heat feedback profile will be coupled with a solid phase combustion solver, such as Thermakin, which in turn will be able to predict material response (pyrolysis and burning rate) given this heat feedback and appropriate material properties. The new model should then be able to predict flame spread and burning rate for different pyrolyzable solids.

Net flame to surface heat flux, q''_{net}, can be determined as follows solely by the inputs of x (height above sample base), $\frac{dm'}{dt}$ (sample burning rate), and T_{surf} (material surface temperature at that height, x). First, q''_{steady} and x_f are defined by equations (18) and (19), respectively. Net heat flux into the sample can then be determined directly with these input quantities by reorganizing the above formulas into the single equation:

$$\begin{aligned} q''_{net} = \quad & (1-(cx+d))\left(q''_{steady} - \frac{(q''_{steady})(T_{surf}-T_{HFg})}{(T_{fl,adiabatic}-T_{HFg})}\right) \\ + \quad & (1-r)(cx+d)\left(q''_{steady}\right) - \sigma(1-r)(T_{surf})^4 \end{aligned} \tag{28}$$

Here, q''_{net}, is expressed for heights $x < 1.0m$ where $x < x_f$; q''_{net} is explicitly defined for $x > x_f$ and $x > 1.0m$ in the appendix.

7. Appendix

7.1 Sample Information

	2cm	3cm	4cm	5cm	6cm
Sample Mass (g)	6.37 +/- 0.19	9.39 +/- 0.2	12.24 +/- 0.18	15.55 +/- 0.25	18.40 +/- 0.51
Glue Mass (g)	0.41 +/- 0.24	0.74 +/- 0.3	1.18 +/- 0.14	1.58 +/- 0.29	1.73 +/- 0.28
Before Burn (g)	26.64 +/- 0.69	32.26 +/- 1.07	38.16 +/- 0.48	44.10 +/- 1.35	49.75 +/- 1.36
After Burn (g)	22.40 +/- 1.55	26.93 +/- 1.92	30.91 +/- 0.69	35.95 +/- 1.36	41.38 +/- 1.03
Drip Mass (g)	0	0.09 +/- 0.07	0.12 +/- 0.03	0.27 +/- 0.12	0.36 +/- 0.13
First drip time	-	5:53 +/- 0:37	6:08 +/- 0:02	5:38 +/- 0:23	5:45 +/- 0:06

	7cm	8cm	9cm	10cm	11cm
Sample Mass	21.85 +/- 0.29	24.33 +/- 2.1	28.10 +/- 0.15	31.25 +/- 0.35	34.25 +/- 0.34
Glue Mass	2.35 +/- 0.32	3.03 +/- 0.47	2.61 +/- 0.75	3.23 +/- 0.81	3.22 +/- 0.82
Before Burn	57.25 +/- 1.92	62.71 +/- 1.57	66.90 +/- 1.08	74.55 +/- 1.52	80.57 +/- 2.16
After Burn	47.40 +/- 2.20	51.47 +/- 2.15	55.90 +/- 1.06	64.16 +/- 3.33	68.10 +/- 1.70
Drip Mass	0.52 +/- 0.18	0.81 +/- 0.41	0.80 +/- 0.17	1.25 +/- 0.72	1.23 +/- 0.93
First drip time	5:22 +/- 0:12	5:15 +/- 0:27	5:10 +/- 0:16	5:10 +/- 0:16	5:13 +/- 0:19

	12cm	13cm	14cm	15cm
Sample Mass	37.33 +/- 0.36	40.40 +/- 0.41	43.93 +/- 0.27	46.34 +/- 0.64
Glue Mass	3.61 +/- 0.60	3.97 +/- 1.36	4.68 +/- 0.29	4.55 +/- 1.62
Before Burn	85.69 +/- 1.25	92.15 +/- 2.40	97.66 +/- 0.40	103.17 +/- 2.01
After Burn	73.08 +/- 1.87	72.17 +/- 24.27	85.34 +/- 0.79	89.02 +/- 3.32
Drip Mass	1.20 +/- 0.72	1.45 +/- 0.83	1.12 +/- 0.39	1.39 +/- 0.94
First drip time	5:24 +/- 0:18	5:19 +/- 0:14	5:20 +/- 0:19	5:11 +/- 0:20

7.2 Visualizing the time intervals used to calculate maximum heat flux at each sample height

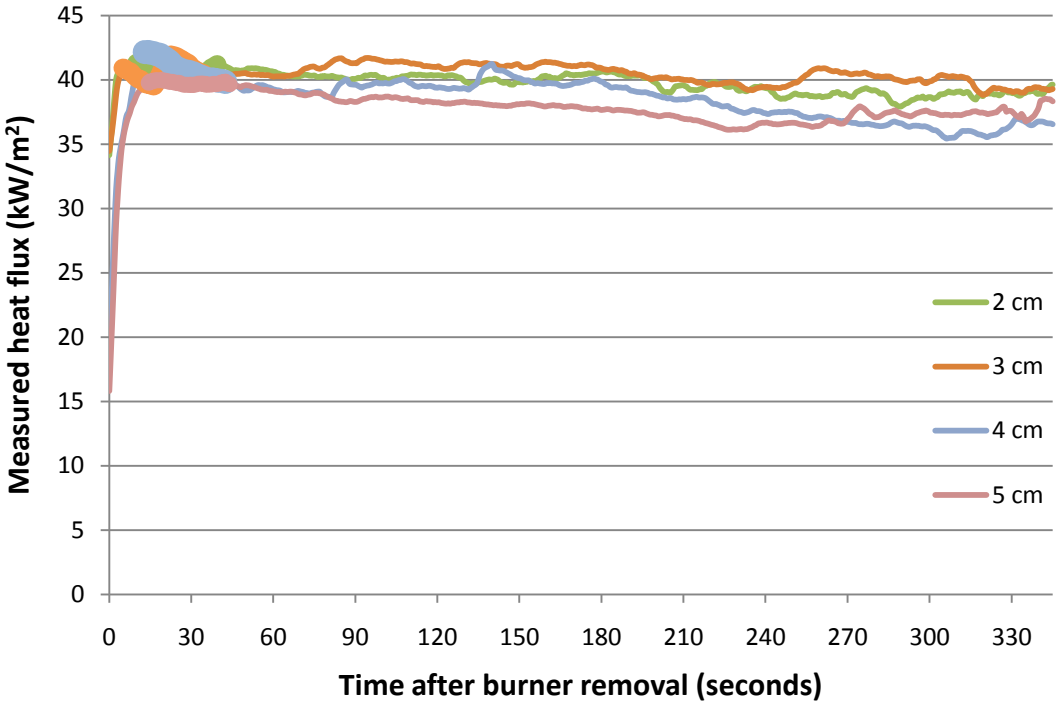

Figure A 1. Time interval used to calculate q''_{steady} for samples 2-5 cm in height.

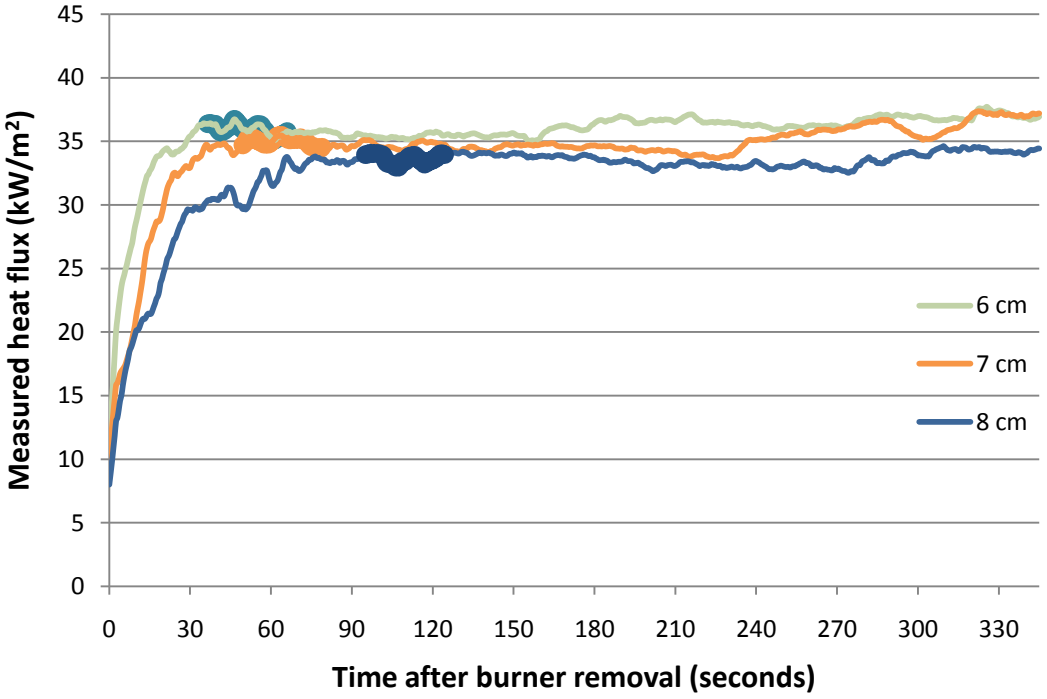

Figure A 2. Time interval used to calculate q''_{steady} for samples 6-8 cm in height.

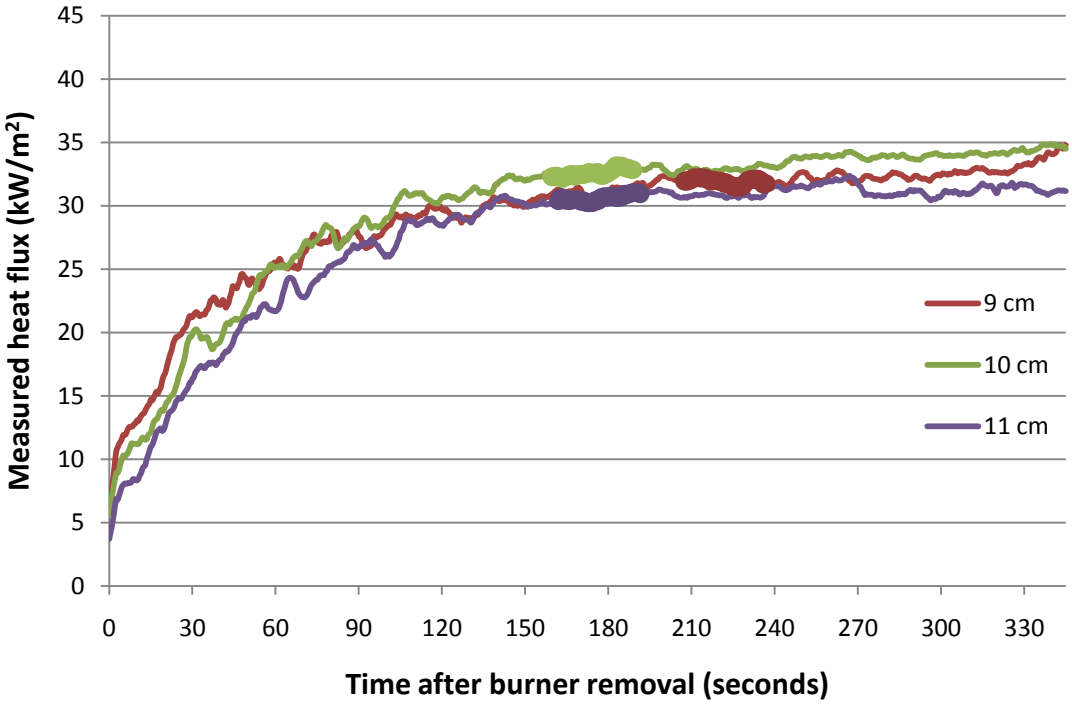

Figure A 3. Time interval used to calculate q"$_{steady}$ for samples 9-11 cm in height.

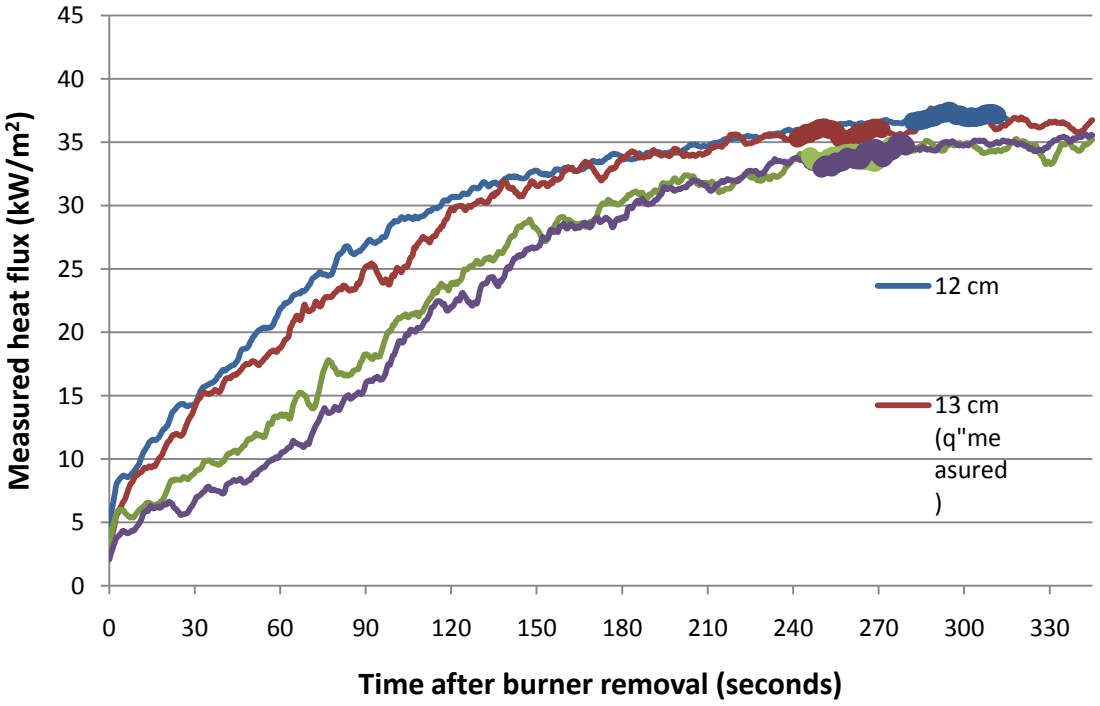

Figure A 4. Time interval used to calculate q"$_{steady}$ for samples 12-15 cm in height.

7.3 Calculated values of q''_{steady}

Table 3. Steady state heat flux values, q''_{steady}, for sample heights from 2-15cm

Height in Sample (cm)	q''_{steady} (kW/m^2)	Fitted q''_{steady} (kW/m^2)
2	40.86	40.56
3	40.74	40.56
4	40.88	40.56
5	39.76	40.56
6	35.94	36.05
7	35.00	34.39
8	33.63	33.90
9	31.91	33.75
10	32.59	33.69
11	30.62	33.69
12	37.04	33.69
13	35.74	33.69
14	33.87	33.69
15	33.92	33.69

From 2-5cm the fitted values of q''_{steady} have been determined as the mean of the four q''_{steady} values calculated over that range. The same averaging is used for heat fluxes reported at heights from 10-15 cm to reflect the previously described concept that that flame to surface heat flux can be regarded as a fire property of the material. From 6 - 9 cm, a sigmoidal fit of the data was used to provide the fitted values of q''_{steady} used in the transition region between these two constant values.

This allows for a representative heat flux, 33.7 kW/m^2, to be presented for PMMA while reporting higher q''_{steady} (as measured) near the base of the sample where the flame is closest to the material's surface. Using these fitted values of q''_{steady} to predict the final heat flux profile as a function of $\frac{dm'}{dt}$ helps to provide smoothed results without the random, though natural, variations seen in experimental data. Figure A 5 provides a qualitative depiction of these results.

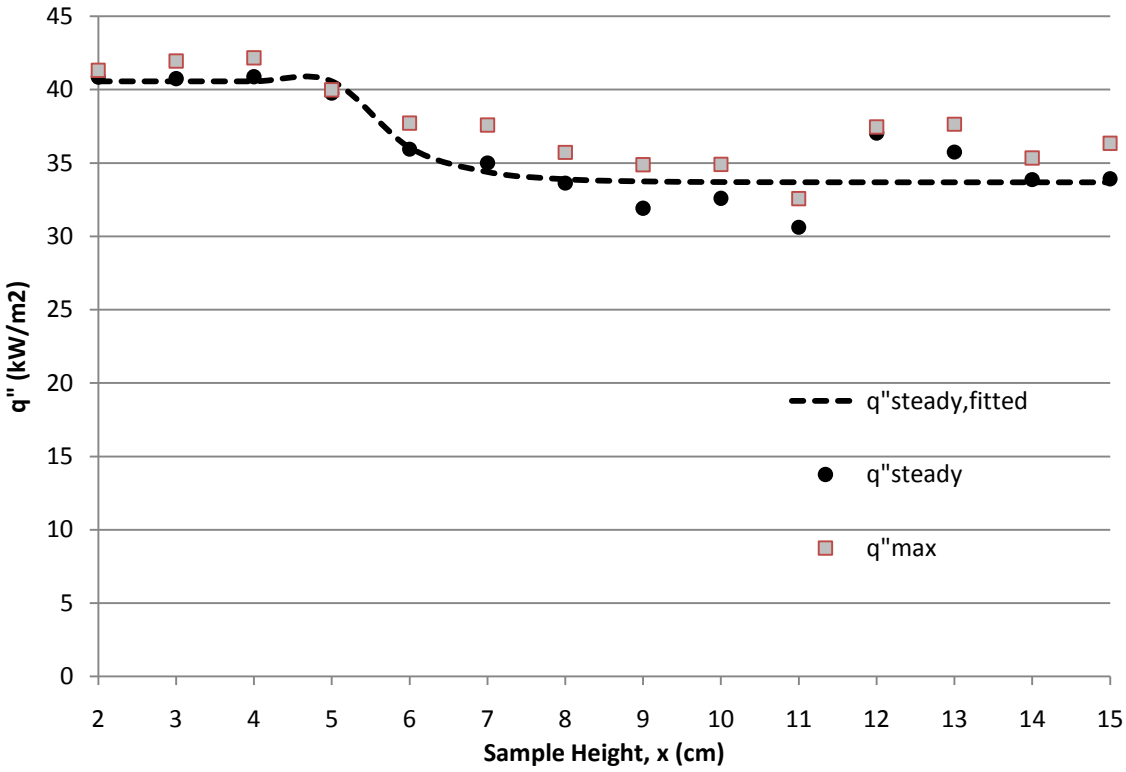

Figure A 5. Peak measured heat flux vs. sample height.

7.4 Accuracy of curve fits used to represent mass loss data

When determining sample mass loss rate, a mass balance with a precision of 0.01 g is used to provide readings at 1 Hz. Mass loss rate is calculated as $\frac{dm}{dt} = \frac{m_t - m_{t+1}}{\Delta t}$ and then normalized by the sample width (5 cm) to provide a new measurement, $\frac{dm'}{dt}$ [g/s-m]. Using this method, the minimum resolution of this measurement ($\Delta\frac{dm'}{dt}$) is 0.2 g/s-m. As average readings throughout the experiment increase from 0.2 to 1.4 g/s-m, this results in a rather low signal to noise ratio as seen Figure A 6.

Also shown in this figure are curves depicting average $\frac{dm'}{dt}$ (15 cm), which is calculated as a third order polynomial fit and a +/-3 s running average. This time interval was selected to match, as closely as possible, the +/-2.5 s interval across which heat flux measurements are treated as quasi-steady. Throughout the length of the experiment, the two curves (fitted and experimental average) differ, on average, by 2.5%.

The constants used to define fitted curves, $\frac{dm'}{dt} = a_0 + a_1 t + a_2 t^2 + a_3 t^3 + a_4 t^4$ can be found in Table 4.

Table 4. Coefficients used to determine polynomial regressions representing sample mas loss rate versus experimetnal time.

	a_0	a_1	a_2	a_3	a_4
3cm	0.2167	$4\cdot10^{-4}$	$2\cdot10^{-6}$	$-5\cdot10^{-9}$	0
5cm	0.234	$2.2\cdot10^{-3}$	$-6\cdot10^{-6}$	$1\cdot10^{-8}$	0
7cm	0.2191	$2.6\cdot10^{-3}$	$-4\cdot10^{-6}$	$6\cdot10^{-9}$	0
9cm	0.217	$1.58\cdot10^{-3}$	$1.16\cdot10^{-5}$	$-6.22\cdot10^{-8}$	$1.06\cdot10^{4}$
11cm	0.225	$1.9\cdot10^{-3}$	$3\cdot10^{-6}$	$-3\cdot10^{-10}$	0
13cm	0.2051	$2.3\cdot10^{-3}$	$-7\cdot10^{-7}$	$1\cdot10^{-8}$	0
15cm	0.2117	$1.9\cdot10^{-3}$	$2\cdot10^{-6}$	$8\cdot10^{-9}$	0

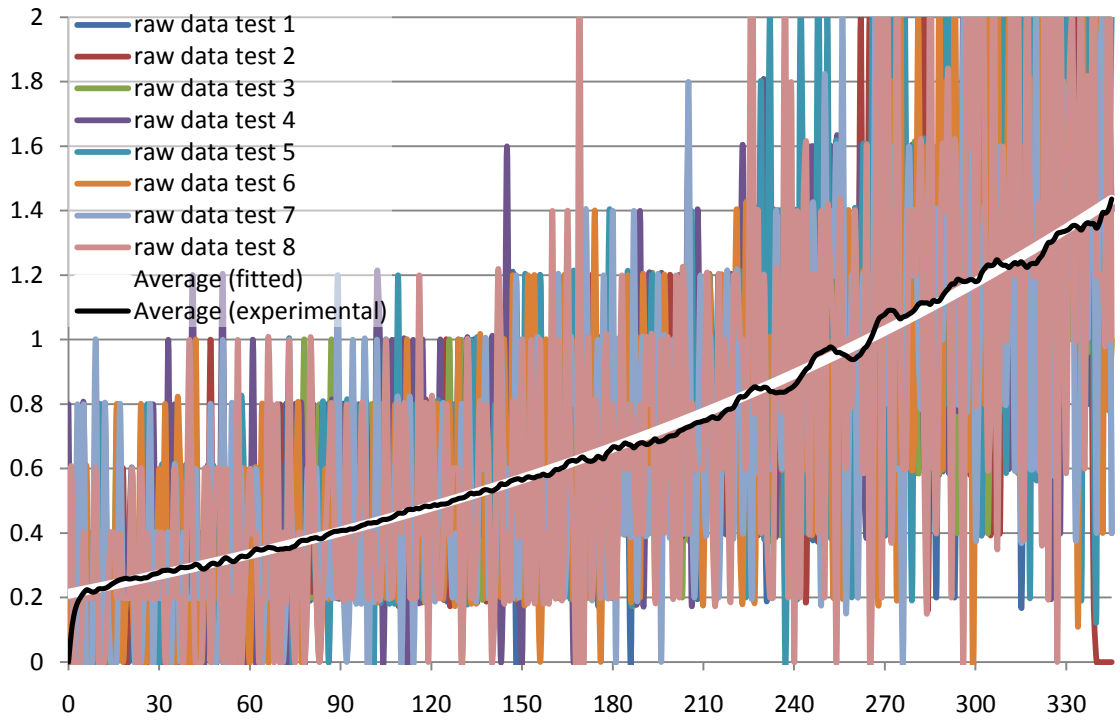

Figure A 6. Raw and fitted mass loss rate data for 15cm samples.

Qualitatively, the fitted polynomial matches the trend in raw measurements exceptionally well; however, to more precisely determine how well it correlates with experimental readings, one dimensional statistics were used to determine the standard deviation of the mean of the fitted curve. This error was determined at each time step in the experiment according to the formula below using experimental data taken in the time interval, $t = t_i \pm 3s$.

$$\sigma_{mean} = \sqrt{\frac{\sum_i^N \left(\dot{m}'_{fitted} - \dot{m}'_i\right)^2}{N(N-1)}}$$

N is defined as $N = 7 \bullet (number\ of\ successful\ tests)$; 7 is used here because the average mass loss rate profile has been smoothed with a 3s running average of data and measurements are taken at 1Hz.

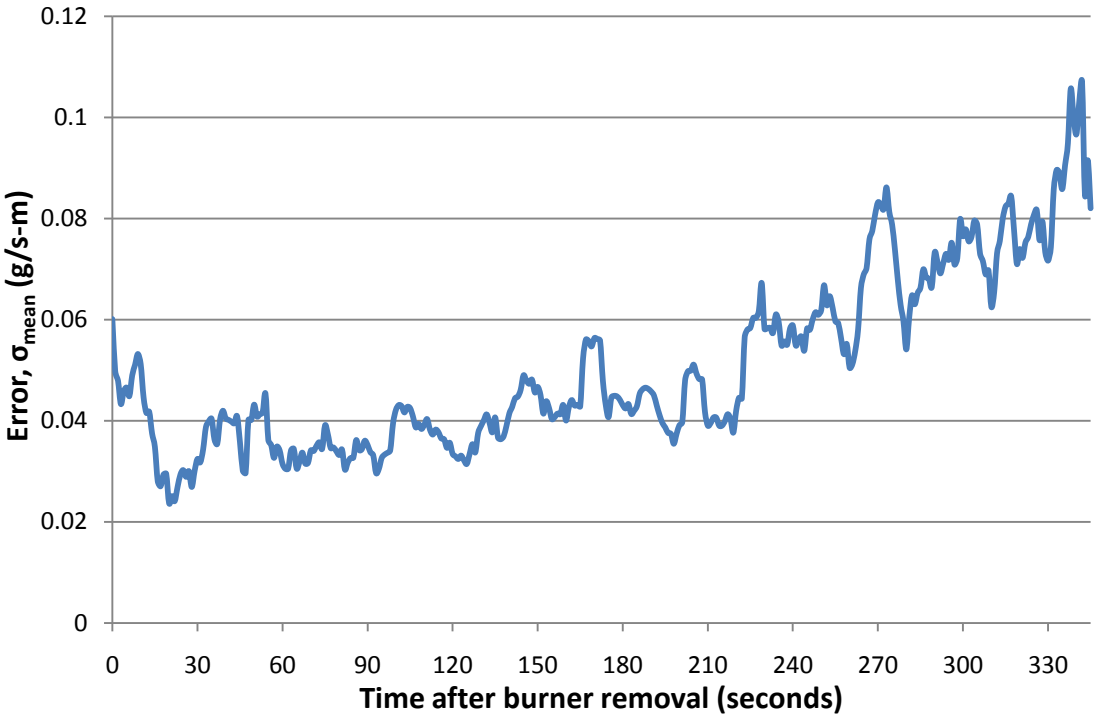

Figure A 7. Difference between fitted and measured average mass loss rate data.

As seen in Figure A 7, the calculated error in this smooth, fitted representation of sample mass loss rate versus experimental measurements remains quite small throughout the test. Although the total value of this error increases with respect to time, $\sigma_{mean}/\frac{dm'}{dt}$ [%] actually decreases in this respect because $\frac{dm'}{dt}$ later in experiments. Throughout the course of an experiment, this error, in absolute terms and as a fraction of total mass loss rate, averages to 0.05 g/s-m and 8.3%, respectively. Figure A 8 plots this result by showing the polynomial fit of sample mass loss rate with a 95% confidence interval equal to $2\sigma_{mean}$.

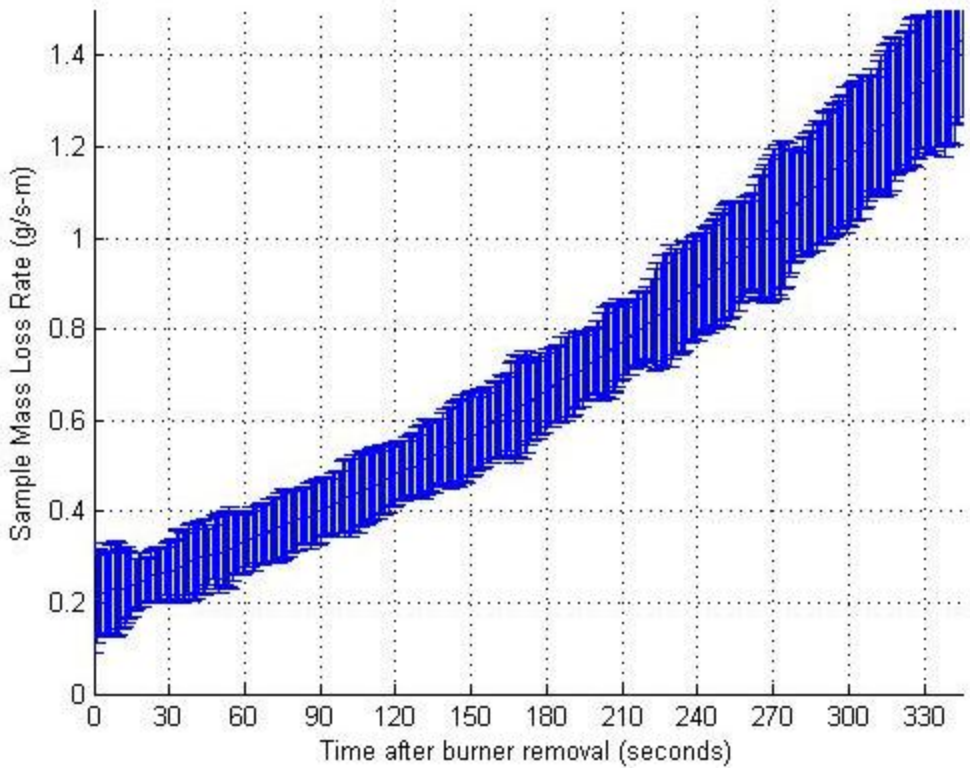

Figure A 8. Normalized sample mass loss rate (+/- $2\sigma_{mean}$) versus experimental time.

7.5 Calculating q"$_{recessed}$

The heat flux reported for tests when the gauge is recessed into the sample is determined by taking the value recorded just prior to flame extinction and subtracting from it the measurement taken shortly thereafter, when $\left|\frac{dq"}{dt} < 1\frac{kW}{m^2 s}\right|$. The points used for such a measurement can be seen in Figure A 9, which shows that the measured flame to recessed gauge heat flux can be calculated as $q" = 20.93 - 8.19 = 12.74\ \mathrm{kW/m^2}$ and $q" = 20.19 - 6.76 = 13.43\ \mathrm{kW/m^2}$ for tests 1 and 2 of this series, respectively.

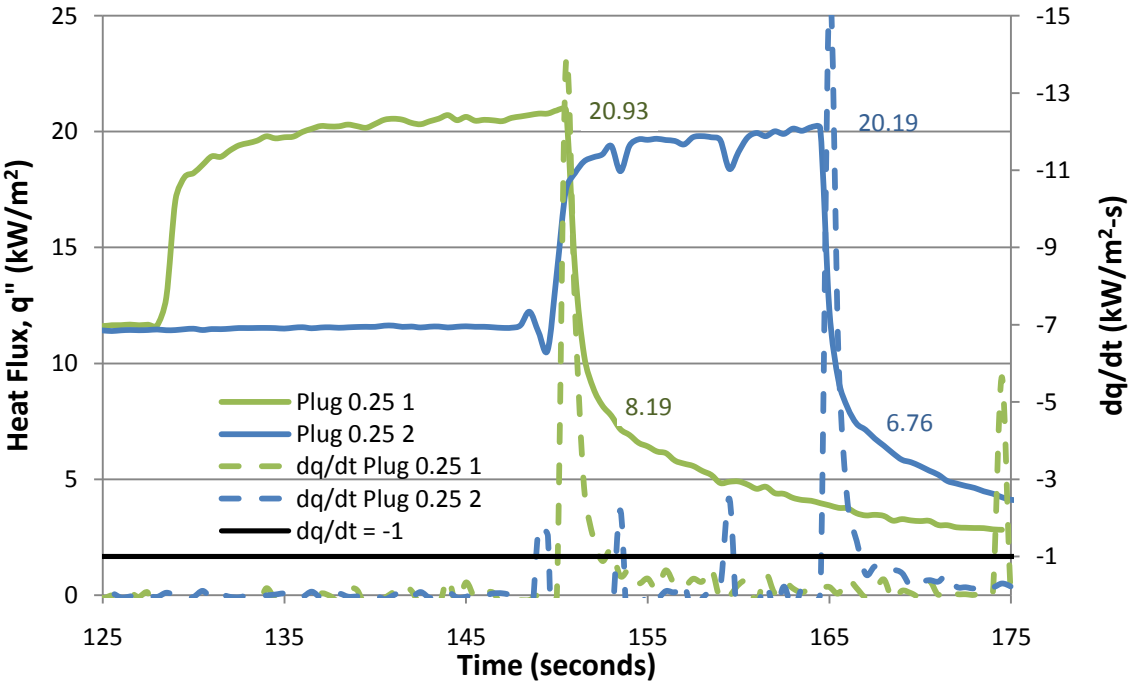

Figure A 9. Recessed gauge heat flux measurement of a propane flame taken at extinction. This same method is used for determining the heat flux to a recessed gauge in a burning sample of PMMA .

Ideally, one would like to measure the flame to surface heat flux before insulating materials surrounding the gauge begin heating up. Unfortunately, this is not possible for experiments on PMMA because there is a delay, during which time the sample and surrounding insulation (that form the walls of the heat flux gauge cavity) heat up, before the flame height has reached that of the heat flux gauge. Subtracting the heat flux that is measured directly following flame extinction effectively eliminates the contributions of these hot surrounding materials.

This calculation is easily and rationally justifiable from a physical perspective and to further ensure that it produces correct quantitative results, the heat flux of a propane flame was measured both immediately after ignition and in the manner described above; heat fluxes measured by these two methods were nearly identical. A propane flame is used as an analogue to that supported by burning samples of PMMA because it a produces similar peak heat flux but can be easily turned on or off and by measuring its flame to surface heat flux directly after ignition, the hot wall/surrounding insulation effects are nonexistent.

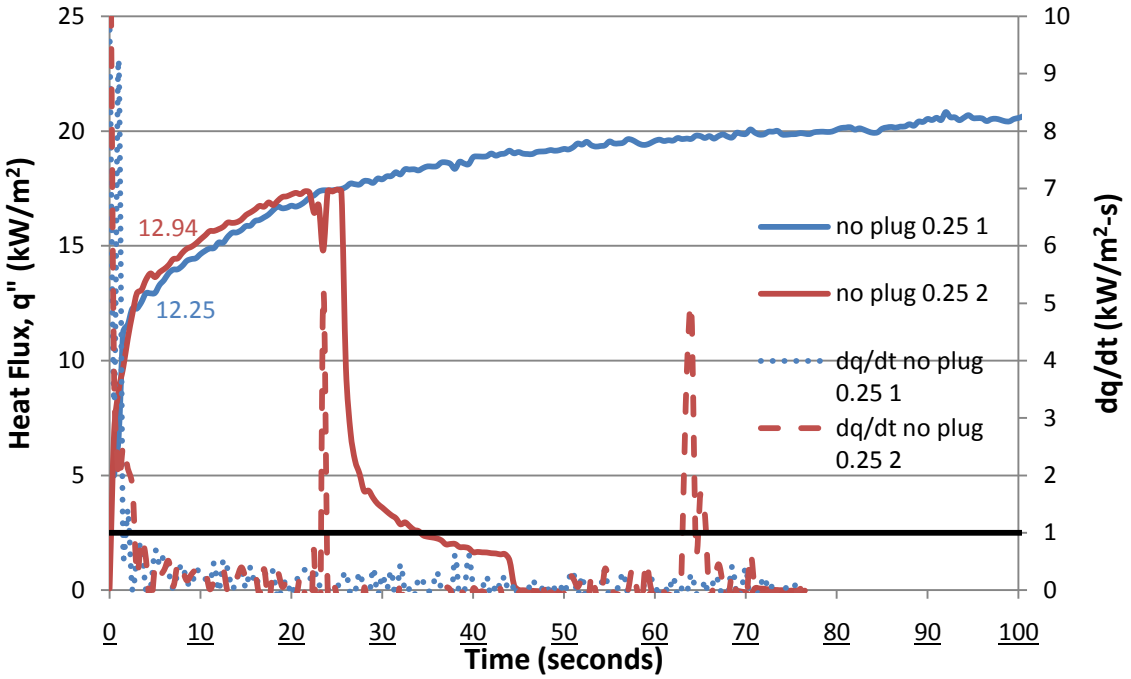

Figure A 10. Recessed gauge heat flux measurement of a propane flame taken at ignition.

Figure A 10 shows two representative tests where heat flux was measured by a recessed gauge immediately after flame ignition. Once again, the values reported here, 12.94 and 12.25 kW/m^2, are determined as the maximum measured value obtained before $\left|\frac{dq"}{dt} < 1 \frac{kW}{m^2 s}\right|$. These measurements are very consistent with those determined at flame extinction (12.74 and 13.43 kW/m^2) and thus the two methods are deemed equivalent and reliable measurements of solely the flame to surface heat flux, without any contributions from the surrounding insulation.

7.6 Radiative View Factor Calculations

7.6.1 Theoretical

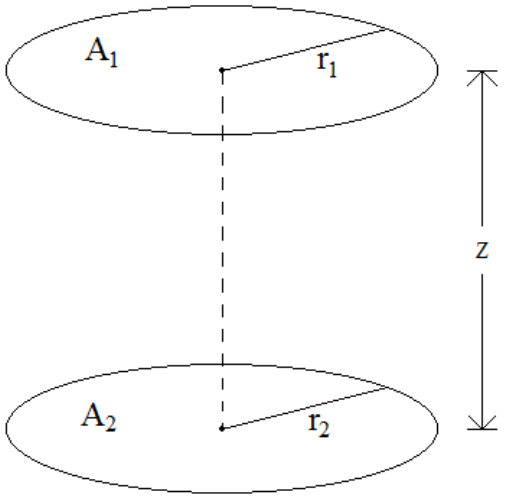

$$R_1 = \frac{r_1}{z} \qquad R_2 = \frac{r_2}{z} \qquad X = 1 + \frac{1+R_2^2}{R_1^2}$$

$$F_1 = \frac{1}{2}\left(X - \sqrt{X^2 - 4\left(\frac{R_2}{R_1}\right)^2}\right)$$

h; $r_1 = r_2 = 3/16$inch

$$R_1 = R_2 = R = \frac{3/16}{1/4} = \frac{3}{4}$$

$$X = 1 + \frac{1+R_2^2}{R_1^2} \rightarrow X = 1 + \frac{1+R^2}{R^2}$$

$$\frac{1+\left(\frac{3}{4}\right)^2}{\left(\frac{3}{4}\right)^2} = \frac{34}{9}$$

$$F_{1\rightarrow 2} = \frac{1}{2}\left(\frac{34}{9} - \sqrt{\left(\frac{34}{9}\right)^2 - 4\left(\frac{R}{R}\right)^2}\right) = 0.286$$

Here, A_1 and A_2 represent the surface area of the opening drilled through the sample/insulation and the front face of the heat flux gauge, respectively. They are calculated assuming $r_1 = r_2 = r_{HFg} =$ ½ (3/8 in) = 0.48 cm. Z is taken as the nominal distance that the heat flux gauge is recessed, 0.64 cm. Above formulas are cited from Holman's *Heat Transfer*. [23]

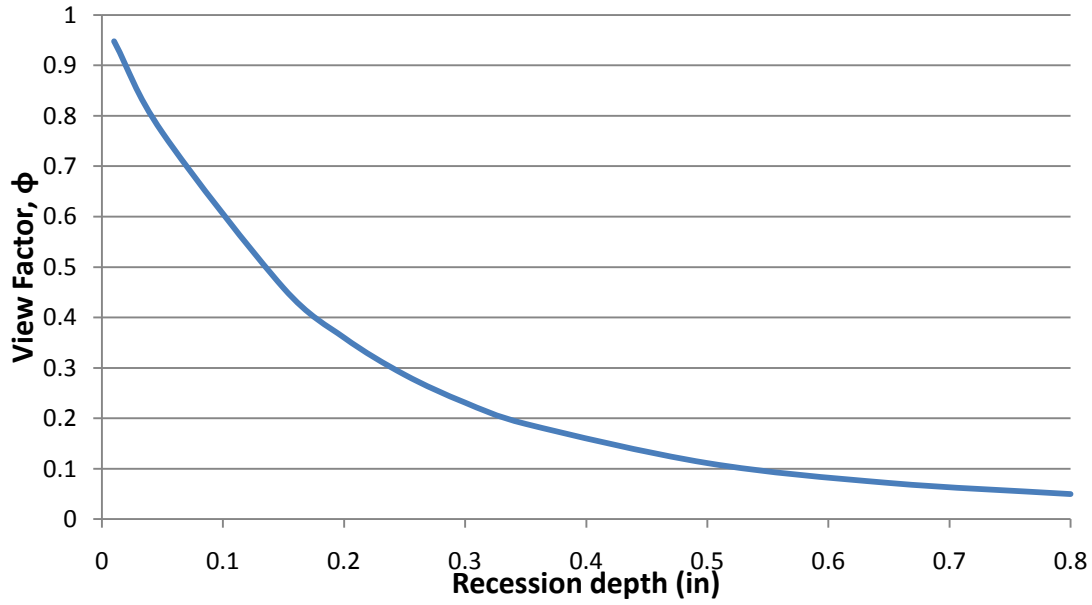

Figure A11. Radiative view factor as a function of recession depth, assuming constant $r1 = r2 =$ $0.48cm$.

7.6.2 Empirical

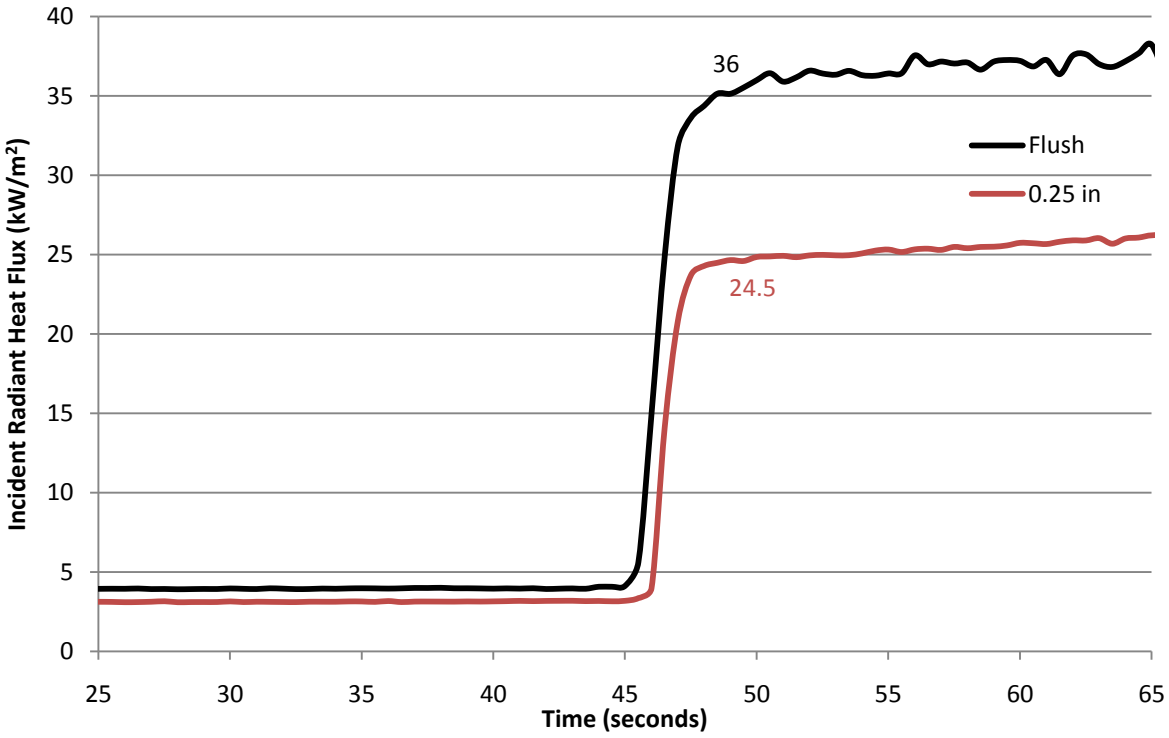

Figure A12. Measured heat flux as a function of heat flux gauge recession depth (inches).

Empirically, the radiative view factor is calculated as $\varphi = \frac{\dot{q}''_{recessed}}{\dot{q}''_{flush}} = \frac{24.5}{36} = 0.77.$

Measured heat flux values shown in the equation and figure above are determined by positioning a heat flux gauge in a prepared sample and placing it normal to the radiant heater of a cone calorimeter. Once in place, the sample and heat flux gauge are shielded by several layers of insulation and the cone heater is turned on until it reaches a steady state value. At this point, the shielding insulation is removed and incident heat flux is determined as the initial reading of the gauge at that time, before measurements slowly begin increasing as the surrounding sample and insulation heats up.

A margin of error of +/- 0.05 is obtained by recognizing that, although shielded, the prepared sample surrounding the heat flux gauge still heats up slightly before direct exposures. When the heat flux gauge is flush with the sample's face, this results in a 1.8 kW/m^2 difference in measured heat flux versus when the gauge is exposed to otherwise identical conditions but openly supported (not surrounded by a sample.) This serves as a fair approximation for the upper bound of errors in this measurement and thus the radiative view factor is reported as:

$$\varphi = 0.77 +/- 0.05$$

7.7 Determining the radiative component of incident radiation

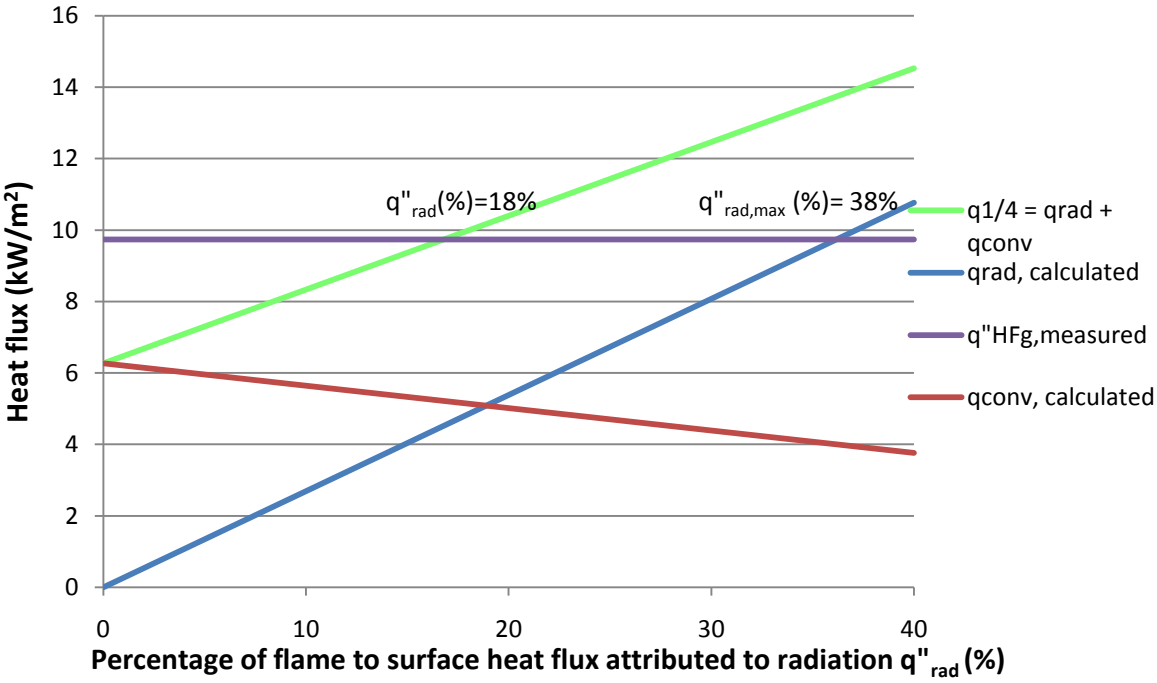

Figure A13. Calculated recessed gauge heat flux reading versus $q''_{rad}(\%)$.
This figure uses measurements taken from a 15cm tall samples.

Once flush and recessed gauge measurements of heat flux are accurately determined, a calculation of the percentage of flame to surface heat transfer that is attributed to radiation, $q''_{rad}(\%) = 100 \bullet \left(\frac{q''_{rad}}{q''_{HFg}}\right)$, can be made. This was done in two ways, the first assuming that the hot flame gases could not reach the heat flux gauge (blue curve) and the second, which allows for such thermal contact (light green curve).

Figure A13, the average heat flux recorded by a gauge recessed ¼ inch behind the sample's surface is plotted as the (purple) horizontal curve, $q'' = 9.74\ \mathrm{kW/m^2}$. The blue curve is a calculation of what the heat flux gauge would measure at a given $q_{rad}(\%)$; it is determined based on the known values of q''_{HFg} and φ as:

$$q''_{rad,calculated} = \varphi\left(q_{rad}(\%)\right)\left(q''_{HFg}\right)$$

The point at which these two curves intersect marks the highest $q_{rad}(\%)$ at which the recessed heat flux gauge's measurement could be attributed solely to radiation. If $q_{rad}(\%)$ is allowed to increase beyond this value, it suggests the nonsensical result that the flame transfers more energy into the material by radiation than was measured. For a 15 cm sample, as seen in Figure A8, this suggests an upper bound for radiation, $q_{rad}(\%) = 38\%$.

As there is physical evidence that hot gases do in fact reach the surface of the heat flux gauge, this calculation is repeated allowing for a non-zero convective component of heat flux. The resulting calculated heat flux ($q''_{¼,\,calculated}$, seen in Figure A13 in green) is then determined as:

$$q''_{1/4\,,calculated} = q''_{rad,calculated} + q''_{conv,calculated}$$

Where $q_{rad,calculated}$ is defined identically as above and $q_{conv\,,calculated}$ is determined as:

$$q''_{conv,calculated} = \varphi_{conv}\left(1 - q_{rad}(\%)\right)\left(q''_{HFg}\right)$$

With this new definition, the predicted $q''_{rad}(\%)$ for this system is found at the point in Figure A13 where the green and purple curves intersect. For a 15cm sample, this results in a flame to surface radiative fraction of $q''_{rad}(\%) = 18\%$. The same analysis is repeated for the 5 other sample heights at which recessed gauge measurements were taken resulting in the data seen in Figure A13

With the addition of Tewarson and Ogden' data, $q''_{rad}(\%)$can be defined as:

$$q''_{rad}(\%) \begin{cases} \dfrac{0.77x}{1cm} + 3.2142 & ; \quad x \le 1m \\ 80 & ; \quad x > 1m \end{cases}$$

7.8 Comparison of fitted curves with the original average heat flux measurements

The coefficients used to produce regressions estimating heat flux, q''_{HFg}, versus experimental time as $q''_{HFg} = a_0 + a_1 t + a_2 t^2 + a_3 t^3 + a_4 t^4 + a_5 t^5$ can be found in Table 5.

Table 5. Coefficients used to determine polynomial regressions representing q''_{HFg} versus experimetnal time**.**

	a_0	a_1	a_2	a_3	a_4	a_5
2cm (0-10.5s)	33.737	3.9149	-0.8253	$8.609 \cdot 10^{-2}$	-4.38310^{-3}	$8.622 \cdot 10^{5}$
2cm (11-14s)	41.251	0	0	0	0	0
2cm (14.5-345s)	41.803	$-4.505 \cdot 10^{-2}$	$4.9 \cdot 10^{-4}$	$-2.236 \cdot 10^{-6}$	$3.292 \cdot 10^{-9}$	0
3cm (0-4.5s)	34.146	2.343	-0.1999	0	0	0
3cm (5-345s)	40.61	$6.344 \cdot 10^{-3}$	$3.0898 \cdot 10^{2}$	0	0	0
4cm (0-13.5s)	18.67	7.43	-1.234	0.1024	$-3.134 \cdot 10^{-3}$	0
4cm (14-345s)	43.539	-0.14345	$1.617 \cdot 10^{-3}$	$-7.094 \cdot 10^{-6}$	$9.977 \cdot 10^{-9}$	0
5cm (0-14s)	15	7.458	-0.922	$5.327 \cdot 10^{-2}$	$-1.131 \cdot 10^{4}$	0
5cm (14.5-345s)	39.934	$-6.819 \cdot 10^{-3}$	$-8.8844 \cdot 10^{-5}$	$2.6831 \cdot 10^{-7}$	0	0
6cm (0-36s)	12.533	2.817	-0.1435	$3.364 \cdot 10^{-3}$	$-2.892 \cdot 10^{-5}$	0
6cm (36.5-345s)	38.809	$-9.187 \cdot 10^{-2}$	$8.24 \cdot 10^{-4}$	$-2.81 \cdot 10^{3}$	$3.353 \cdot 10^{-9}$	0
7cm (0-35s)	10.947	1.318	$-1.867 \cdot 10^{2}$	0	0	0
7cm (35.5-345s)	32.265	$8.323 \cdot 10^{-2}$	$8.694 \cdot 10^{-4}$	$3.353 \cdot 10^{-6}$	$-4.104 \cdot 10^{-9}$	0
8cm (0-83.5s)	9.286	1.2926	$-3.077 \cdot 10^{-2}$	$3.483 \cdot 10^{-4}$	$-1.48 \cdot 10^{-6}$	0
8cm (84-98s)	33.547	0	0	0	0	0
8cm (98.5-345s)	18.183	0.337	$-2.506 \cdot 10^{-3}$	$7.572 \cdot 10^{-6}$	$-7.956 \cdot 10^{-9}$	0

9cm (0-315s)	8.78	0.5128	$-5.474 \cdot 10^{-3}$	$3.07 \cdot 10^{-5}$	$-8.403 \cdot 10^{-9}$	$8.812 \cdot 10^{-11}$
9cm (315.5-345s)	32.552	0	0	0	0	0
10cm (0-345s)	7.376	0.423	$-2.694 \cdot 10^{-3}$	$7.697 \cdot 10^{-6}$	$-8.069 \cdot 10^{-9}$	0
11cm (0-345s)	5.498	0.407	$-2.482 \cdot 10^{-3}$	$6.8 \cdot 10^{-6}$	$-6.971 \cdot 10^{-9}$	0
12cm (0-302s)	6.916	0.27	$7.085 \cdot 10^{-5}$	$-1.034 \cdot 10^{3}$	$4.528 \cdot 10^{-8}$	$-5.966 \cdot 10^{-11}$
12cm (302.5-345s)	37.1	0	0	0	0	0
13cm (0-345s)	5.475	0.287	$-9.044 \cdot 10^{-4}$	$9.712 \cdot 10^{-7}$	0	0
14cm (0-345s)	4.611	0.114	$9.111 \cdot 10^{-4}$	$-5.578 \cdot 10^{-6}$	$7.903 \cdot 10^{-9}$	0
15cm (0-330.5s)	4.023	$3.54 \cdot 10^{-2}$	$1.832 \cdot 10^{-3}$	$-9.064 \cdot 10^{-6}$	$1.228 \cdot 10^{-8}$	0
15cm (331s-345s)	35.21	0	0	0	0	0

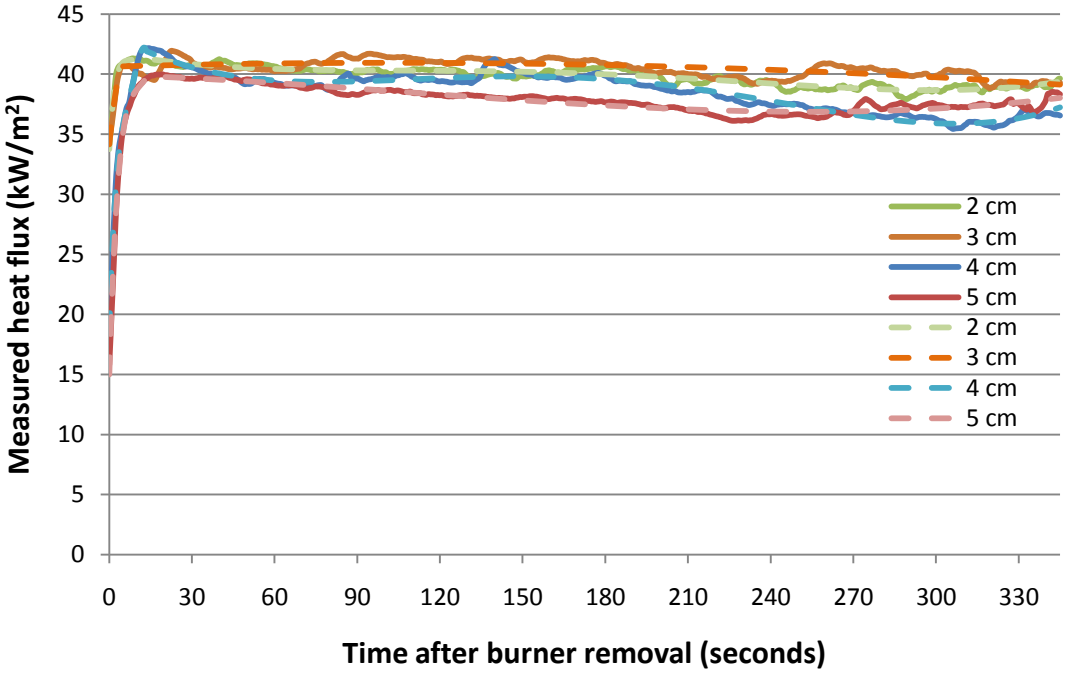

Figure A 14. Measured average and calculated fitted heat flux measurements for 2-5 cm tall samples. Solid curves denote measured average data.

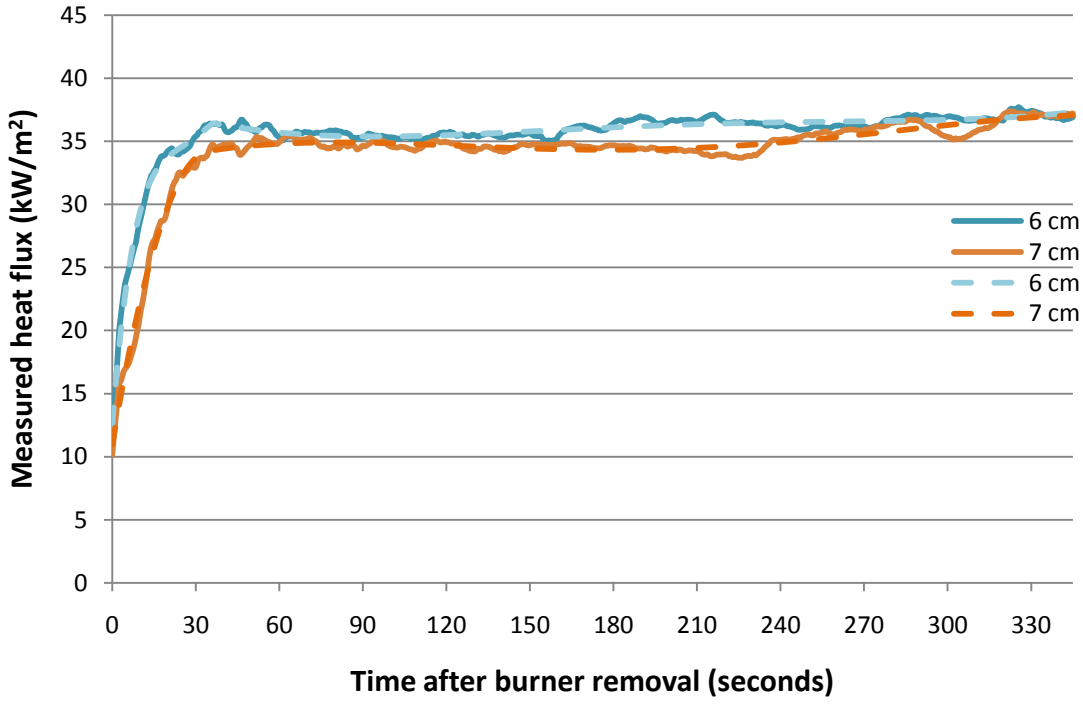

Figure A 15. Measured average and calculated fitted heat flux measurements for 6-7 cm tall samples. Solid curves denote measured average data.

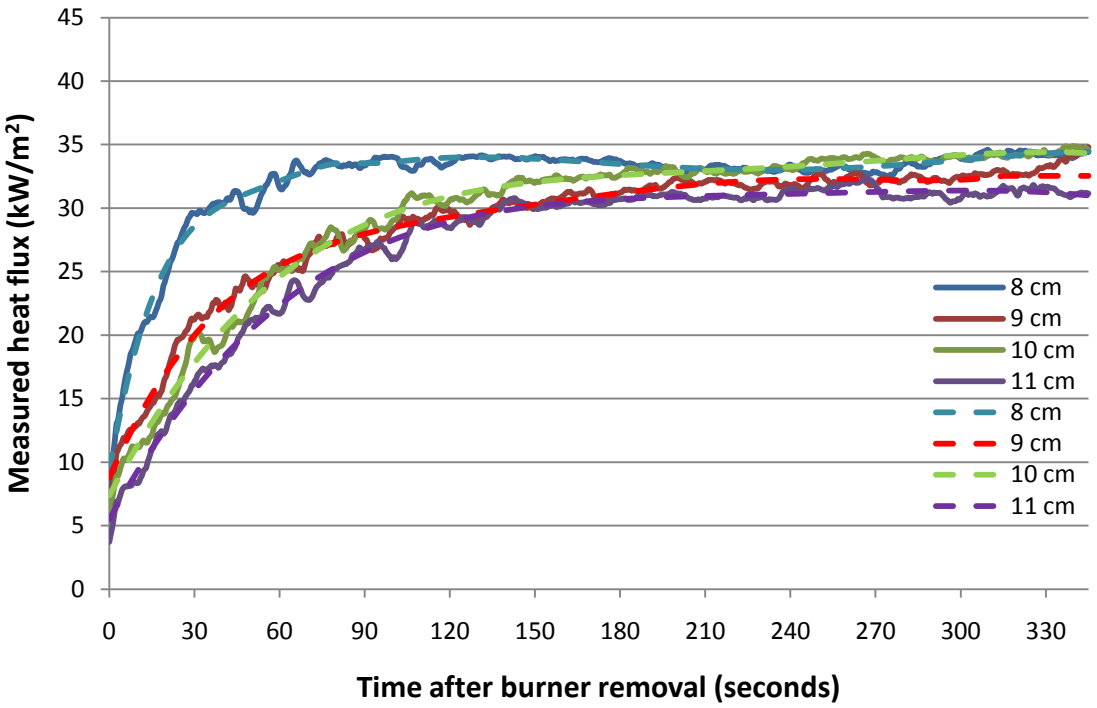

Figure A 16. Measured average and calculated fitted heat flux measurements for 8-11 cm tall samples. Solid curves denote measured average data.

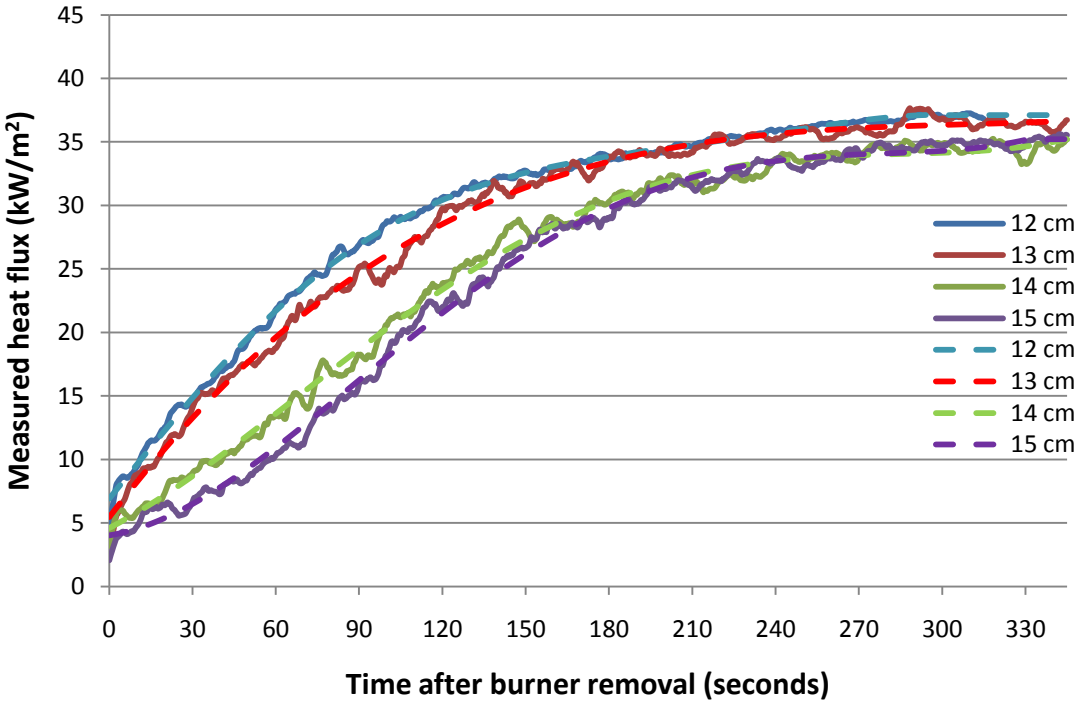

Figure A 17. Measured average and calculated fitted heat flux measurements for 12-15 cm tall samples. Solid curves denote measured average data.

7.9 Determining Flame Height, x_f, as a Function of Mass Loss Rate, dm'/dt

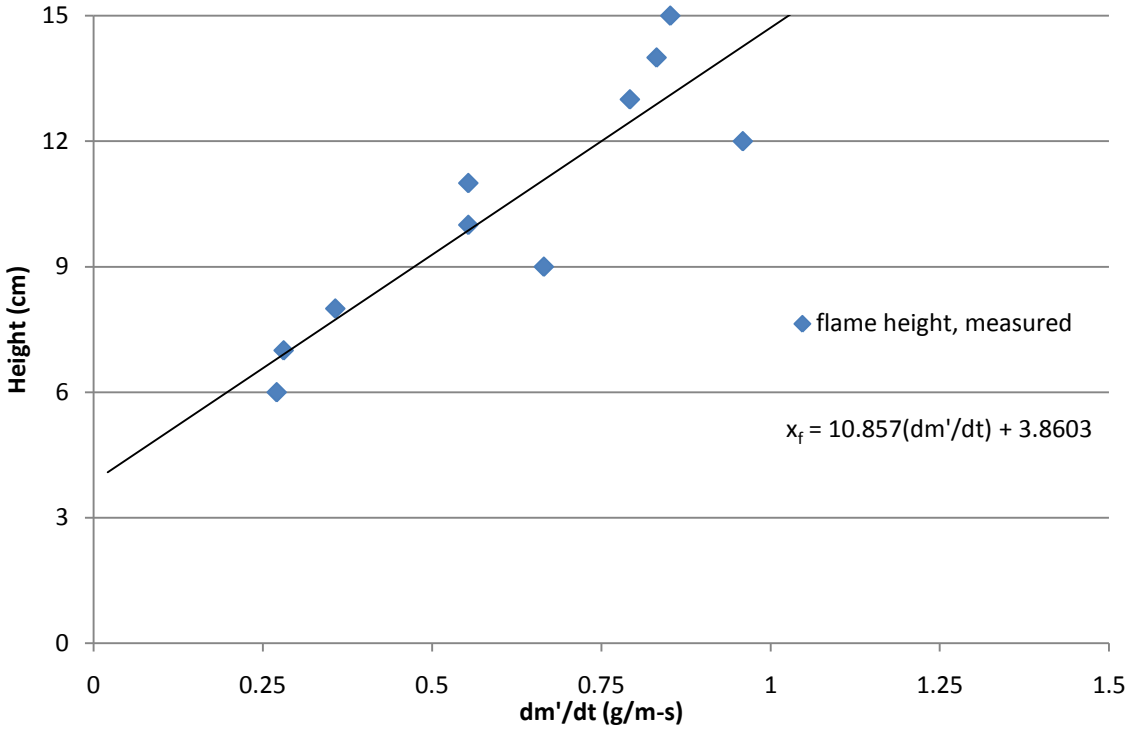

Figure A 18. Measured flame height (q"=0.975q"$_{steady}$) versus mass loss rate.

7.10 Stoichiometric Adiabatic Flame Temperature of Methyl Methacrylate, Calculations

Table 6. Heat of Formation and Specific Heat of Selected Substances

Substance	$\Delta\tilde{h}_f^\circ$ (kJ/mole, at 25°C and 1atm)	C_P (J/K-mole at 1400K)
$C_5H_8O_2$(PMMA)	-184.5	-
O_2	0	-
N_2	0	34.52
CO_2	-393.5	57.83
H_2O	-241.8	46.06

All values in this chart, except for the enthalpy of formation of PMMA [44], are taken from the NIST chemistry webbook [45]. Specific heats are taken at an average value between ambient, 25°C, and the adiabatic flame temperature. Once an adiabatic flame temperature is calculated, corrected values of C_p are determined and the calculation of $T_{fl,\,adiabatic}$ is reiterated until a constant value is obtained. The calculation below is representative of the final iteration of this process.

$$C_5H_8O_2 + 6(O_2 + 3.76N_2) \rightarrow 5CO_2 + 4H_2O + 22.56N_2$$

$$\sum H_{reactants} = \sum H_{products}$$

$$H = \Delta\tilde{h}_f^\circ + C_P\Delta T$$

$$\left[(1mol)\left(-184.5\frac{kJ}{mol}\right) + 6\left((1mol)\left(0\frac{kJ}{mol}\right) + (3.76mol)\left(0\frac{kJ}{mol}\right)\right)\right] =$$

$$\left[(5mol)\left(-393.5\frac{kJ}{mol}\right) + (4mol)\left(-241.8\frac{kJ}{mol}\right) + (22.56mol)\left(0\frac{kJ}{mol}\right)\right]$$

$$+$$

$$\left[\left((5mol)\left(57.83\frac{J}{mol-K}\right) + (4mol)\left(46.06\frac{J}{mol-k}\right) + (22.56mol)(34.52\frac{J}{mol-K}\right)\right.$$
$$\left.\bullet\left(10^{-3}\frac{kJ}{J}\right)(T_{fl,adiabatic} - 298K)\right]$$

$$-184.5kJ = -2934.7kJ + \left(1.24\frac{kJ}{K}\right)(T_{fl,adiabatic} - 298K)$$

$$T_{fl,adiabatic} = 2{,}217.9K \approx 2{,}220℃$$

7.11 Free Convection Heat Transfer on a Vertical Flat Plate: Theoretical Predictions of the Convective Heat Transfer Coefficient

g	9.81m/s^2
T_{fl}	2493K
T_w	630K
B=1/T_{avg}	0.00128K^{-1}
ν(1550K)	2.42E-04m^2/s
Pr (1550K)	0.705
k(1550K)	0.0973W/m-K

$$h = \frac{2k}{\delta} \qquad Ra = GrPr$$

$$\frac{\delta}{x} = 3.93Pr^{-\frac{1}{2}}(0.952 + \mathrm{Pr})^{1/4}Gr_x^{-1/4}$$

$$Gr_x = \frac{g\beta(T_w - T_\infty)x^3}{\nu^2}$$

Representative calculation of $h_{conv,theory}$at 10cm. Correlations and required thermal properties of air are taken from Holman. [23]

$$Gr_{10cm} = \frac{(9.81m/s^2)(0.0128K^{-1})(2493K - 630K)(0.1m)^3}{(2.42 \bullet 10^{-4}m^2/s)^2} = 4 \bullet 10^5$$

$$Ra = 4 \bullet 10^5(0.705) = 2.82 \bullet 10^5$$

$$\delta = (0.1m)\left[3.93(0.705)^{-\frac{1}{2}}(0.952 + 0.705)^{\frac{1}{4}}(4 \bullet 10^5)^{1/4}\right] = 0.0148m$$

$$h = \frac{2(0.0973\ W/mK\ )}{0.0148m} = 13.075W/m^2K$$

7.12 Determining q''_{net} as a function of sample mass loss rate

7.12.1.1 $x \leq 1.0$ m; $x/x_f \leq 1$

$$q''_{net} = (1-(cx+d))\left(q''_{steady} - \frac{(q''_{steady})(T_{surf}-T_{HFg})}{(T_{fl,adiabatic}-T_{HFg})}\right) + (1-r)(cx+d)\left(q''_{steady}\right) - \sigma(1-r)(T_{surf})^4$$

7.12.1.2 $x < 1.0$ m; $x/x_f > 1$

$$q''_{net} = (1-(cx+d))\left(q''_{steady}\left(\frac{x}{x_f}\right)^{\tau+\omega\bullet\left(1-\exp\left(\gamma\bullet\left(\frac{dm'}{dt}\right)\right)\right)} - \frac{(q''_{steady})\,(T_{surf}-T_{HFg})}{(T_{fl,adiabatic}-T_{HFg})}\right)$$

$$+(1-r)(cx+d)\left(q''_{steady}\left(\frac{x}{x_f}\right)^{\tau+\omega\bullet\left(1-\exp\left(\gamma\bullet\left(\frac{dm'}{dt}\right)\right)\right)}\right) - \sigma(1-r)(T_{surf})^4$$

7.12.2.1 $x \leq 1.0$ m; $x/x_f \leq 1$

$$q''_{net} = (1-e)\left(q''_{steady} - \frac{(q''_{steady})(T_{surf} - T_{HFg})}{(T_{fl,adiabatic} - T_{HFg})}\right) + (1-r)(e)\left(q''_{steady}\right) - \sigma(1-r)(T_{surf})^4$$

7.12.2.2 $x < 1.0$ m; $x/x_f > 1$

$$q''_{net} = (1-e)\left(q''_{steady}\left(\frac{x}{x_f}\right)^{\tau+\omega\bullet\left(1-\exp\left(\gamma\bullet\left(\frac{dm'}{dt}\right)\right)\right)} - \frac{(q''_{steady})\,(T_{surf} - T_{HFg})}{(T_{fl,adiabatic} - T_{HFg})}\right)$$

$$+(1-r)(e)\left(q''_{steady}\left(\frac{x}{x_f}\right)^{\tau+\omega\bullet\left(1-\exp\left(\gamma\bullet\left(\frac{dm'}{dt}\right)\right)\right)}\right) - \sigma(1-r)(T_{surf})^4$$

Bibliography

1. *Heat Release Rate: The Single Most Important Variable in Fire Hazard.* **Babrauskas, Vytenis.** 1992, Fire Safety Journal, Volume 18, pp. 255-272.

2. *Characterization of Flame Spread over PMMA Using Holographic Interferometry Sample Orientation Effects.* **Kashiwagi, Takashi and Ito, Akihiko.** 1988, Combustion and Flame, pp. 189-204.

3. *Width effects on the early stage of upward flame spread over PMMA slabs: Experimental observations.* **Pizzo, Y., et al.** 2009, Fires Safety Journal.

4. *Flame Spread Over Combustible Surfaces for Laminar Flow Systems, Part I: Excess Fuel and Heat Flux.* **Annamalai, A. and Sibulkin, M.** 1979, Combustion Science and Technology, pp. 167-183.

5. **Underwriters Laboritories .** UL 94. *UL.* [Online] http://www.ul.com/global/eng/pages/offerings/industries/chemicals/plastics/testing/flame/.

6. *The Application of Flame Spread Theory to Predict Material Performance.* **Quintiere, James G.** 1988, Journal of the Research of the National Bureau of Standards, pp. 61-70.

7. *Controlling Mechanisms of Flame Spread.* **Fernandez-Pello, A.C and Hirano, T.** 1983, Comustion Science and Technology, pp. 1-31.

8. *On the Flame height definition for upward flame spread.* **Consalvi, J.L., et al.** 2007, Fire Safety Journal, pp. 384-392.

9. *Numerical Model of upward flame spread on practical wall materials.* **Brehob, E.G., Kim, C.I. and Kulkarni, A.K.** 2001, Fire Safety Journal, pp. 225-240.

10. *Wall Flames and Implications for Upward Flame Spread.* **Quintiere, James, Harkleroad, Margaret and Hasemi, Yuji.** 1986, Combustion Science and Technology, pp. 191-222.

11. **Thomas, P.H. and Lawson, D.I.** *On the minimum speed of flame propagation in fabrics.* Borehamwood, UK : Joint Fire Reserach Organization, 1957.

12. *Spread of a Laminar Diffusion Flame.* **DeRis, J. N.** s.l. : National Bureau of Standards, 1969, Proceedings of the Combustion Institute, pp. 241-252.

13. *Flame Spread Over Combustible Surfaces for Laminar Flow Systems, Part II: Flame Heights and Fire Spread Rates.* **Annamalai, K and Sibulkin, M.** 1979, Combustion Science and Technology, pp. 185-193.

14. *A theoretical model for the upward laminar spread of flames ove vertical fuel surfaces.* **Fernandez-Pello, A.C.** 1978, Combustion and Flame , pp. 135-148.

15. *Upward Turbulent Flame Spread.* **Saito, K, Williams, F.A. and Quintiere, J.G.** Gaithersburg, MD : Hemisphere Publishing Co., 1985. International Association for Fire Safety Science. pp. 75-86.

16. *Fire Behavior of Polymethylmethacrylate.* **Tewarson, A. and Ogden, D.** 1992, Combustion and Flame, pp. 237-259.

17. *Upward Flame Spread: The Width Effect.* **Tsai, K.C. and Wan, F.** 2005. Proceedings of the Eigth International Symposium. pp. 409-419.

18. *Upward flame spread on a vertically orientated fuel surface : The effect of finite width.* **Rangwala, Ali S., Buckley, Steven G. and Torero, Jose L.** 2007, Proceedings of the Combustion Institute, pp. 2607-2615.

19. *Upward Turbulent Flame Spread on Wood Under External Radiation.* **Saito, K., et al.** 1989, Journal of Heat Transfer, pp. 438-445.

20. *Experimental observations of the steady state burning rate of a vertically orientated PMMA slab.* **Pizzo, Y., et al.** 2008, Combustion and Flame, pp. 451-460.

21. *Upward Laminar Flame Spread Under the Influence of Externally Applied Thermal Radiation.* **Fernandez-Pello, A.C.** 1977, Combustion Science and Technology, pp. 87-99.

22. *Characterization of Flame Spread over PMMA Using Holographic Interferometry Sample Orientation Effects.* **Kashiwagi, Ito.** 1988, Combustion and Flame, pp. 189-204.

23. **Holman, J. P.** *Heat Transfer, Ninth Edition.* New York : McGraw Hill, 2002.

24. *Numerical analysis of the heating process in upward flame spread over thick PMMA slabs.* **Consalvi, J.L., Pizzo, Y. and Porterie, B.** 2008, Fire Safety Journal, pp. 351-362.

25. *Upward turbulent fire spread and burning of fuel surface.* **Orloff, L., DeRis, J. and Marksteain, G.H.** 1974. Fifteent Symposium (International) on Combustion. pp. 183-192.

26. *Unsteady-state upward flame spreading velocity along vertical combustible solid and influence of external radiation on the flame spread.* **Hasemi, Y., et al.** 1991. Proceedings of the Third International Symposium of Fire Safety Science. pp. 197-206.

27. *Flame heights in turbulent wall fires with significant flame radiation.* **Delichatsios, M.A.** 1984, Combustion Science and Technology, pp. 195-214.

28. **Stoliarov, Stanislav I. and Lyon, Richard E.** *Thermo-Kinetic Model of Burning.* s.l. : Federal Aviation Administration, 2008.

29. *Upward flame spread: heat transfer to the unburned surface.* **Tsai, Kuang-Chung, et al.** Edinburgh : s.n., 1991. Fire Safety Science- Proceedings of the Seventh International Symposium. pp. 117-128.

30. *Flame Heat Fluxes and Correlations of Upward Flame Spread Along Vertical Cylinders in Various Oxygen Environments.* **Delichatsios, Michael A.** 2000, Proceedings of the Combustion Institute, pp. 2899-2904.

31. *The dependence of flame propagation on surface heat transfer II Upward Burning.* **Sibulkin, M. and Kim, J.** 1977, Combustion Science and Technology, pp. 39-49.

32. *Concurrent Turbulent Flame Spread.* **Zhou, L. and Fernandez-Pello, A.C.** 1991. Twenty-Third Symposium (International) on Combustion. pp. 1709-1714.

33. *Prediction of the Burning Rates of Non-Charrring Polymers.* **Stoliarov, Stanislav I.** 2009, Combustion and Flame, pp. 1068-1083.

34. **Quintiere, James G.** *Fundamentals of Fire Phenomena.* s.l. : Wiley & Sons Ltd., 2006.

35. **Lattimer, Brian Y.** Heat Fluxes from Fires to Surfaces. *SFPE Handbook of Fire Protection, Third Edition.* Quincy, Massachusetts : NFPA, 2002.

36. *Model Calculations of steady upward flame spread over a thin solid in reduced gravity.* **Jiang, Ching-Biau, T'ien, James S. and Shih, Hsin-Yi.** 1996, Twenty Sixth Symposium (International) on Combustion, pp. 1353-1360.

37. *Effect of Oxygen on flame heat flux in horizontal and vertical orientations.* **Beaulieu, Patricia A. and Dembsey, Nicholas A.** 2008, Fire Safety Journal, pp. 410-428.

38. **Beaulieu, Patricia A. and Dembsey, Nocholas A.** *Effect of Oxygen on flame heat flux in horizontal and vertical orientations.* 2008. pp. 410-428.

39. **Cyro.** Acrylite FF & GP Acrylic Sheet. *US Plasstic Corp.* [Online] 03 20, 2002. http://www.usplastic.com/catalog/files/44200MSDS05-2002.pdf. 04902.

40. **Kulkarni, A.K., et al.** *Turbulent Upward Flame Spread on a Vertical Wall Under External Radiation.* Gaithersburg, MD : NIST, 1994.

41. **Thermal Ceramics.** Kaowool Low Temperature Boards. *Thermal Ceramics.* [Online] [Cited: September 12, 2011.] http://www.fabricationspecialties.com/pdf/lowtemp.pdf.

42. *Radiation Attenuation characteristics of pyrolysis volatiles of solid fuels and their effect for radiant ignition model.* **Zhou, Y. and al., et.** 2010, Combustion and Flame, pp. 167-175.

43. *Heat transfer by radiation and convection in fire testing.* **Wickström, Ulf.** 2004, Fire and Materials, pp. 411-415.

44. *Laser- Induced Incandescence Measurements of Soot Production in Steady and Flicker Methane, Propane and Ethylene Diffusion Flames.* **Shaddix, Christopher, R. and Smyth, Kermit C.** 107, Gaithersburg : The Combustion Insitute, 1996.

45. *Advances in Heat Flux Measurement.* **Diller, T.E.** Boston : Academic Press, 1997, Advances in Heat Transfer, Vol. 23.

46. **Walters, Richard N., Hackett, Stacey M. and Lyon, Richard E.** *Heat of combustion of high temperature polymers.* Atlantic City, NJ : Federal Aviation Administration.

47. **NIST.** Nist Chemistry Webbook. [Online] 2011. [Cited: October 1, 2011.] http://webbook.nist.gov/chemistry/. 69.